TYNER

Technical and Economic Evaluation of a Solid-Particle/Air Direct-Contact Heat Exchanger

Herbert J. Green
Cécile M. Leboeuf
Mark S. Bohn

SERI

Technical and Economic Evaluation of a Solid-Particle/Air Direct-Contact Heat Exchanger

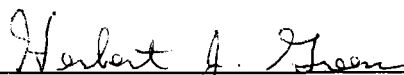Herbert J. Green
Cécile M. Leboeuf
Mark S. Bohn

October 1986

PREFACE

The research and development described in this document was conducted within the U.S. Department of Energy's Storage Technology Program. The Solar Energy Reserch Institute (SERI) is the lead laboratory for research, technology, and system analyses and assessments for thermal energy storage for solar thermal applications and for thermal energy transport.

The goal of SERI's Solar Energy Storage Program is to identify economical energy storage and transport subsystems for the industrial sector and to bring the corresponding technologies to the point where they can be transferred from research and development. The strategy to accomplish this goal is to conduct research in advanced thermal energy storage technologies for solar thermal electric power and solar thermal industrial process heat applications, and in energy transport technologies for industrial process heat applications.
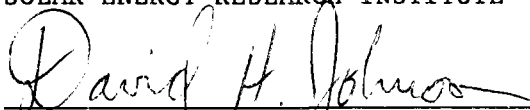
The focus of the program is to develop containment techniques and heat exchange for high temperatures and to define thermochemical transport systems. This report documents a technical and economic evaluation of a solid-particle/ air direct-contact heat exchanger to heat pressurized air using solid particles heated in a solar thermal central receiver. This study was done in cooperation with Sandia National Laboratories in Livermore, California, where the development of central receivers using solid particles as the heat transfer media is currently under way for the Solar Thermal Technologies Program. This report was done for the Solar Energy Storage Program in FY 1984 under funding from the Division of Energy Storage Technologies of the U.S. Department of Energy.
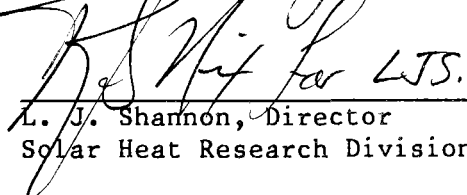
We wish to acknowledge the contributions of Elizabeth Fisher and David H. Johnson who surveyed pertinent literature and prepared a critical review of the state of the art of particle-gas heat exchange, which served as the starting point for this study. We also wish to thank Ron West of Colorado University and Jill Hruby of Sandia National Laboratories, Livermore, for their reviews of this report and their constructive comments.

Herbert J. Green
Associate Engineer

Approved for

SOLAR ENERGY RESEARCH INSTITUTE

David H. Johnson, Manager
Thermal Sciences Research Branch

L. J. Shannon, Director
Solar Heat Research Division

SUMMARY

Objective

The objective of this research is to determine the technical and economic feasibility of heating pressurized air in a direct-contact heat exchanger (DCHX) with hot solid particles from a solar thermal central receiver.

Discussion

High-temperature applications (above $650^\circ C$) of solar thermal central receivers may use solid particles as the heat transfer medium. Some high-temperature applications such as Brayton-cycle electric power generation require pressurized hot air. A direct-contact heat exchanger configuration appears attractive for these applications because of the absence of heat transfer surfaces. In this report, two conceptual designs of solid-particle/ air heat exchanger systems are presented including a multistage fluidized-bed heat exchanger, solid-particle feeders and defeeders, and cyclones. The first system is based on state-of-the-art technology while the second system assumes reasonable technical progress resulting from future development activities. Both systems are designed for $1000^\circ C$ solid particles heating air at 10 atm at a 100 MW_t heat rate. Both the technical and economic feasibilities of these systems are evaluated. As an alternative to direct contact, a shell-and-tube heat exchanger is evaluated as well.

Conclusions

The DCHX system is technically feasible though additional development is needed in some areas. In particular, the operating temperatures for valves handling solid particles must be increased and data on particle attrition in a central receiver system is needed for accurate cyclone design. The annual levelized cost per unit of delivered energy for a DCHX system based on state-of-the-art technology is estimated to be $6.66/GJ ($7.04/10^6 Btu). If reasonable assumptions are made about the technical progress resulting from future development activities, the cost drops to $2.30/GJ ($2.43/10^6 Btu). Most of the cost is for the solids-handling equipment and not in the heat exchanger itself. The cost of a shell-and-tube heat exchanger for the same service was estimated to be $2.91/GJ ($3.07/10^6 Btu), about one-third that of the DCHX. This makes the shell-and-tube configuration competitive with the DCHX, although the applicability of this configuration at high temperatures is yet to be determined.

These costs were calculated using a cost methodology developed by the SERI Solar Energy Storage Program. In addition, a cost methodology from the Solar Thermal Technology Program was used to allow comparison to the Solar Thermal cost goals. Using the Solar Thermal methodology, the state-of-the-art configuration costs $4.64/GJ ($4.90/10^6 Btu), the configuration that assumes reasonable technical progress costs $1.56/GJ ($1.65/10^6 Btu), and the shell-and-tube configuration costs $2.03/GJ ($2.14/10^6 Btu). All these costs are high compared to the Solar Thermal cost goal of $8.52/GJ ($9.00/10^6 Btu) for thermal energy delivered from a solar central receiver.

TABLE OF CONTENTS

LIST OF FIGURES

LIST OF FIGURES (Concluded)

LIST OF TABLES

NOMENCLATURE

a	surface area per unit volume
A_1	surface area (m^2)
c_{pa}	specific heat of air (J/kg K)
c_{ps}	specific heat of solid particles (J/kg K)
C_c	corrosion allowance (in.)
C_d	drag coefficient
C_f	capacity factor
C_m	cost of electricity ($/kWh)
C_t	total cost of insulation plus cost of lost heat ($)
dp	particle diameter (m)
d_s	particle diameter (cm)
d_{sh}	inner shell diameter (in.)
D	orifice diameter (in.)
D_h	hydraulic diameter
D_i	inside diameter of the tubes
D_o	outside diameter of the tubes
E_j	joint efficiency
F	friction factor adjustment for finned tube geometry
g	981 cm/s^2
h	heat transfer coefficient (W/m^2 K)
h_f	operating bed depth
h_m	static bed depth
h_{sh}	total height of the heat exchanger shell (m)
H	bed height
H_a	air-side heat transfer coefficient (W/m^2 K)
H_p	particle-side heat transfer coefficient (W/m^2 K)
k	thermal conductivity of air (W/m K)
k_1	thermal conductivity of internal insulation (W/m K)
k_2	thermal conductivity of external insulation (W/m K)
K_a	thermal conductivity of air
K_s	thermal conductivity of alumina
K_w	wall thermal conductivity
L	tube length

<div align="center">

NOMENCLATURE (Continued)

</div>

$\dot{m}_a$	mass flow rate of air (kg/s)
$\dot{m}_s$	mass flow rate of solid particles (kg/s)
Nu_a	air-side Nusselt number
P	internal pressure (psig)
P_b	pressure drop in the bed (N/m^2)
Pe	Peclet number
Pr	Prandtl number
Pr_a	air-side Prandtl number
P_t	pressure drop in the multistage fluidized-bed heat exchanger (N/m^2)
q	heat loss, heat flux (W/m^2)
Q	heat duty (MW)
R_a	air-side fouling resistance
Re	Reynolds number
Re_a	air-side Reynolds number
Re_p	particle-side Reynolds number
R_p	particle-side fouling resistance
S	maximum allowable stress (psi)
t_{sh}	thickness of the shell (in.)
t_1	thickness of internal insulation (m)
$T_{ai,n}$	air inlet temperature for stage n
$T_{ao,n}$	air outlet temperature for stage n
$\overline{T}_{s,n}$	average particle temperature for stage n
u_{mf}	minimum velocity for fluidization (cm/s)
u_o	operating air velocity (cm/s)
u_s	superficial gas velocity (m/s)
u_t	particle terminal velocity (cm/s)
U	overall heat transfer coefficient
U_a	volumetric heat transfer coefficient
U_c	air inlet velocity (m/s)
V_a	velocity of air
V_c	cyclone air inlet velocity (m/s)
V_1	total volume of internal insulation (m^3)
V_{1h}	volume of internal insulation required for an ellipsoidal head (m^3)

NOMENCLATURE (Concluded)

V_{1sh} volume of internal insulation required for the shell (m^3)

V_o bed velocity

W pumping power (kW)

W_h weight of head (kg)

W_s solids efflux rate (lb/s ft^2)

W_{sh} weight of the shell (kg)

W_t total weight of the heat exchanger vessel (lb)

Y_w wall thickness

γ_b bulk density

Δ_p pressure drop (N/m^2)

ΔT temperature difference ($^\circ C$)

ΔT_{1M} log-mean temperature difference

ε void fraction

ε_m void fraction in the static bed

ε_{mf} bed voidage at minimum fluidization

η collection efficiency

η_a heat exchanger efficiency on the air side

η_c compressor efficiency

η_m motor efficiency

η_s heat exchanger efficiency on the particle side

μ air viscosity (Ns/m^2)

ρ_a air density (g/cm^3)

ρ_b particle bulk density (g/cm^3)

ρ_{cs} density of carbon steel (lb/ft^3)

ρ_s particle density (g/cm^3)

ϕ_s particle sphericity
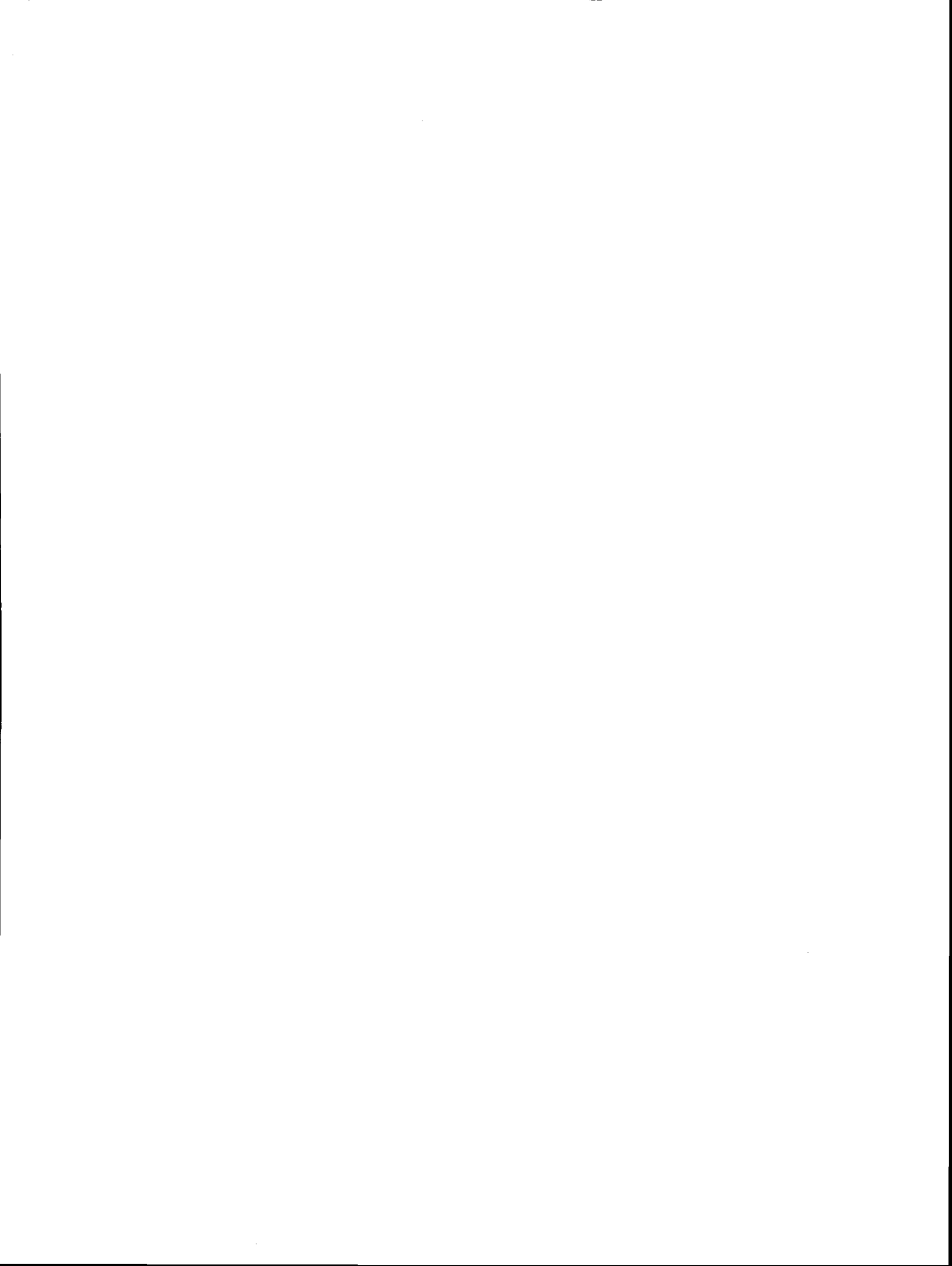
1.0 INTRODUCTION

Solid particles have been studied as a heat transfer and storage medium for central receiver solar thermal systems (Burolla et al. 1984; Falcone et al. 1985; Martin and Vitko 1982). Figure 1-1 shows a conceptual design of a solid-particle receiver. Solid particles show potential to operate at higher temperatures by virtue of their chemical stability, essentially zero vapor pressure, and ability to withstand high incident flux levels. Applications for high-temperature central receiver systems include industrial process heat, production of fuels and chemicals, and cogeneration of steam and electricity.
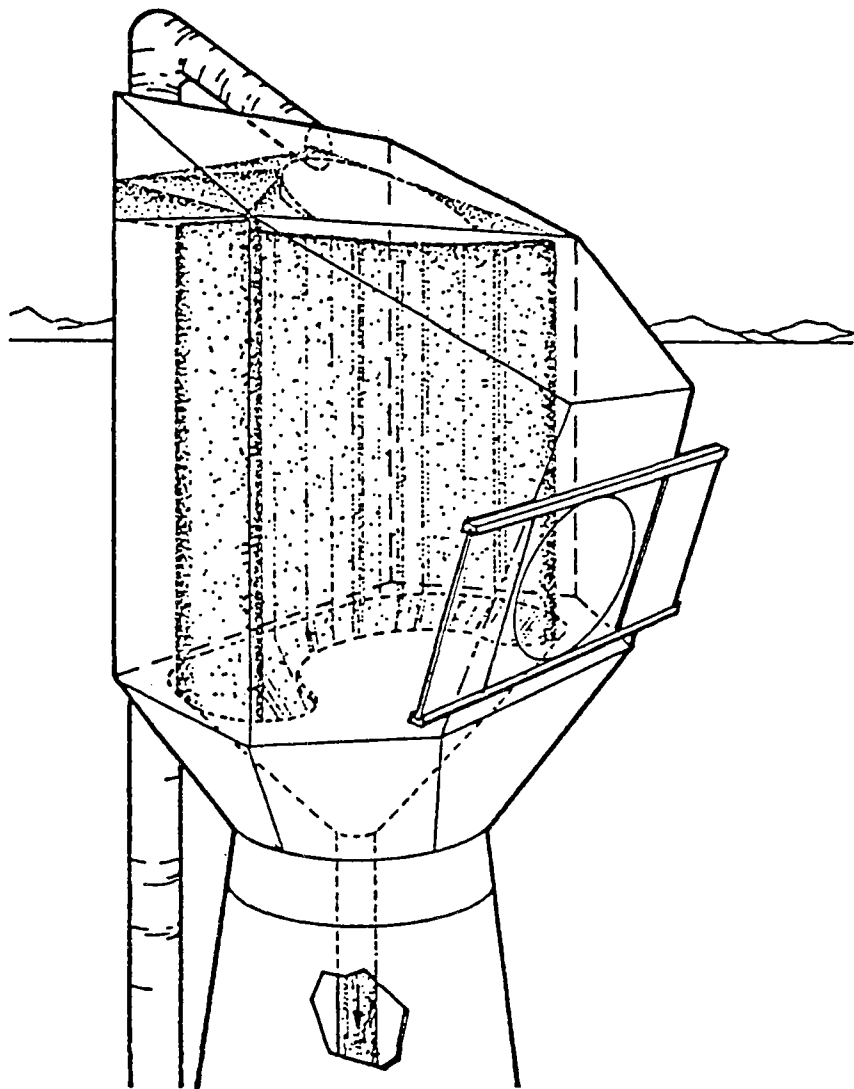
Figure 1-1. Conceptual Design of Solid-Particle Receiver (Sandia National Laboratories, Livermore)

Many of these applications require pressurized hot air. Delivering hot air from a solid-particle central receiver system requires a solid-particle-to-air heat exchanger. Figure 1-2 is a schematic of a simplified system where solid particles from high-temperature storage pass to a heat exchanger and on to low-temperature storage. A direct-contact configuration for the heat exchanger is an attractive option for such a system. Eliminating heat transfer surfaces reduces the problem of strength limitations of these surfaces at high temperature and, thus, has the potential to reduce costs. Also, there has been considerable commercial experience with solid particles as a heat transfer medium using direct contact (Martin and Vitko 1982).

The subject of this report is the conceptual design and costing of a solid-particle/air direct-contact heat exchanger (DCHX). The objective of the study was to determine the economic and technical feasibility of a solid-particle/air heat exchanger to supply pressurized hot air to an industrial process or to a Brayton-cycle gas turbine. Economic feasibility is addressed by calculating the annual levelized cost of the DCHX per unit of thermal energy delivered. The calculation will be based on a cost methodology developed by the SERI Solar Energy Storage Program. A cost methodology from the Solar Thermal Technology Program will also be used to compare the cost of the DCHX to the Solar Thermal Program cost goal of $8.52/GJ ($9.00/10^6 Btu) for thermal energy delivered by a central receiver system. Technical feasibility is determined by evaluating the heat exchanger conceptual design parameters in light of state-of-the-art technology and commercially available equipment.
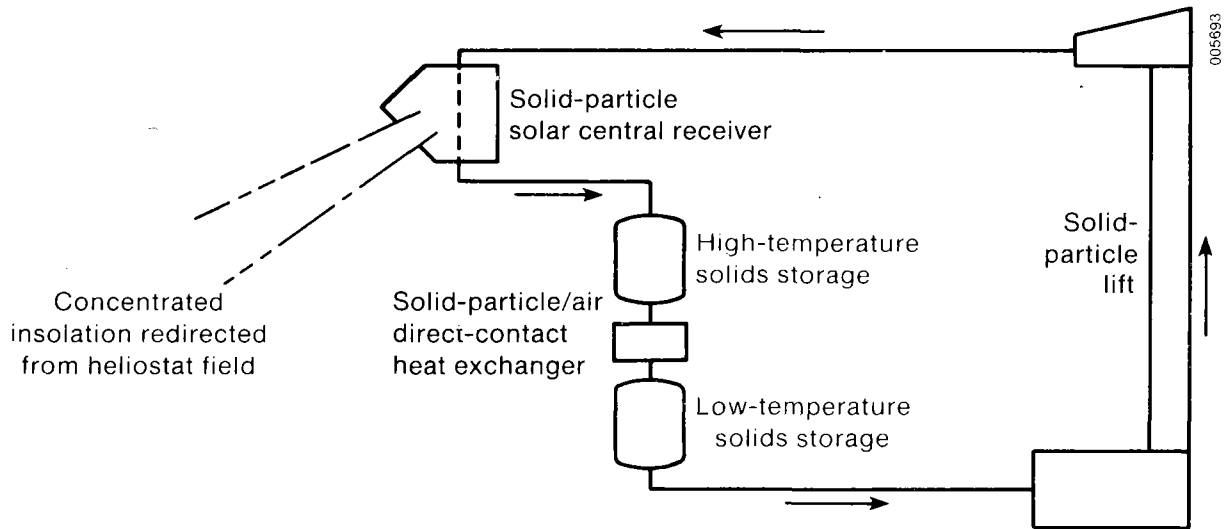
Figure 1-2. Solid-Particle Central Receiver System

We selected the following parameters for the study:

- 100-MW$_t$ capacity
- 1000°C solid-particle inlet temperature to DCHX
- 0.5-mm particle size
- Alumina particles
- 10 atm delivered air pressure
- Delivered air quality adequate for use in a gas turbine.

The complete heat exchanger system includes the apparatus to feed the particles into and out of the heat exchanger and to clean the outlet air stream. The compressor to supply air to the heat exchanger is not included, but the portion of the compressor operating cost attributable to pressure drop in the heat exchanger and the air cleaner is included. This is reasonable since, for a gas turbine application, the compressor is an integral part of the turbine. For an industrial process requiring pressurized hot air, a compressor is required regardless of the choice of heat exchanger.

In the following chapters, we will select a conceptual design of a DCHX system and size and cost the system using the parameters listed above. This design, referred to hereafter as the original configuration, will be based on the best information available on the state of the art of each of the technologies required by the design. We will also present the size and cost of a "best case" configuration for which we will assume progress in several technologies that will result from future development activities. Finally, we will evaluate a shell-and-tube design as an alternative to direct contact.

2.0 CONCEPTUAL DESIGN

The essential components of the DCHX system include the heat exchanger itself, feeders and defeeders to get the particles into and out of the high-pressure heat exchanger, and a separator to clean residual particles out of the heated air stream. We reviewed pertinent literature concerning possible designs and performance of each of these components. The results of this review are in the notes in Appendix B.

Figure 2-1 shows the specific components recommended for the DCHX as a result of this review. For each component, we selected a baseline design that offers the best performance and for which sufficient information exists to size and cost the component. In addition, we selected optional designs that hold promise for improved performance but for which additional information is needed to predict performance and cost. The baseline design for the feeder shown in Figure 2-1 is not the same as that given in Appendix B. The switch from a piston feeder to a lockhopper feeder was made after the initial review. Additional evaluation revealed that the lockhopper is the only design that is now technically feasible at 1000°C and that lockhopper operational costs caused by vent gas losses are smaller than originally thought.

Feeder			Air cleaner
Baseline: lockhopper			Baseline: staged cyclone
Option: inertial plug			Option: electrocyclone for last stage(s)
	Solid-particle/air direct-contact heat exchanger		Baseline: multistaged fluidized bed
			Option: falling bed
Defeeder			Compressor
Baseline: lockhopper			
Option: inertial plug			

005694
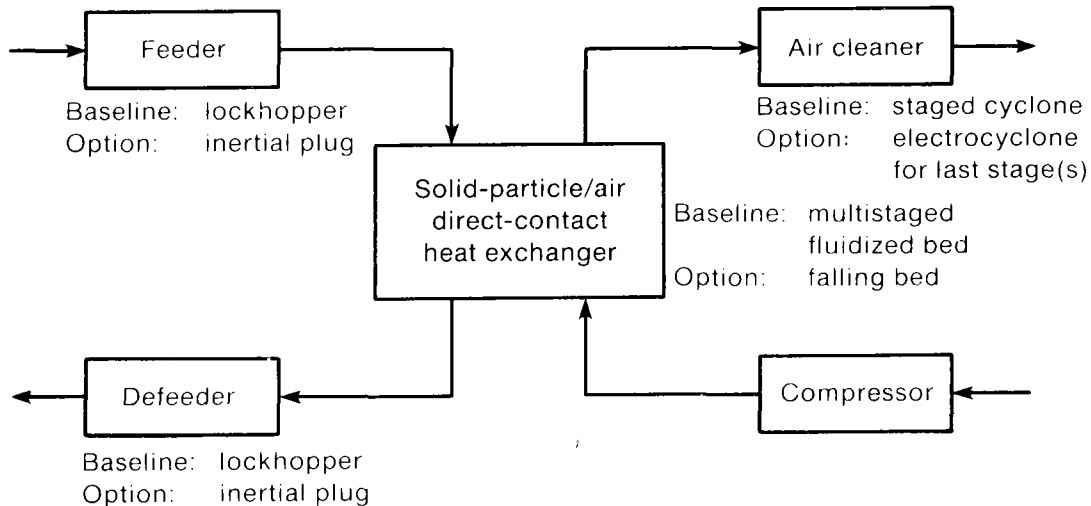
Figure 2-1. Direct-Contact Heat Exchanger Subsystems Baselines and Options to Be Explored

Once we selected the components, we completed a conceptual design of each. Figures 2-2 through 2-4 show these conceptual designs. The feeders, shown in Figure 2-2, include three lockhoppers that will be sized so that any two can deliver the required flow rate of particles. The third lockhopper can be off-line for valve repair. Isolation valves are located above and below each lockhopper for this purpose. The capability for valve repairs during operation was provided because we anticipated that frequent overhauls would be required for valves handling high-temperature solids. Buffer storage above and below the lockhoppers is provided because the flow to and from the lockhoppers is intermittent while the flows to the DCHX and from the solid-particle transport system are continuous. All of the vessels are constructed of carbon steel and have adequate internal insulation to keep the steel at 316°C as recommended in the ASME codes (Peters and Timmerhaus 1980).
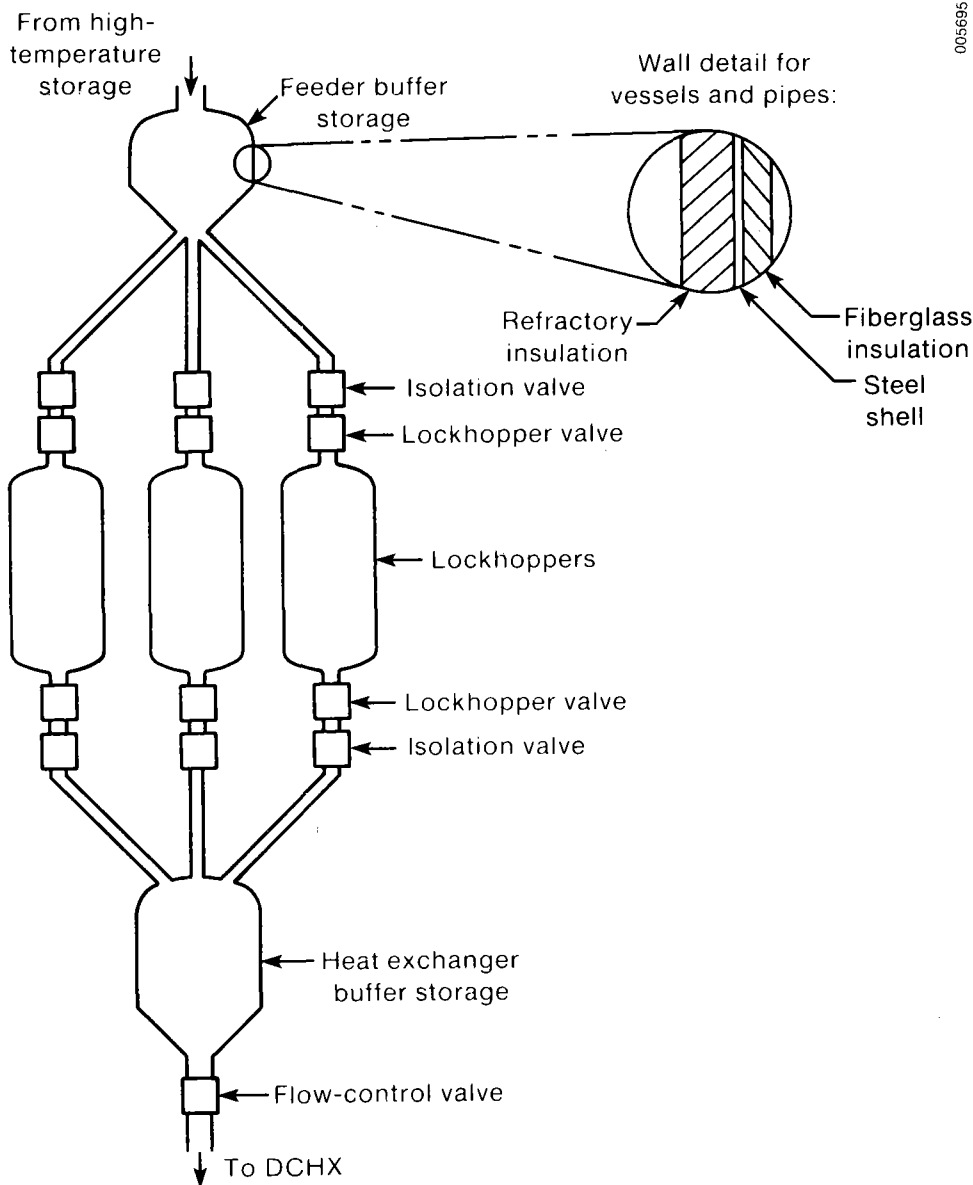
Figure 2-2. Solid-Particle Feeder Subsystem Schematic
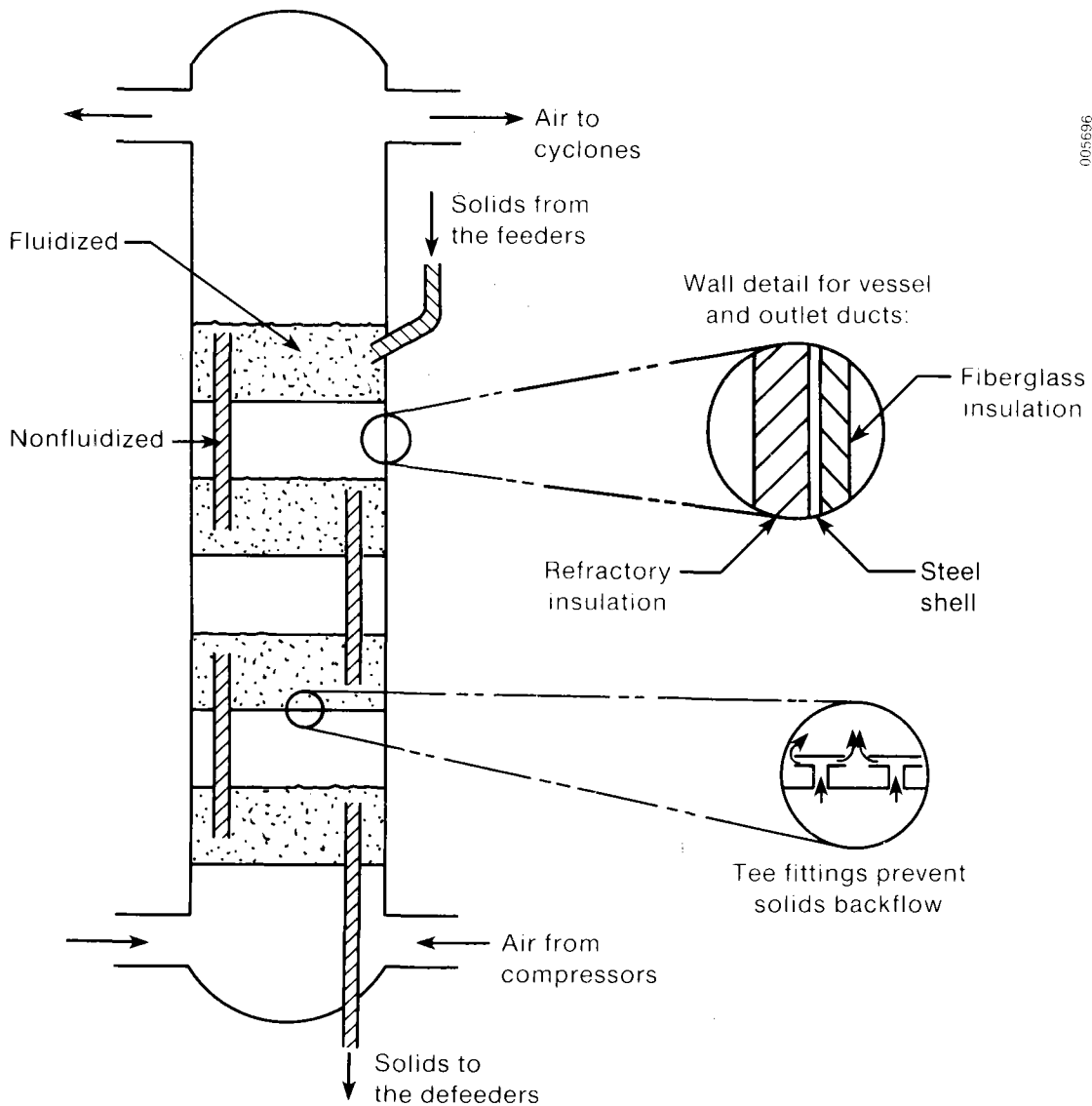
Figure 2-3. Direct-Contact Heat Exchanger Schematic

The defeeders are similar to the feeders. Their internal insulation is less thick than that of the feeders because the particles being handled have a lower temperature. Isolation valves are located above the defeeder lock-hoppers, but none are required below because the adjoining buffer storage is at atmospheric pressure. Also no flow-control valve is required.

Figure 2-3 shows the conceptual design of the DCHX. Although only one down-comer is shown between each stage, more than one might be required in a final design. Each grid (the air distributor and floor of the bed) is equipped with tee fittings as shown. These fittings leave an unfluidized layer of particles on the grid providing an insulating layer between the grid and the fluidized
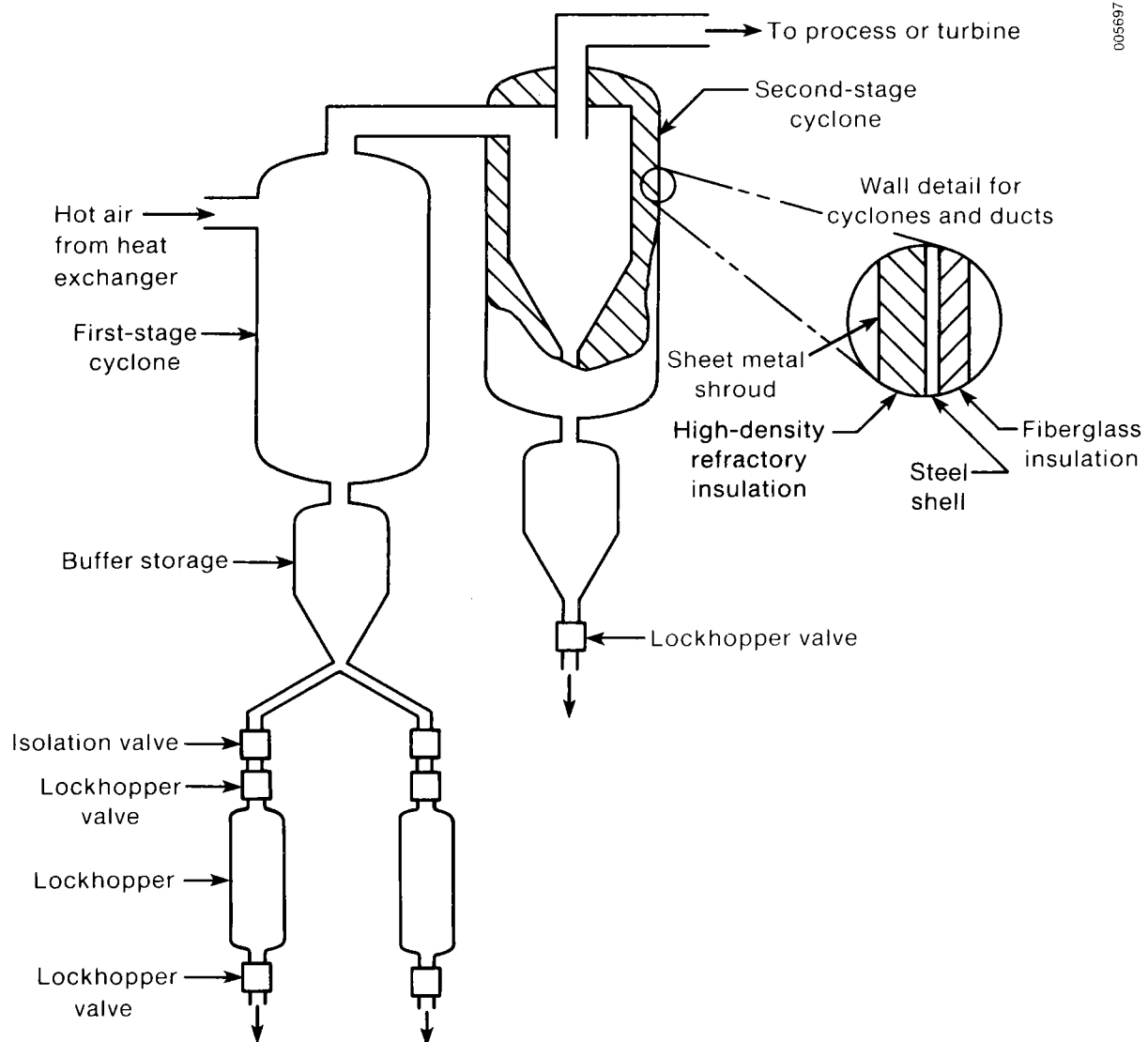
Figure 2-4. Hot Air Cleaning Subsystem Schematic

bed. This allows a lower operating temperature for the grid, which may be important in the uppermost and hottest bed. The fittings may also be used on the lower beds to prevent drain down when the heat exchanger is not in use. The actual number of stages will be specified once we have analyzed the performance of the heat exchanger. Space is allowed below the bottom stage as a manifold for the incoming air. Similarly, a space is provided above the top stage to disengage particles entrained from that stage.

The cyclones, as shown in Figure 2-4, will be contained in a cylindrical pressure vessel. The appropriate installation of internal insulation, as shown in the figure, gives the bottom of each cyclone its familiar conical shape. We will analyze cyclone performance to determine the actual number of stages and

7

the number of cyclones per stage. The outlet duct is internally insulated and internally shrouded to prevent particles of insulation from contaminating the cleaned air stream. Below the first-stage cyclone, there are two lockhoppers so that valves may be serviced during plant operation as described for the feeders. For the following stage (or stages), the collection rate of solid particles is very low so that the buffer storage can be drained once per day when the system is down and not at pressure.

3.0 COMPONENT DESIGN AND SIZING

3.1 Fluidized-Bed Heat Exchanger

3.1.1 Heat Transfer

Hydrodynamic requirements, rather than heat transfer requirements, determine the depth of the fluid bed stages. To demonstrate this, we will show that, because of the very large heat transfer surface area provided by the small particles, thermal equilibrium is reached for very short stage heights. Following this, we will develop a generalized method to predict the performance of a multistage fluidized bed.

Whitaker's (1972) correlation for packed beds estimates the heat transfer between the particles and the gas. This estimate will be compared to the rate of heat transfer expected in a fluidized bed.

$$\frac{hd_p}{k} = \frac{1-\varepsilon}{\varepsilon}\left(0.5\ Re_p^{0.5} + 0.2\ Re_p^{2/3}\right)Pr^{1/3} \ , \qquad (3\text{-}1)$$

where

h = heat transfer coefficient $(W/m^2\ K)$

d_p = particle diameter (m)

k = thermal conductivity of air $(W/m\ K)$

ε = void fraction.

The Prandtl number is defined as:

$$Pr = \frac{\mu c_{pa}}{k} \ , \qquad (3\text{-}2)$$

where

μ = air viscosity (Ns/m^2)

c_{pa} = specific heat of air $(J/kg\ K)$.

The Reynolds number for the particle is:

$$Re_p = \frac{\rho_a d_p u_s}{\mu} \ , \qquad (3\text{-}3)$$

where

ρ_a = air density (kg/m^3)

u_s = superficial gas velocity (m/s) .

The superficial gas velocity u_s is approximately 0.5 m/s for an 8-m diameter tower flowing 150-kg/s air (100-MW_t rating). For particle diameters of 0.5 mm and air properties of 20 atm at 1000 K, we obtain a particle Reynolds number of 37, which gives a heat transfer coefficient of 409 W/m^2 K. The surface area per unit volume is:

$$a = (1 - \varepsilon)\frac{6}{d_p} . \tag{3-4}$$

For a void fraction of 0.5, $a = 6000 \text{ m}^2/\text{m}^3$, so the volumetric heat transfer coefficient U_a is

$$U_a = ha \tag{3-5}$$

$$= 2.5 \times 10^6 \text{ W/m}^3 \text{ K} .$$

The volume per meter of height v of an 8-m diameter tower is 51.7 m^2. For a 10-stage heat exchanger with inlet temperatures of 300°C (air) and 1000°C (particles), a log mean temperature difference per stage will be approximately $\Delta T_{LM} = 35$°C. For a 10-MW_t per stage heat duty Q, the bed height H required for thermal equilibrium is:

$$H = 10^8 Q/U_a v \Delta T_{LM} \tag{3-6}$$

$$= 0.2 \text{ cm} .$$

Thus, very little bed height is required for the air entering the bottom of a stage to equilibrate with the particle temperature in the stage. The requirement for good fluidization and bubbling action in the bed, not heat transfer requirements, will determine the bed height.

Since the air rapidly equilibrates with the particle temperature, we equate the air outlet temperature for stage n, $T_{ao,n}$, with the average particle temperature for stage n (see Figure 3-1):

$$T_{ao,n} = \overline{T}_{s,n} . \tag{3-7}$$

Neglecting radiative heat transfer and wall losses, a thermal balance on stage n gives:

$$\dot{m}_s c_{ps}(\overline{T}_{s,n+1} - \overline{T}_{s,n}) = \dot{m}_a c_{pa}(T_{ao,n} - T_{ai,n}) , \tag{3-8}$$

where

$\dot{m}_s$ = mass flow rate of solid particles (kg/s)

$\dot{m}_a$ = mass flow rate of air (kg/s)

c_{ps} = specific heat of solid particles (J/kg K)

$T_{ai,n}$ = air inlet temperature for stage n (K).

Since $T_{ai,n} = T_{ao,n-1} = \overline{T}_{s,n-1}$ and $\gamma = \dot{m}_a c_{pa}/\dot{m}_s c_{ps}$,

$$\overline{T}_{s,n+1} - \overline{T}_{s,n} = \gamma(\overline{T}_{s,n} - \overline{T}_{s,n-1}) , \tag{3-9}$$

or

$$\overline{T}_{s,n-1} = \frac{(1 + \gamma)\overline{T}_{s,n} - \overline{T}_{s,n+1}}{\gamma} . \qquad (3\text{-}10)$$

The stage-to-stage drop in particle temperature is:

$$\Delta T_{s,n} \equiv \overline{T}_{s,n+1} - \overline{T}_{s,n} = \gamma(\overline{T}_{s,n} - \overline{T}_{s,n-1}) . \qquad (3\text{-}11)$$

This temperature drop decreases by a factor of γ for each stage. At the top of a heat exchanger with N stages (see Figure 3-2),

$$\Delta T_{s,N-1} \equiv \overline{T}_{s,N} - \overline{T}_{s,N-1} , \qquad (3\text{-}12)$$

but $\overline{T}_{s,N} = T_{ao}$. So from Equation 3-10,

$$\overline{T}_{s,N-1} = \frac{(1 + \gamma)\overline{T}_{s,N} - \overline{T}_{s,N+1}}{\gamma} = \frac{(1 + \gamma)T_{ao} - T_{si}}{\gamma} , \qquad (3\text{-}13)$$

and

$$\begin{aligned}
\Delta T_{s,N-1} &= T_{ao} - \frac{(1 + \gamma)T_{ao} - T_{si}}{\gamma} \\
&= \frac{T_{si} - T_{ao}}{\gamma} . \qquad (3\text{-}14)
\end{aligned}$$
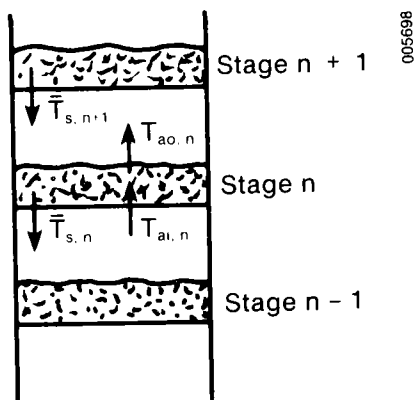
Figure 3-1. Notation for Solid-Particle and Air Temperatures in a Multistage Fluidized Bed
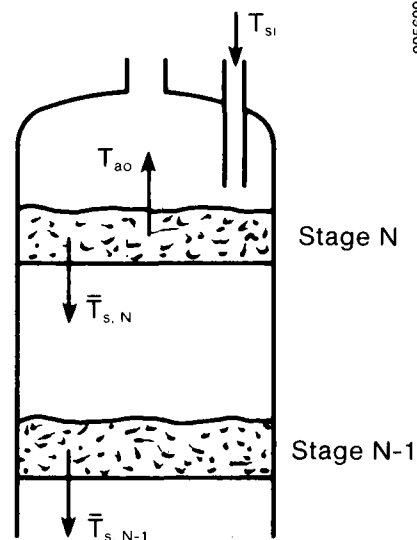
Figure 3-2. Notation for Solid-Particle and Air Temperatures at the Top of a Multistage Fluidized Bed

From Eq. 3-14, $\Delta T_{s,N} = (T_{si} - T_{ao})$, therefore

$$\Delta T_{sn} = \frac{T_{si} - T_{ao}}{\gamma^{N-n}} \, . \tag{3-15}$$

The overall swing in particle temperature is:

$$T_{si} - T_{so} = \sum \Delta T_{sn} = (T_{si} - T_{ao}) \sum_{n=1}^{N} \gamma^{n-N} \, . \tag{3-16}$$

Define x as:

$$x = \sum_{n=1}^{N} \gamma^{n-N} \, , \tag{3-17}$$

which expands into:

$$x = \frac{\gamma(\gamma^{-N} - 1)}{(1 - \gamma)} \, ,$$

so

$$T_{si} - T_{so} = x(T_{si} - T_{ao}) = \gamma(T_{ao} - T_{ai}) \, . \tag{3-18}$$

Finally, the outlet temperatures are:

$$T_{ao} = \frac{x T_{si} + \gamma T_{ai}}{\gamma + x} \tag{3-19}$$

$$T_{so} = \frac{T_{si}(\gamma + x - \gamma x) + \gamma x T_{ai}}{\gamma + x} \, . \tag{3-20}$$

Defining the heat exchanger efficiencies on the air and particle sides:

$$\eta_a \equiv \frac{T_{ao} - T_{ai}}{T_{si} - T_{ai}} = \frac{x}{\gamma + x} \tag{3-21}$$

$$\eta_s \equiv \frac{T_{si} - T_{so}}{T_{si} - T_{ai}} = \frac{\gamma x}{\gamma + x} \, . \tag{3-22}$$

The efficiency therefore depends only on γ and the number of stages. Figure 3-3 plots values of η_a for five values of γ versus the number of stages. Figure 3-4 is a similar plot for η_s.

This analysis does not account for two possible modes of heat transfer between stages. The first is radiation heat transfer between stages. The second is carryover of particles from a given stage into the stage above due to entrainment in the air stream. These modes of heat transfer are, in effect, thermal back mixing between adjacent stages. This back mixing will affect heat exchanger performance only to the extent that it reduces the temperature of the top stage and, thus, reduces T_{ao}. We will show later that the temperature difference between the top two stages is small. Thus, the radiant back mixing
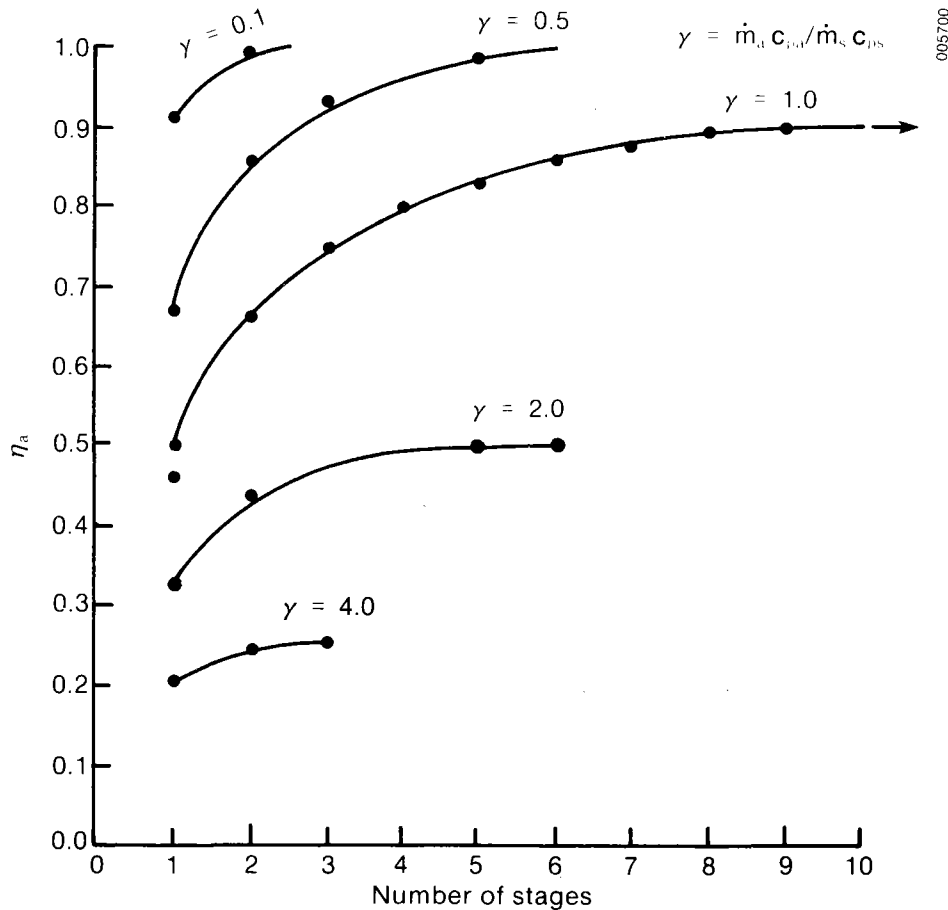
Figure 3-3. Heat Exchanger Air-Side Efficiency versus Number of Stages

is small and can be ignored. As for the entrained particles, only those few that hit the holes in the grid above pass through to the stage above while the rest strike the grid itself and fall back. Because so few particles are carried over, the thermal back mixing is small.

For this study, we selected a four-stage heat exchanger with an outlet air temperature of $970^{\circ}C$. Table 3-1 summarizes the operating conditions for this heat exchanger. Because C_{pa} very nearly equals C_{ps}, γ can be expressed as the ratio of mass flow rates, $\dot{m}_a/\dot{m}_s$. , The height and diameter of the heat exchanger and the pressure drop will be determined in the following section based on the design of the fluidized beds.
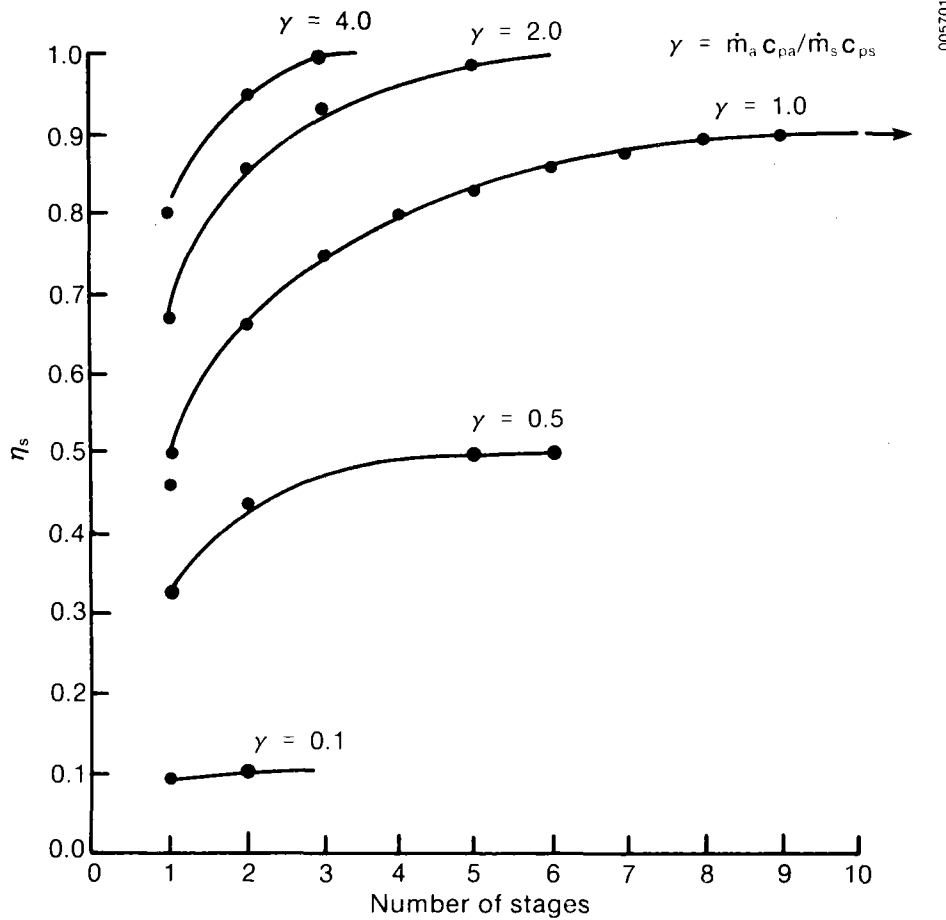
Figure 3-4. **Heat Exchanger Particle-Side Efficiency versus Number of Stages**

3.1.2 Fluidized-Bed Design

When the velocity of a gas passing upward through a bed of particles is gradually increased, the bed is first fluidized and then begins to bubble (see Figure 3-5). The minimum velocity for fluidization, u_{mf}(cm/s), given by Kunii and Levenspiel (1977), is:

$$\frac{1.75}{\phi_s \epsilon_{mf}^3}\left(\frac{d_s u_{mf} \rho_a}{\mu}\right)^2 + \frac{150(1-\epsilon_{mf})}{\phi_s^2 \epsilon_{mf}^3}\left(\frac{d_s u_{mf}\rho_a}{\mu}\right) = \frac{d_s^3 \rho_a(\rho_s - \rho_a)g}{\mu^2} \quad , \quad (3-23)$$

Table 3-1. Operating Parameters of a Four-Stage Fluidized-Bed Heat Exchanger

Outlet pressure = 10 atm

Heat rate $\quad$ = 100 MW$_t$

$\gamma = \dot{m}_a/\dot{m}_s \quad$ = 0.51

$\dot{m}_a \quad$ = 111 kg/s

$\dot{m}_s \quad$ = 217 kg/s

$d_{sh} \quad$ = 7.15 m

	T_s ($^{\circ}$C)	T_a ($^{\circ}$C)	u_o (cm/s)
Inlet	1000	150	--
First stage (top stage)	581	581	67.2
Second stage	801	801	84.5
Third stage	914	914	93.4
Fourth stage (bottom stage)	971	971	97.9
Outlet	581	971	--
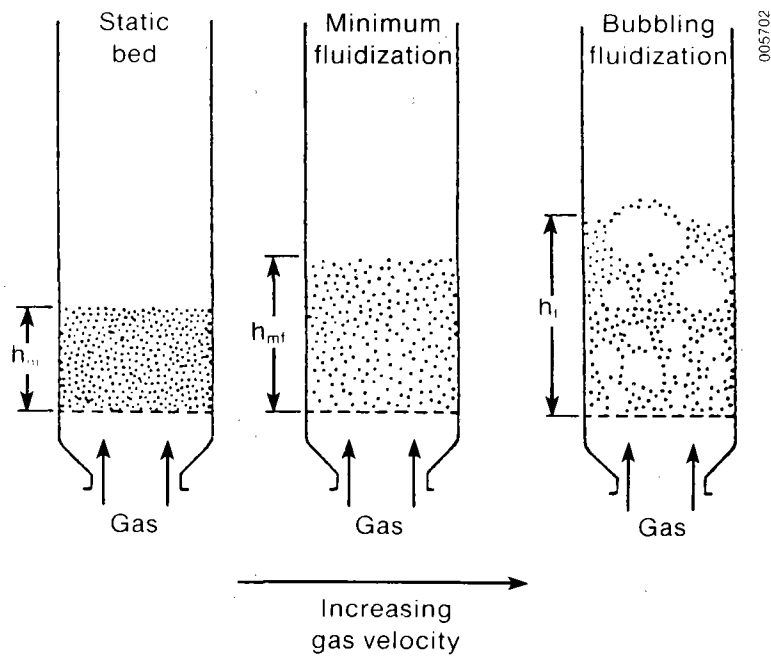
Figure 3-5. Minimum and Bubbling Fluidization

where

ϕ_s = particle sphericity

ε_{mf} = bed voidage at minimum fluidization

d_s = particle diameter (cm)

ρ_s = particle density (g/cm^3)

ρ_a = air density (g/cm^3)

μ = air viscosity (g/cm s)

g = 981 cm/s^2.

We assumed values of ε_{mf} = 0.5 and ϕ_s = 0.9. (Particle sphericity is defined as the volume of the particle divided by the volume of a sphere having the same surface area as the particle.) From Section 1.0, d_s = 0.5 mm and ρ_s = 4 g/cm^3 for alumina. For a vigorously bubbling bed, Kunii and Levenspiel recommend that the operating air velocity u_o be at least twice the minimum fluidization velocity. Vigorous bubbling ensures good mixing and, thus, a uniform temperature in the bed. Kunii and Levenspiel also note that, for stable operation, u_o should be less than one-third of the particle terminal velocity u_t (cm/s):

$$u_t = \left[\frac{4gd_s(\rho_s - \rho_a)}{3\rho_a C_d} \right]^{1/2} , \qquad (3\text{-}24)$$

where the drag coefficient $C_d = 10/\text{Re}^{1/2}$ and:

$$\text{Re} = \frac{d_s \rho_a u_t}{\mu} . \qquad (3\text{-}25)$$

We determined velocities in the heat exchanger by setting the velocity at the top stage to $1/3$ u_t and checking the lower stages to verify that the bubbling criteria $u_o = 2u_{mf}$ was met for each stage. The cross-sectional area of the heat exchanger was held constant for all stages. We then calculated the heat exchanger diameter of 7.15 m given the mass flow rate of air and the air velocity and density for the first stage.

Figure 3-6 is a schematic of the four-stage fluidized bed heat exchanger. The height of the heat exchanger is the sum of the transport disengaging height (TDH), the heights of the beds, the interstage gaps (IG), and the air inlet manifold (M). The TDH is an empty space above the uppermost bed of the heat exchanger. This height allows particles that have been thrown out of the bed by bubbles bursting at the surface to disengage from the air stream and fall back into the bed. The TDH is defined as the height at which the rate of decrease of entrainment of particles in the air stream approaches zero. Placing the outlets to the cyclones above TDH ensures that the air entering the cyclones has the least possible particle loading.

Bed height should be kept small since it does not affect the heat transfer but does influence the size of the heat exchanger. Ideally, experiments with the particles in question would determine the minimum stable operating height of the bed as well as the bed expansion during fluidization. The literature offers little guidance as to these quantities and none for the pressures and particles under consideration. A static bed depth h_m = 0.305 m (1 ft) and an

Figure 3-6. **Schematic Layout of Multistage Fluidized-Bed Heat Exchanger**
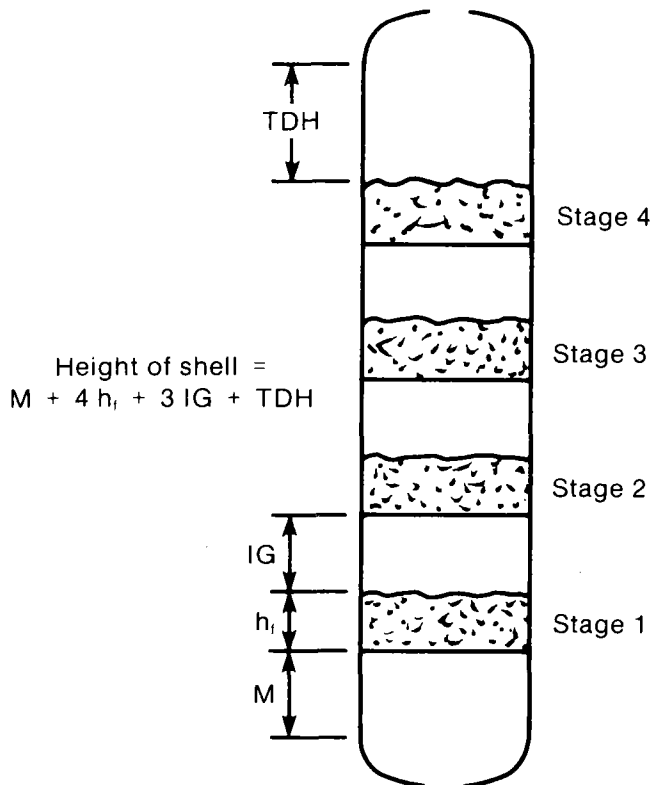
operating bed depth h_f = 0.61 m (2 ft) were assumed. This operating height should be adequate to provide stable operation of the beds without making the heat exchanger excessively tall.

We assumed that the interstage gap was equal to the operating bed depth, which allows clearance between the bed and the grid above as the bed height fluctuates during operation. We allowed a height of 1 m for the air inlet manifold. Zenz (1983) correlates TDH with superficial velocity $u_s = u_o - u_{mf}$ and bubble diameter. Assuming a bubble diameter of 15.24 cm (6 in.) and given a superficial velocity of 74 cm/s, the TDH is 1.52 m. Using the equation in Figure 3-6, total height of the heat exchanger shell h_{sh}(m) is:

$$h_{sh} = 1 + (4 \times 0.61) + (3 \times 0.61)$$

$$+ 1.52 = 6.8 \text{ m} . \qquad (3-26)$$

The pressure drop in a fluidized bed must include the drop in the bed and the drop through the grid. The pressure drop in the bed P_b(N/m^2) is simply the weight per unit area of particles in the bed:

$$P_b = h_m(1 - \epsilon_m)\rho_s g/10 ,$$

where ϵ_m is the void fraction in the static bed. A pressure drop in each grid of at least 30% of the drop in the bed is recommended for air distribution to all parts of the grid (Zenz 1982). Thus, the pressure drop in the multistage fluidized-bed heat exchanger P_t is:

$$P_t = 1.3 \times 4 \times P_b = 37,340 \text{ N/m}^2 .$$

Entrance and exit losses to and from the heat exchanger have not been included.

3.1.3 Vessel Design

The heat exchanger is essentially an internally insulated pressure vessel with 2:1 ellipsoidal heads. Given the required height and diameter of the heat exchanger from the previous sections, we now can size the vessel.

To determine the required inner diameter of the shell, we must first calculate the thickness of the internal insulation. Ceramic firebrick was chosen for the internal insulation because it provides a rigid, durable inner wall for the vessel. The ceramic firebrick has a thermal conductivity k_1 of 0.17 W/m K and a cost of $809/m^3 (Bohn 1983). The heat lost through 1 m^2 of this insulation is:

$$q = k_1 \Delta T / t_1 , \tag{3-27}$$

where

q = heat loss (W/m^2)

ΔT = temperature difference (K)

t_1 = thickness of internal insulation (m).

The temperature difference is 684 K, which is the particle inlet temperature, 1000°C, minus the shell temperature 316 K. Assuming a cost of $9/GJ for thermal energy, the value of the heat lost at a rate of 1 kW over a year (350 days of operation) is $272. Over a 30-year life, the value of this heat loss will be $272 times the present worth factor 9.427 (30 years, 10% interest), or $2566/kW. Thus, the total cost of the insulation plus the cost of the lost heat C_t is:

$$C_t = t_1 \ \$809/m + \$2566/kW . \tag{3-28}$$

This equation was differentiated and set to zero, $dC_t/dt_1 = 0$, and solved for t_1 giving a thickness of 0.6 m. Thus, the required shell diameter d_{sh} is the heat exchanger diameter plus twice the insulation thickness, or 8.35 m.

Peters and Timmerhaus (1980) give the required thickness of the shell t_{sh} (cm) of a pressure vessel.

$$t_{sh} = 2.54 \left[P d_{sh}/(2 \ SE_j - 1.2 \ P) + C_c \right] , \tag{3-29}$$

where

P = internal pressure (psig)

d_{sh} = diameter of shell (in.)

S = maximum allowable stress (13,700 psi at 650°F)

E_j = joint efficiency = 1

C_c = corrosion allowance = 0.125 in.

We assumed the same thickness for the heads, a reasonable approximation when P is much less than S. The weight of the shell is given by:

$$W_{sh} = \rho_{cs} \pi h_{sh} \left[(t_{sh} d_{sh}/100) + (t_{sh}^2/10,000) \right] , \tag{3-30}$$

where

W_{sh} = weight of the shell (kg)

ρ_{cs} = density of carbon steel (7833 kg/m^3)

h_{sh} = height of shell (m)

d_{sh} = inner diameter of shell (m).

The weight of an ellipsoidal head is given by:

$$W_h = \rho_{cs} \pi t_{sh} (1.23\ d_{sh} + t_{sh}/100)^2/4 \ , \qquad (3-31)$$

where

W_h = weight of head (kg).

The total weight of the heat exchanger vessel W_t (kg), including an additional 20% for nozzles, manholes, etc., is:

$$W_t = 1.2(W_{sh} + 2\ W_h) \ . \qquad (3-32)$$

The capital cost of the vessel is based on this total weight plus the cost of insulation, both internal and external, and the cost of the grids for the fluidized beds. In the following section on costs, the grids will be treated as bubble cap trays using the cost method given by Peters and Timmerhaus (1980).

The cost of the insulation is based on the volume required. Equations for calculating these volumes are taken from Peters and Timmerhaus (1980). The volume of internal insulation required for the shell V_{1sh} (m^3) will be:

$$V_{1sh} = \pi h_{sh}(t_1 d_{sh} + t_1^2) \ . \qquad (3-33)$$

The volume required for an ellipsoidal head V_{1h} (m^3) is:

$$V_{1h} = \pi t_1 (1.23\ d_{sh} + t_1)^2/\ 4 \ . \qquad (3-34)$$

The total volume of internal insulation V_1 (m^3) is:

$$V_1 = V_{1sh} + 2\ V_{1h} \ . \qquad (3-35)$$

To find the thickness of external insulation, the heat flux through the wall of the vessel is calculated:

$$q = k_1 \Delta T/t_1 \ , \qquad (3-36)$$

where

q = heat flux (W/m^2)

ΔT = temperature difference ($684^o C$).

We then use this flux to calculate the required thickness of the external fiberglass insulation t_2 (m):

$$t_2 = k_2 \Delta T/q \ . \qquad (3-37)$$

The temperature difference, ΔT, for this calculation was the shell temperature, $316^o C$, minus the ambient temperature, $30^o C$. The thermal conductivity of the fiberglass insulation k_1 was assumed to be 0.4 W/m K. We calculated a

value of 0.05 m for t_2. We calculated the total volume of the external insulation using the same equations as for the internal insulation.

For the aluminum lagging, we calculated the required surface area A_1 (m^2) as follows:

$$A_1 = \pi h_{sh} d + 2.17 \, d^2 , \qquad\qquad (3\text{-}38)$$

where $d = d_{sh} + 2(t_2 + t_{sh}/100)$.

Figure 3-7 shows the major dimensions and the stage temperatures for the heat exchanger.
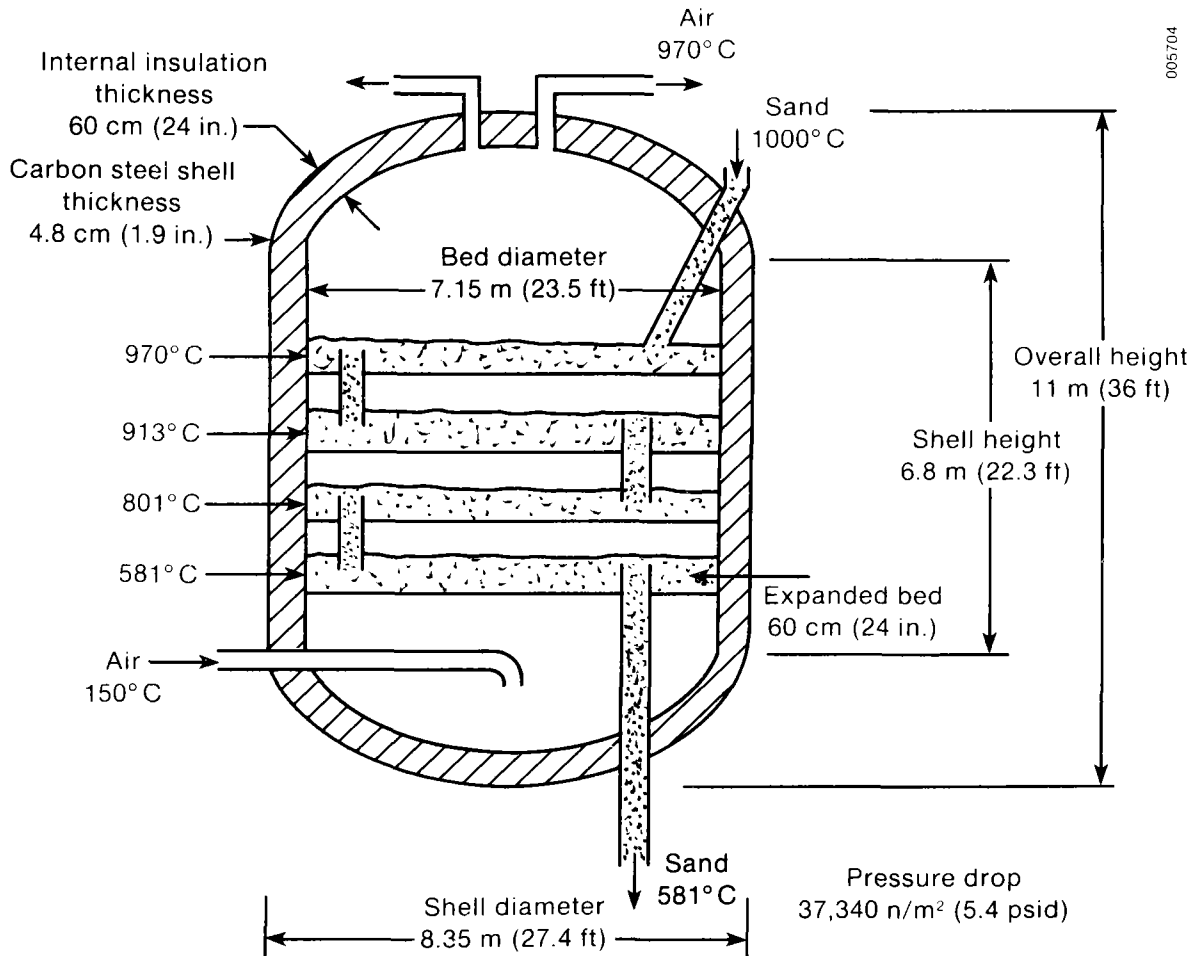
Figure 3-7. Schematic of Four-Stage Fluidized Bed

3.2 Feeders and Defeeders

The lockhoppers and buffer storage vessels are pressure vessels with internal insulation. They each have a shell with an aspect ratio of 2:1, height to diameter, and the heads are 2:1 ellipsoidal heads. The feeder lockhoppers go through a four-stage cycle. First, the upper valve is opened and the lockhopper is filled with hot particles. Next, the upper valve is closed and the lockhopper is pressurized. Third, the bottom valve is opened and the particles are discharged. And fourth, the bottom valve is closed and the lockhopper is depressurized. The defeeder lockhopper cycle is similar except the discharge step is at ambient pressure.

There is a trade-off between lockhopper size and the number of cycles required per unit time. We prefer that a low cycle rate be used to reduce wear on the lockhopper valves. We chose a 15-minute cycle time to determine the required lockhopper volume, which results in 4 valve cycles per hour and 40 cycles for a 10-hour day. We further assumed that 45% of the cycle time was for charging, 45% was for discharging, and the remaining 10% was for cycling of valves and pressurization or depressurization. As mentioned in Section 2.0, two lockhoppers handle the required particle flow in both the feeder and defeeder; the spare lockhoppers are available for valve maintenance or simply held in reserve.

Using these assumptions and the particle volumetric flow rate, we determined the valve size and lockhopper volume. The mass flow rate of 217.4 kg/s was given in the previous section. Alumina particles have a particle density of 4 g/cm^3. Assuming a void fraction ε_m of 0.4, the particle bulk density is 2.4 g/cm^3 and the volumetric flow rate is 0.09 m^3/s. The lockhopper valves must be oversized by 10% to pass one-half the required flow rate while open only 45% of the time. The lockhopper volume must be sufficient to accept this flow rate of particles for 45% of 15 minutes, or 6.75 minutes. The feeder and defeeder buffer storage vessels are sized for twice the volume needed to contain the 0.14 m^3/s flow for 1.5 minutes (10% of 15 minutes).

We applied similar assumptions to the cyclone defeeders. The particle flow rate from the first-stage cyclone was assumed to be 1% of the heat exchanger flow rate. For the second-stage cyclone, a particle flow rate of 0.025% of the heat exchanger flow rate was assumed. These flow rates are generous and will lead to adequate defeeder capacity regardless of cyclone performance. Only one of the first-stage cyclone lockhoppers is used at any time. The second is held in reserve. Thus, these lockhoppers are the same size as the first-stage buffer storage vessel. The second-stage buffer storage vessel must be sized so that it need only be emptied once per 10-hour day. We found a vessel identical in size to the first-stage vessels to be adequate.

We assumed that the required volume for all of these vessels was contained within the shell alone. The heads add less than 20% additional volume, which will be allowed as ullage. We used the same methods as in the previous section on the heat exchanger to determine the thickness and volume of insulation

and the size and weight of the various vessels required for the feeders and defeeders. The only difference is that less insulation is required in the defeeders because of their lower operating temperature of 580°C. Using the same method described previously to calculate the most economical thickness of insulation, the internal insulation thickness for the defeeders is 37 cm and the thickness of external insulation is 12 cm. Table 3-2 gives the major dimensions and weight of each of the vessels.

In some lockhopper applications, vent gas losses are a significant operating cost. For the DCHX, the volume of gas lost in the operation of the feeders and defeeders is approximately the same as the volumetric flow rate of solids. The volumetric flow rate of air through the heat exchanger is over 100 times larger than the volumetric flow rate of solids. Thus, the vent gas losses are small and no accounting of them is made in this analysis.
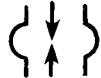
3.3 Lockhopper Valves

Table 3-3 summarizes the service conditions for the lockhopper valves required for the DCHX. These valves must handle high-temperature abrasive solids while providing a pneumatic seal for the lockhoppers. Table 3-4 shows the relative hardness of various solids media and valve materials. The hardness of alumina relative to that of the alloys indicates the problem of abrasion in this type of valve. The ceramic materials that have the required hardness are not commonly used in commercially available valves. The capability of a valve in this type of service can be expressed as some combination of the three interrelated parameters of temperature, pressure, and life time (number of cycles before service is required to maintain acceptable leak rates).

Table 3-2. Dimensions and Weights of the Feeder and Defeeder Vessels

Vessel	Operating Pressure (atm)	Quantity	Shell Diameter (m)	Overall Height (m)	Weight (kg)
Feeder buffer storage	1	1	3.4	6.0	6,280
Feeder lockhoppers	10	3	4.2	8.0	28,800
DCHX buffer storage	10	1	3.4	6.0	14,920
Defeeder buffer storage	10	1	2.9	5.8	10,820
Defeeder lockhoppers	10	3	3.7	7.8	22,240
Cyclone lockhoppers and buffer storage	10	4	1.8	2.2	1,930

SERI ◉

Table 3-3. Lockhopper Valve Service Conditions

Application	Configuration	Temperature of Solid Particles ($^{\circ}$C [$^{\circ}$F])	Pressure (atm)
Feeders to DCHX	solids flow / pressure	1000 (1830)	10
Defeeders from DCHX	pressure / solids flow	600 (1100)	10
Defeeders from cyclones	pressure / solids flow	1000 (1830)	10

The DOE Morgantown Energy Technology Center began a program in 1976 to test state-of-the-art lockhopper valves and to develop prototype valves capable of operating under more severe conditions than the state-of-the-art valves. Their assessment of the capabilities of state-of-the-art valves as of 1982 was 15,000 cycles at 1.38×10^6 N/m^2 (200 psi) and 540°C (1000°F) (DOE 1983). Prototype valves were tested at much higher pressures and temperatures with materials such as silicon carbide and alumina. The final report on those tests is due in 1985.

Discussions with representatives of valve companies reveal similar assessments of the state of the art (personal communications with Kamyr-Neles Inc., Mogas Industries Inc., and Everlasting Valve Co.). Temperature limits of 650° to 760°C (1200° to 1400°F) are considered reasonable for solids-handling valves. Valve seat materials are commonly noted as a limiting factor. Valves have been supplied to the petroleum industry for handling alumina-based catalysts at high temperature and pressure. Costs in the range of \$35,000 to \$65,000 for 6-in. valves were suggested as typical for this type of application.

The valves required for the DCHX defeeder lockhoppers can be considered state of the art. Valves for the feeders and cyclone defeeders will require development but appear to be feasible. The valves are sized according to the equation given by Zenz (1962) for the flow of solids into an orifice:

$$W_s = 1.2 \, \rho_s D^{1/2} \, , \qquad (3-39)$$

where

ρ_s = solids bulk density (lb/ft^3)

Table 3-4. Relative Hardness of Solids Media and Hard-Facing Materials

Material	Equivalent Vickers Hardness Number (VHN)
Solids media	
Coal[a]	<40
Limestone	110 – 130
Dolomite	130 – 150
Fused ash	800 – 2000
Aluminum oxide	1800 – 2100
Hard-facing alloys	
316 Stainless steel	160 – 290
Stellite No. 6	400
Stellite No. 1	580
Haynes No. 40	630
Tribaloy T-800	650
METCO 19-E	600 – 700
Cermet and ceramic materials	
Silicon nitride	1400
Tungsten carbide	1600 – 1750
Silicon carbide	1900 – 3300
Boron carbide	3000
Tungsten titanium diboride over tungsten carbide (TMT-745)	≅5000

[a]This is for carbonaceous material and is not representative of siliceous and other common mineral inclusions. The hardness on these ranges from 100 to over 1000.

Source: DOE 1983.

D = orifice diameter (in.)

W_s = solids efflux rate (lb/s ft^2).

Valve sizes have all been rounded to the next largest even size in inches according to standard industry practice. Based on the particle flow rates determined above, the feeder and defeeder lockhopper valves and the flow control valve are all 12-in. valves while 2-in. valves are needed for the cyclone defeeder.

3.4 Cyclones

This section describes the method used to calculate the performance of the cyclones that remove small particles from the fluidized-bed heat exchanger outlet air before the air passes to a turbine or an industrial process.

First, we must describe the particles leaving the fluidized bed. As a base-line, we have chosen a nominal particle size of 500 μm in the bed itself. We assume that through attrition, these particles will be ground down producing a distribution of smaller particles. The largest of these particles will remain in the fluidized bed because the operating gas velocity is chosen somewhat below the terminal velocity of 500 μm particles. Smaller particles will be carried over into the exhaust stream and must be removed before leaving the system. For example, if the bed operates at 10 atm, the terminal velocity for the 500-μm particles is 269 cm/s (assuming a particle density of 4 g/cm^3). Under these conditions the minimum fluidization velocity is 36 cm/s, and if we choose an operating velocity three times the minimum fluidization velocity we get 108 cm/s. The particle diameter for which 108 cm/s is a terminal velocity is approximately 200 μm; that is, particles smaller than about 200 μm will be carried out of the fluidized bed at an operating velocity of 108 cm/s. Larger particles will remain in the fluidized bed.

There is no sure way of predicting the loading and size distribution of fines that might be generated in a central receiver plant. Clearly the probability of a particle existing should increase with the particle diameter since we assume that the small particles result from grinding of larger particles. A simple particle-size distribution that satisfies this criterion is the Gates-Gaudin-Schumann distribution, which is:

$$\log L = b + a \log d , \tag{3-40}$$

where L is the quantity of particles with diameters less than d in parts per million (ppm) of mass. We can determine the constants a and b from the largest diameter in the sample and, for example, the diameter below which 1% of the mass exists. In the overall system analysis, we will let the largest particle diameter entering the cyclone be determined by the fluidized bed operating velocity, as calculated above. We will arbitrarily set the 1% point at 1 μm.

Lastly, we must choose the total loading of particles elutriated from the fluidized bed. For the study, we assume that 1% (10,000 ppm) of the total particle flow is carried over into the cyclones. This is surely a worst case since in 100 passes through the DCHX, a mass of particles equivalent to the entire plant inventory would be carried into the cyclones. The assumed dis-tribution of elutriated particles is a straight line on a log-log plot, as shown in Figure 3-8.

Next, we must prescribe the desired exit air quality in terms of particle loading. The best analysis of the state of the art of turbine technology is that of Boericke et al. (1980) based on turbine tests with various dusty gases. They recommend keeping the total loading below 100 ppm (based on the mass of the air flow) with 98% of the particles smaller than 10 μm.

A cyclone removes particles from gas streams by centrifugal force. The particle-laden gas stream enters a cylindrical vessel tangentially and the particles are thrown to the outer wall by centrifugal force, slide down the wall, and are collected by a conical bottom. The gas exits through a central opening in the top of the cyclone. Figure 3-9 shows a cyclone with typical dimensional ratios. Since centrifugal force is the separation mechanism, larger particles are more efficiently removed from the gas stream than are
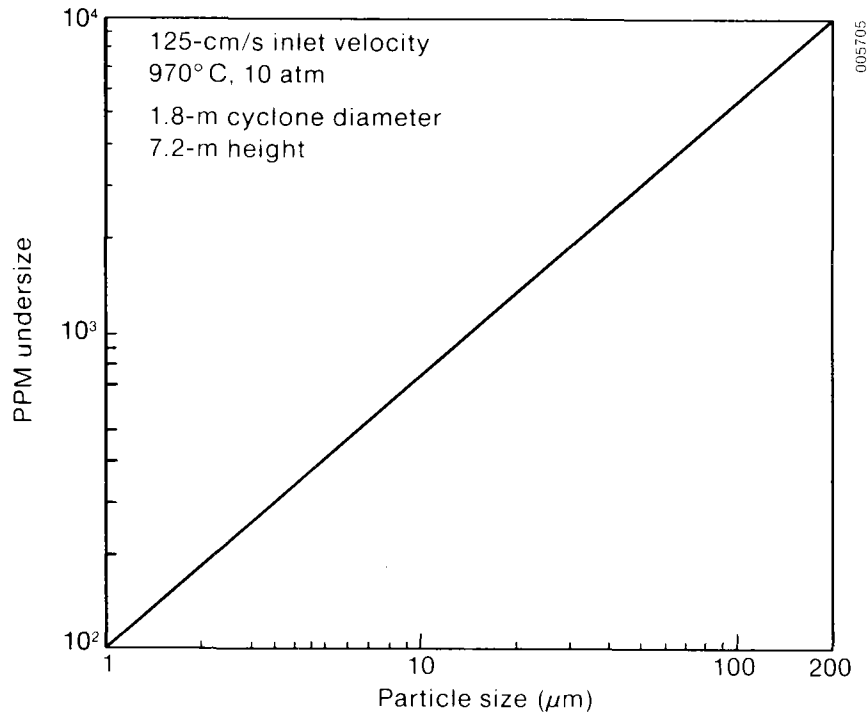
Figure 3-8. **Size Distribution of Particles Carried over from the DCHX Expressed as ppm of the Total Mass Flow Rate of Solids**
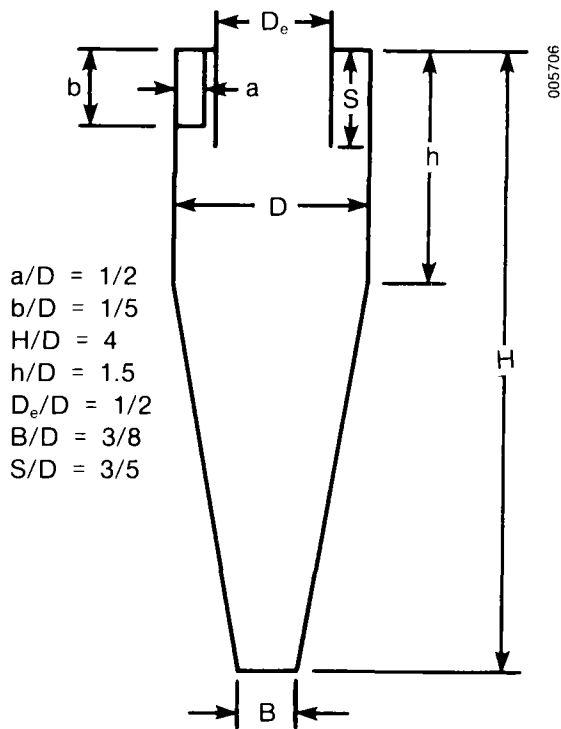
Figure 3-9. **Cyclone with Typical Dimensional Ratios**

a/D = 1/2
b/D = 1/5
H/D = 4
h/D = 1.5
D_e/D = 1/2
B/D = 3/8
S/D = 3/5

smaller particles. Other mechanisms are apparently at work at the high pressure and temperature at which these cyclones operate. As shown by Parker et al. (1981), classical cyclone efficiency correlations fail at high pressure and temperature. Typically, high pressure increases cyclone efficiency and high temperature reduces cyclone efficiency. Parker has developed a correlation based on high-pressure and high-temperature data (pressure up to 20 atm and temperature up to 693°C) in a 15-cm diameter cyclone, and it is upon this correlation that we will base our cyclone efficiency. Some of the data presented by Parker suggest that cyclone efficiency is reduced by increasing the cyclone size, but at the present time there is no way to estimate this effect. This presents one source of uncertainty in using Parker's correlation.

The Parker correlation, Figure 3-10, presents a 90% collection diameter versus a dimensionless parameter constructed from the cyclone Reynolds number and the Stokes number:

$$d_{90\%} = f(Re \times Stk^{1/2}) \ . \tag{3-41}$$

The data follow a straight line on a log-log plot decreasing from 30 to 2 μm as the abscissa increases from 300 to 100,000. The only data beyond that value of the abscissa are the data of Knowlton and Backhorchin (1978), which give a constant 90% diameter of 6.4 μm for abscissa values greater than 10^6. The jump in 90% diameter near abscissa values of 100,000 has not been explained in the literature according to one of the authors of the Parker paper, but the jump may be caused by Knowlton and Backhorchin's larger cyclone (100 mm versus 50 mm for Parker) or because Knowlton and Backhorchin only ran at ambient temperatures. At any rate, the discrepancy occurs near our operating point and thus creates an uncertainty in collection efficiency. Because of this uncertainty, we will evaluate two cases. The liberal case will be based on the straight line shown in Figure 3-10. The conservative case will assume a constant 90% diameter of 6.4 μm.

The 90% collection diameter must be related to an efficiency-versus-diameter curve so that we may specify the cyclone inlet particle-loading distribution and predict the outlet distribution. To do this we refer to Parker's data for combined high pressure and temperature. We will fit a straight line from the 90% diameter efficiency to the 0,0 point:
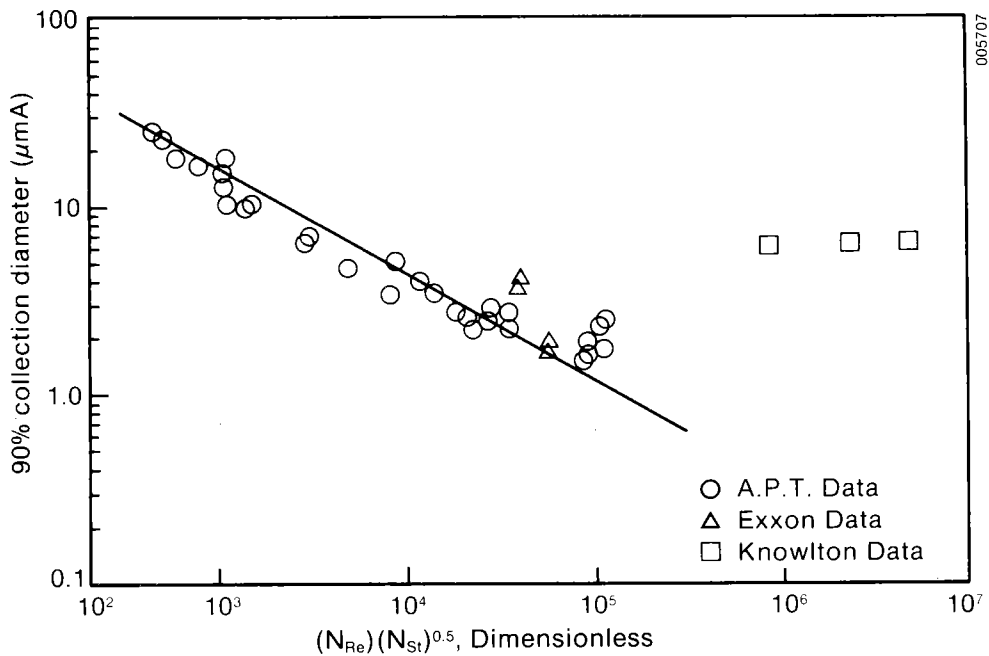
Source: Parker, Jain, and Calvert 1981.

Figure 3-10. Cyclone Performance at High Temperature and Pressure

$$\eta = (d/d90)*0.9 \quad d<d90 , \tag{3-42}$$

where η = collection efficiency.

The efficiency curves level out for diameters greater than the 90% diameter, and from Parker's data it is difficult to prescribe a curve shape. The shape of the curve beyond the 90% diameter is very important because a substantial fraction of the inlet particles will be in this range, and the choice of curve shape beyond the 90% diameter strongly affects effluent distribution. The best data available for this purpose are from the commissioning test of the pressurized fluidized-bed coal combustion facility at Grimethorpe, England (National Coal Board 1983). That operation ran at a pressure and temperature similar to our operation, and the particle distribution and loading were also close (mass mean particle diameter was approximately 100 μm and loading was approximately 18,000 ppm). The data shown in Figure 3-11 give efficiency versus diameter and go well beyond the 90% diameter that was 5.62 μm. The data go out to the 99+% diameter and with slight extrapolation, one can project the 99.9% diameter to be 31.6 μm. A good representation of the Grimethorpe data beyond the 90% diameter is:

$$\eta = 1 - 10^{-[1+2.666 \log(d/d_{90})]}$$

$$= 1 - 0.1(d/d_{90})^{-2.666} . \tag{3-43}$$

Equations 3-41 and 3-42 will be used to generate efficiency-versus-diameter curves given the 90% diameter.

Figures 3-12a and b show the predicted cyclone performance based on the preceding assumptions. Results for both the liberal and conservative assumptions for 90% collection efficiency diameter are given. With the liberal assumption, one stage is more than adequate to meet the goal of 100-ppm total loading. Using the conservative assumption, two stages are needed to reach that goal.

The cyclone pressure drop may be estimated from an equation recommended by Leith and Mehta (1973):

$$\Delta p = \frac{U_c^2 \Delta H}{2} \rho_a , \tag{3-44}$$

where

Δp = pressure drop (N/m^2)

U_c = air inlet velocity (m/s)

$\Delta H = 16\ ab/D_e^2$ (refer to Figure 3-9)

ρ_a = air density (kg/m^3).

For the design and cost of the DCHX system, we obtained a vendor quote for cyclones operating at 970°C and 10 atm from Aerodyne Development Corp. The quote called for 5 units per stage with a capacity of 9.4 m^3/s (20,000 cfm) each and a pressure drop of 1.5 kPa (0.217 psi). The cyclones were internally insulated and lined. Assuming that two stages of cyclones are required, 10 units total will be included in the DCHX system.
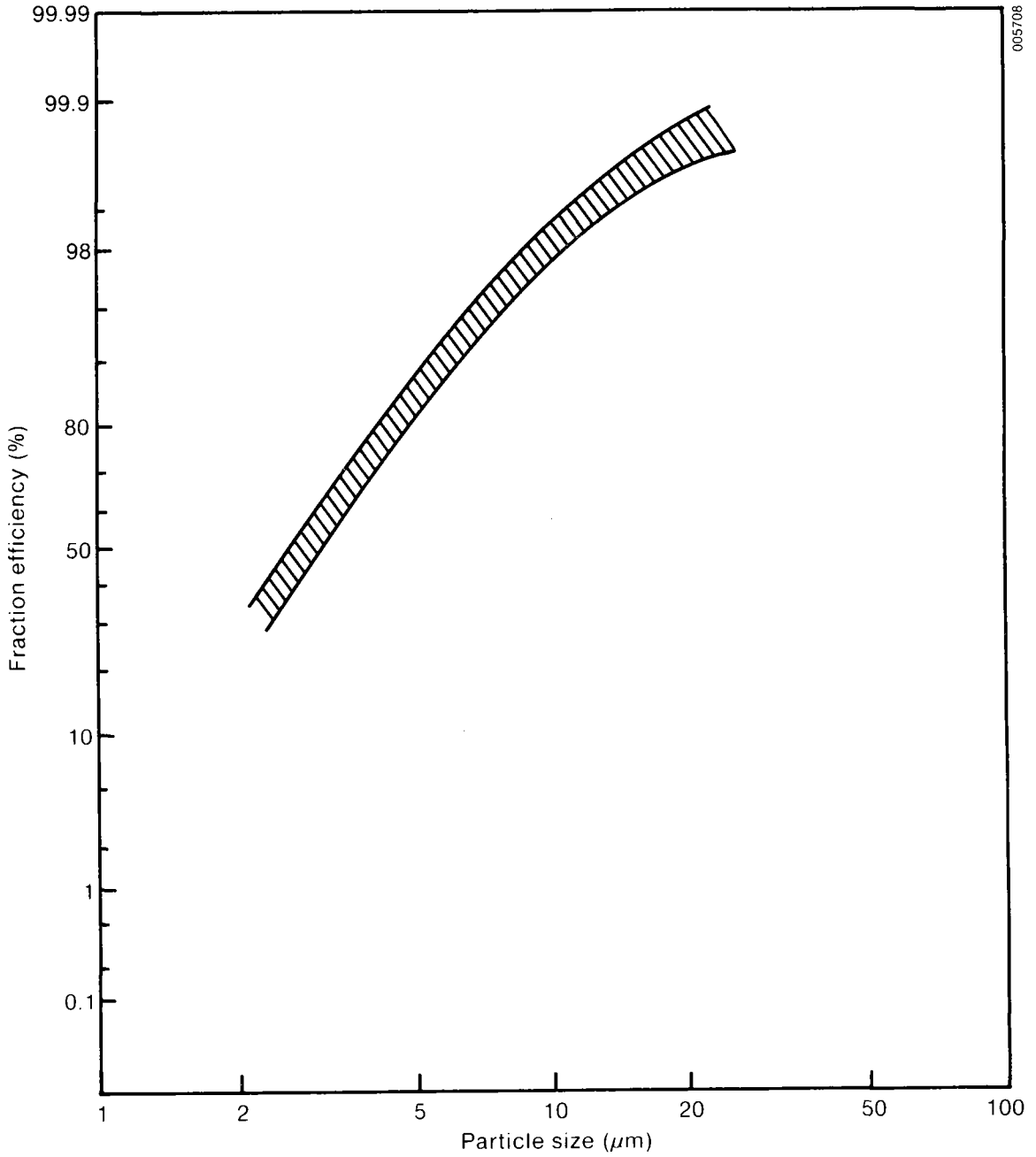
Figure 3-11. Cyclone Fraction Efficiency
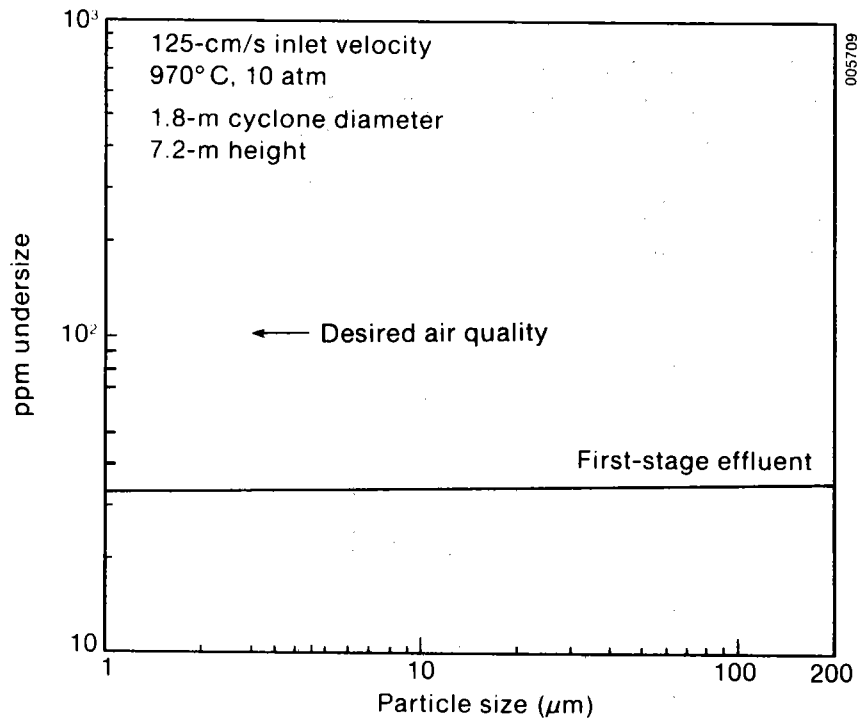
Figure 3-12a. Cyclone Performance Based on the Liberal Assumption for the 90% Collection Efficiency Diameter
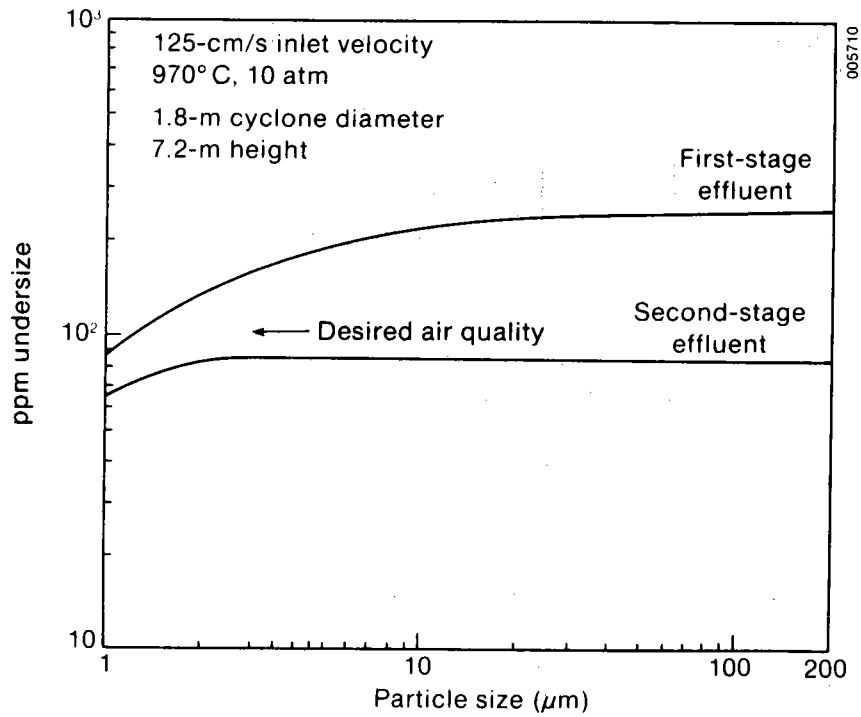
Figure 3-12b. Cyclone Performance Based on the Conservative Assumption for the 90% Collection Efficiency Diameter

3.5 Ducting and Piping

The ducting from the outlets of the heat exchanger and the cyclones will be internally insulated and internally shrouded. The internal insulation maintains a temperature that keeps the walls of the ducts structurally sound, and the internal shroud prevents contamination of the air stream that is caused by spalling of the refractory insulation. We evaluated the cost and performance of this type of ducting for the pressurized fluidized-bed combustion of coal (General Electric 1978). Researchers successfully tested a section of ducting up to $1000^{\circ}C$ ($1850^{\circ}F$) with transients as high as $400^{\circ}C/h$ ($700^{\circ}F/h$). Although the tests were performed at ambient pressure, the ducting is designed to deliver hot pressurized gases to gas turbines. Ducting with a 36 in. inside diameter was priced at \$2300/ft in 1978 dollars. Tees and elbows in the same size were priced at \$33,000 apiece. For this study, the cost of the ducting was assumed to vary linearly with diameter; the diameter was sized for 100-ft/s air velocities.

The balance of piping and ducting for the heat exchanger was costed at 4% of the total installed capital cost (Peters and Timmerhaus 1980, p. 171). This is a typical value for a solids-processing plant.

4.0 ECONOMIC ANALYSIS

4.1 Methodology

The cost of the DCHX system is expressed as an annual levelized cost (ALC). This is the constant annual cost (in fixed dollars) that, if paid over the lifetime of the heat exchanger, would have a present value equal to the present value of the actual costs incurred over the lifetime of the heat exchanger. The actual costs include both capital costs and annually recurring operating and maintenance costs. The costing methodology for SERI's Solar Energy Storage Program detailed in Appendix A is used to calculate the ALC from the capital and annual costs. Parameters used in the calculation include:

> Discount rate--10%
> Lifetime--30 yr
> Corporate tax rate--50%
> First year of operation--1990
> General inflation--6%
> Escalation rate for capital costs--6%
> Escalation rate for annual costs--6%.

Only one capital cost (CC) is considered, the cost of the original purchase and installation. The annually recurring costs (AC) include both an operating and maintenance (O&M) cost and the cost of the pumping power to overcome the pressure drop in the heat exchanger and cyclones. Given these assumptions and the method in Appendix A, the ALC is expressed as:

$$ALC = 0.2228 \ CC + 1.886 \ AC \ . \tag{4-1}$$

All costs are in 1981 dollars. The DCHX cost is also expressed as the cost per unit of energy transferred ALC/Q where Q,MWh is:

$$Q = 8760 \ C_f(100 \ MW_t) = 350,400 \ MWh_t \ , \tag{4-2}$$

where 8760 is the number of hours per year and the capacity factor C_f is assumed to be 0.4, which implies 10 hours of operation per day.

A costing methodology used in the Solar Thermal Technology Program will also be used to facilitate comparison to the Solar Thermal cost goal of \$8.52/GJ (\$9.00/10^6 Btu) for thermal energy delivered from a solar central receiver (Williams 1985). For this method, the ALC is expressed as:

$$ALC = 0.1766 \ CC + 1.0 \ AC \ .$$

In the following text, the Solar Thermal cost methodology will be specifically noted whereever it is used. In all other cases, the Storage Program methodology is used.

4.2   Capital Costs

The valve costs suggested by vendors (Section 3.3) were $35,000-$65,000 for 6-in. valves or $6,000-$11,000 per inch of inner diameter. These state-of-the-art valves are suitable for the DCHX defeeder valves, and a cost of $10,000 per inch is assumed. A higher cost of $15,000 per inch is used for the feeder and cyclone defeeder valves.

For the lockhopper and buffer storage vessels, we use a method given by Peters and Timmerhaus (1980) to calculate the cost of a pressure vessel based on the weight W (lb) of the vessel. The cost in 1979 dollars is given as:

$$\$/lb = 50 \ W^{-0.34} \ . \tag{4-3}$$

This equation is applicable to vessels up to 100,000 lb, which is heavier than any of the lockhopper or buffer storage vessels. These costs are increased by a factor of 4, the Lang Factor, to account for delivery and installation (Peters and Timmerhaus 1980). Added to the cost of the vessel is the cost of insulation, both internal and external. The installed costs are (Bohn 1983):

    Ceramic firebrick--$809/m^3
    Fiberglass--$265/m^3
    Aluminum lagging--$25/m^2.

The total cost, vessel and insulation, was converted to 1981 dollars assuming 6% inflation.

The DCHX vessel was costed in the same manner with two exceptions. First, the vessel weighs over 100,000 lb. At 100,000 lb, the equation gives a cost of $1/lb ($2.203/kg). This was the base cost used for the vessel. Second, the cost of the grids for the fluidized beds was added to the vessel cost:

$$\text{cost of grids} = (\$431/m^2)4\left(\frac{\pi d_{sh}^2}{4}\right) \ . \tag{4-4}$$

Peters and Timmerhaus (1980) recommend this equation for the cost of bubble cap trays.

The vendor quote on the cyclones was $300,000 per unit in 1981 dollars. With 2 stages of cyclones and 5 cyclones per stage, the total cost with the Lang Factor is 12×10^6. In 1978 dollars, General Electric (1978) gives costs of $2300/ft for the internally insulated and shrouded ducting at the outlet of the DCHX and the cyclones and $33,000 a piece for tee and elbow fittings, all with 36-in. inner diameter. These costs are equivalent to $82.50/cm of inner diameter (ID) per meter for ducting and $361/cm of ID for the fittings (tees and elbows), both in 1978 dollars (see also Section 3.5). The balance of piping in the system was taken as 4% of the total capital cost. As before, all costs not in 1981 dollars were converted using an inflation rate of 6%.

4.3   Annual Costs

The annually recurring costs for the DCHX are O&M costs and auxiliary power costs. Battleson (1981) estimates the O&M cost of a solar central receiver power plant as 2% to 3% of the capital costs. This agrees with the EPRI

Technical Assessment Guide (1978), which gives the O&M cost for atmospheric fluidized-bed combustion of coal. Excluding the consumables (limestone for desulfurization), the cost was 3% of the total capital cost. We expect the DCHX to have higher maintenance costs because of its high operating temperature and because the particles are very abrasive. The lockhopper valves, in particular, will be more costly to maintain than conventional valves. In chemical processing plants, maintenance costs alone are usually above 3% with 5%-9% considered average and 10% or more possible under severe operating conditions (Peters and Timmerhaus 1980). For the annual O&M cost, a value of 6% of the total capital cost is assumed.

The auxiliary power cost is based on the pumping power required to overcome the pressure drop in the heat exchanger and the cyclone. The power required to bring the air to the delivery pressure of 10 atm is not included. Given the total pressure drop in the system, P_d in N/m^2, the pumping power is given by:

$$W = \frac{P_d m_a}{\rho_a \eta_c \eta_m 10^3} , \tag{4-5}$$

where

$\quad$ W = pumping power (kW)

$\quad$ m_a = mass flow rate of air (kg/s)

$\quad$ ρ_a = density of air (kg/m^3)

$\quad$ η_c = compressor efficiency = 0.7

$\quad$ η_m = motor efficiency = 0.96 .

Assuming a cost of electricity C_m in 1990 of $0.0464/kWh (in 1981 dollars) as recommended in Appendix A, the annual cost of the auxiliary power AC_m is:

$$AC_m = WC_f C_m \; 8760 . \tag{4-6}$$

4.4 Results

Figure 4-1 shows the complete DCHX system. It has an overall height of 81 m, only 11 m of which is the DCHX. Most of the height is made up of the numerous feeder and defeeder vessels. There are, altogether, 24 pressure vessels in addition to the DCHX. The height of the system presents a construction problem in itself. The system should be installed as part of the receiver tower, if possible, to avoid the additional cost of a superstructure to support the various vessels.

Table 4-1 summarizes the system costs and shows a cost per unit of delivered energy of $6.66/GJ. Most of the system cost is in the solids-handling equipment and not in the heat exchanger itself. The feeders and defeeders alone have a capital cost more than three times that of the DCHX. The cyclones cost
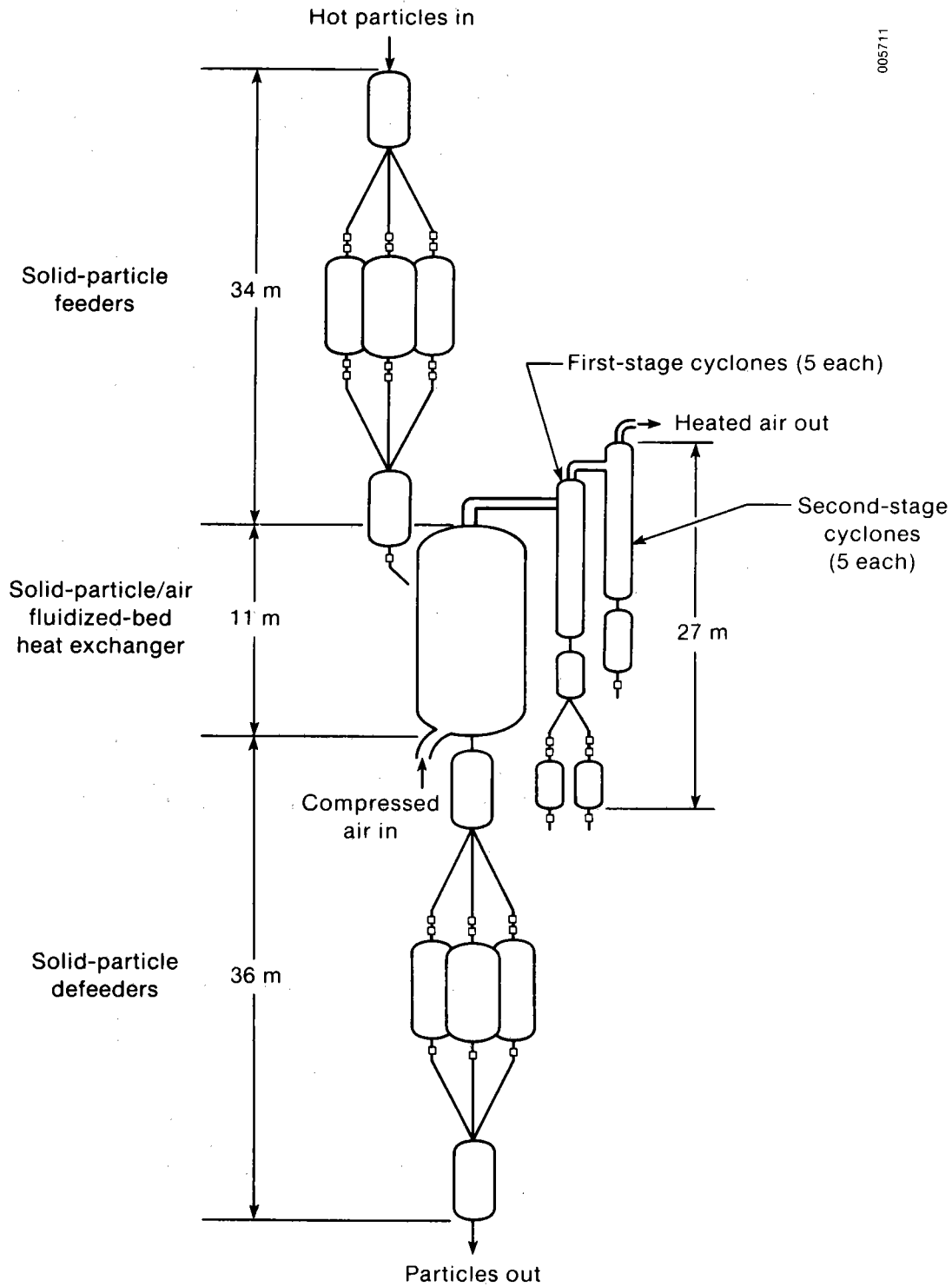
Figure 4-1.   Solid-Particle/Air Direct-Contact Heat Exchanger System Schematic

Table 4-1. Direct-Contact Heat Exchanger Costs in 1981 Dollars

	Total (10^6 $)	Annual Levelized (10^6 $)
Capital investment		
Fluidized-bed heat exchanger	2.16	0.48
Feeders	4.29	0.96
Defeeders	2.55	0.57
Cyclones	12.0	2.67
Cyclone defeeders	0.48	0.11
Ducting	1.59	0.35
Piping	0.92	0.21
Total capital investment	24.00	5.35
Annual costs		
Heat exchanger auxiliary power	0.17	0.32
Cyclone auxiliary power	0.01	0.02
Operation & maintenance	1.44	2.72
Total annual costs	1.62	3.06
Total annual levelized cost		8.41
Annual levelized cost per unit of energy transferred		0.024 $/kWh 6.66 $/GJ 7.04 $/$10^6$ Btu

nearly six times as much as the DCHX. The pie chart in Figure 4-2 more clearly shows how the capital and annual costs contribute to the ALC. The cost of the valves is 61% of the feeder total cost, 48% of the defeeder cost, and 49% of the cyclone defeeder cost.

Using the Solar Thermal Technology Program's cost methodology, the DCHX cost is $4.64/GJ. This cost is high compared to a cost goal of $8.52/GJ ($9.00/10^6 Btu) for thermal energy delivered from a solar central receiver.

4.5 Best Case Configuration

Because of the high cost of the original configuration of the DCHX, we costed a second configuration as well. While the original configuration was based on state-of-the-art technology, the best case configuration assumes progress in several key technologies that have a significant impact on system cost. The assumed progress was limited to technologies that have a reasonable oppor-tunity for progress as a result of future development. Whereas continuing research in these technologies may also create opportunities for cost reduction, these opportunities and their impact are more difficult to project. We have limited our best case assumptions to the development and resulting maturity of existing technologies.
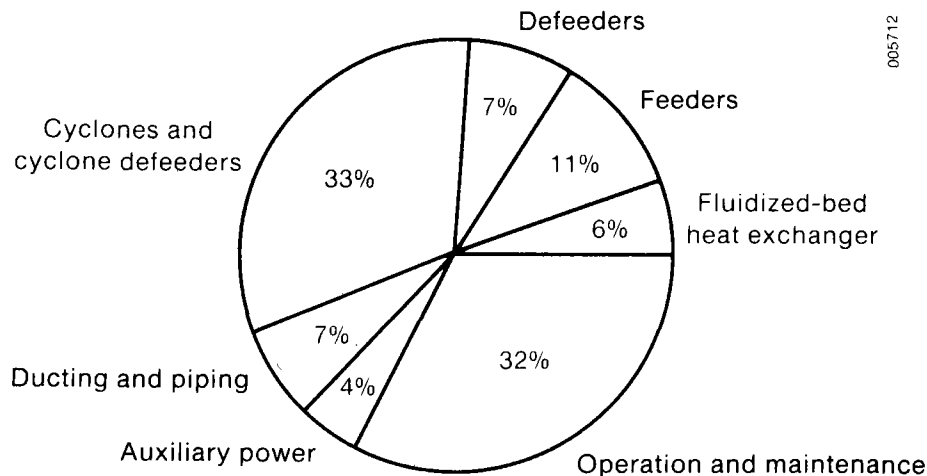
Figure 4-2. Breakdown of Annual Levelized Cost for Direct-Contact Heat Exchanger

For the best case configuration the heat exchanger is unchanged, but we made new assumptions that will lower the cost of the solids-handling equipment. These new assumptions are:

o   High-reliability valves--With valves of sufficient reliability, we would not have to allow for maintenance of valves while the plant is on-line. This eliminates the need for the third lockhopper and the isolation valves. Assuming 6 months between plant shutdowns, the system would require valves with lifetimes of about 10,000 cycles between overhauls.

o   No buffer storage--The lockhopper cycles are timed to have one feeder and one defeeder lockhopper available to service the heat exchanger at all times.

o   No flow control valve--The lockhopper valves alone can adequately control flow rate.

o   One stage of cyclones--This is feasible if the particle loading into the cyclones is lower than estimated in Section 3.4 or if adequate performance can, in fact, be gained from one stage.

For this configuration, the cost of the heat exchanger remains the same. The feeders, defeeders, and valves are sized and costed using the same methods as before. Instead of vendor quotes, cyclones were sized and costed using the methods previously described for costing pressure vessels. The cyclones were treated as pressure vessels with height-to-diameter ratios of 4 to 1. The calculation of cyclone pressure drop is given in Section 3.4. Cyclone size was reduced by increasing the inlet air velocity. A trade-off study of cyclone size versus pressure drop resulted in a least cost configuration consisting of four cyclones 6.5 m in height and 1.6 m in diameter with inlet velocities of 30 m/s.

These assumptions had a significant impact on the size and the cost of the system. Figure 4-3 shows a schematic of the configuration. The overall height is 41 m compared to 81 m for the original configuration. Table 4-2 gives costs for the best case configuration. The delivered energy cost is $2.30/GJ. Within the feeder and defeeder totals, 24% is the cost of valves and 76% is the cost of the lockhopper pressure vessels. Figure 4-4 gives a breakdown of the system cost. This breakdown shows that O&M costs are the single largest contributor to the annual levelized cost. If O&M costs were lower than we assumed, the total cost would be significantly reduced. If the O&M costs were 3% instead of the assumed 6% of total capital costs, the delivered energy would cost $1.96/GJ.

Using the Solar Thermal Technology Program's cost methodology, the cost of the best case configuration is $1.56/GJ. This cost, too, is high compared to the $8.52/GJ ($9.00/10[6] Btu) cost goal.

This configuration costs about one-third as much as the original configuration and indicates what might be possible with additional progress in the development of solids-handling valves, additional information on O&M costs, and information on the adequacy of a single stage of cyclones. In Section 1.0, we surmised that a direct-contact configuration would be economically attractive because of the elimination of heat transfer surfaces. This is true in that the fluidized-bed heat exchanger itself is not high in cost. However, the cost of the solids-handling equipment required by a direct-contact configuration--feeders, defeeders, and cyclones--results in a DCHX system cost that is high as shown by the comparison to the Solar Thermal cost goal.

Hot particles in

Solid-particle
feeders

15 m

Heated air out

Solid-particle/air
fluidized-bed
heat exchanger

Cyclones
(4 each)

13 m

11 m

Cyclone
defeeder
(1 each)

Compressed
air in

15 m

Solid-particle
defeeders

Particles out

005713
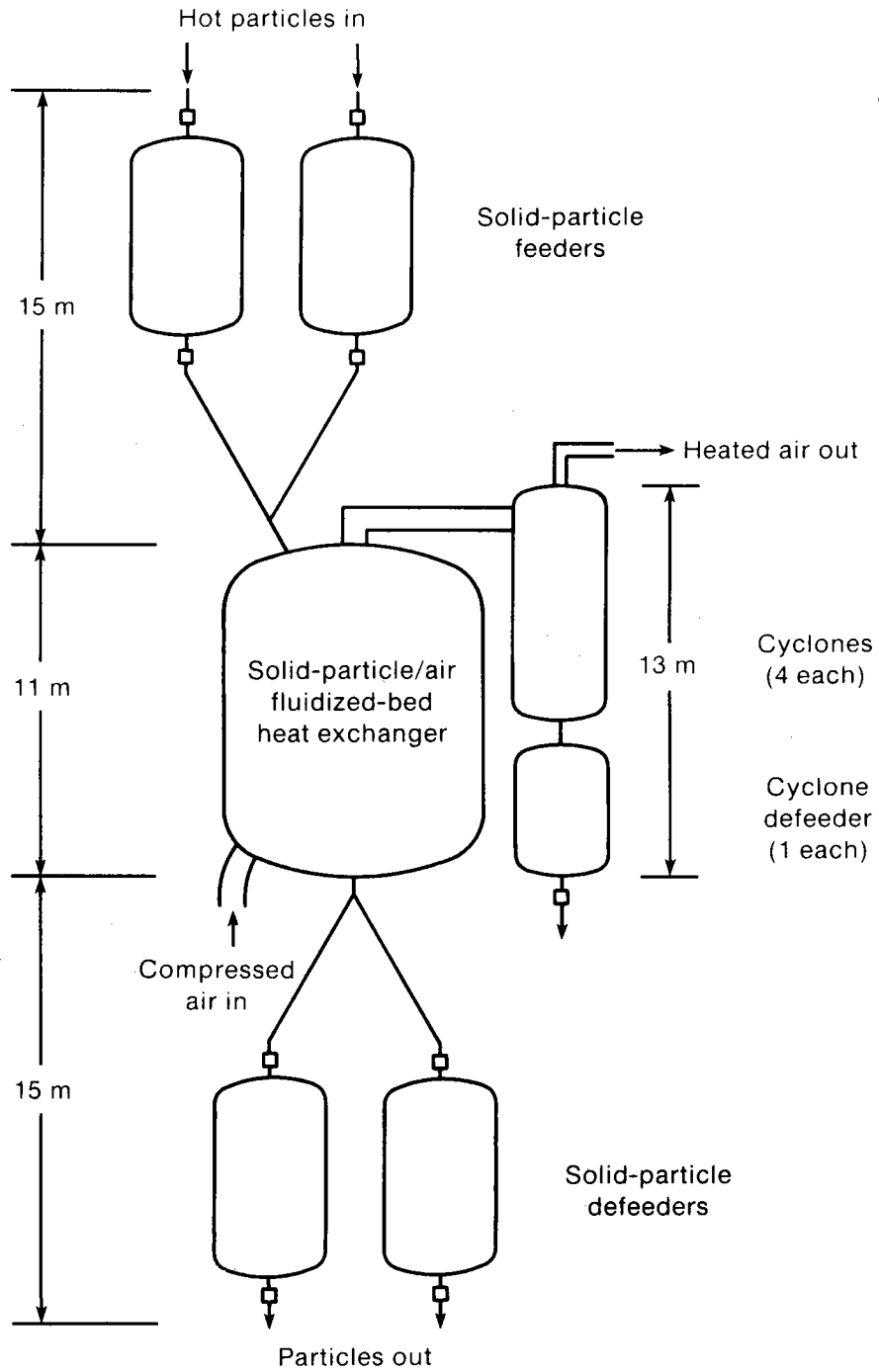
**Figure 4-3.   Solid-Particle/Air Direct-Contact Heat Exchanger System,
Best Case Configuration**

Table 4-2.   Direct-Contact Heat Exchanger Costs, Best Case Configuration, in 1981 Dollars

	Total (10^6 \$)	Annual Levelized (10^6 \$)
Capital investment		
Fluidized-bed heat exchanger	2.16	0.48
Feeders	1.67	0.37
Defeeders	1.23	0.27
Cyclones	0.93	0.21
Cyclone defeeders	0.16	0.04
Ducting	1.02	0.23
Piping	0.29	0.06
Total capital investment	7.46	1.66
Annual costs		
Heat exchanger auxiliary power	0.17	0.32
Cyclone auxiliary power	0.04	0.07
Operation & maintenance	0.45	0.85
Total annual costs	0.66	1.24
Total annual levelized cost		2.90
Annual levelized cost per unit of energy transferred		0.0083 \$/kWh$_t$ 2.30 \$/GJ 2.43 \$/10^6 Btu

005714
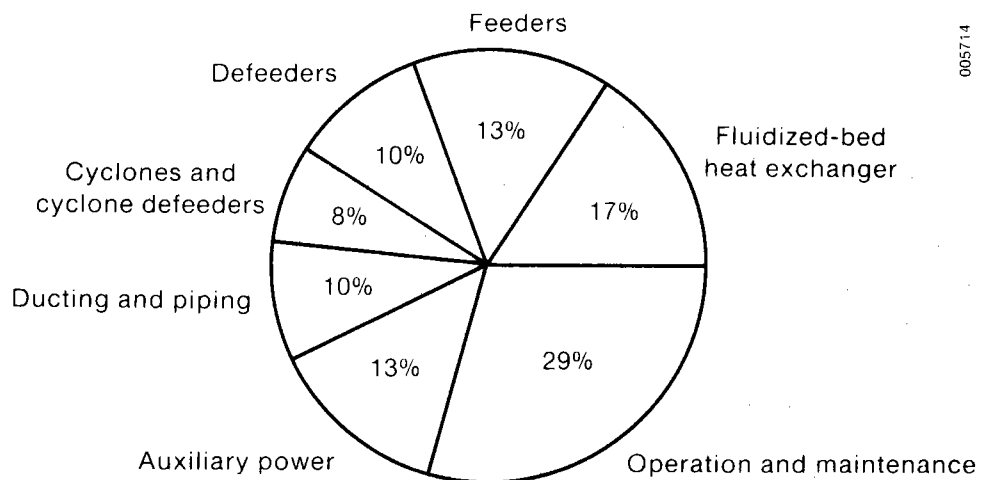
Figure 4-4.   Breakdown of Annual levelized Cost for Direct-Contact Heat Exchanger, Best Case Configuration

5.0 SHELL-AND-TUBE CONFIGURATION

Given the high costs estimated for the DCHX, we decided to evaluate a shell-and-tube heat exchanger configuration as well. In a shell-and-tube config-uration, the solid particles are always at ambient pressure, eliminating the need for feeders and defeeders. The air is never in contact with the par-ticles so that cyclones are not required. Because a shell-and-tube heat exchanger does not require such solids-handling equipment, it may be an attractive alternative. This section presents a parametric analysis of shell-and-tube heat exchanger requirements for this application. We assess heat transfer coefficients, required area, flow rates, pressure drops, and cost.

Although a prototype of a moving bed shell-and-tube heat exchanger has not yet been built, several investigators have performed significant research. In a study aimed at the 10-MW solar thermal central receiver pilot plant, Wright et al. (1981) of Babcock and Wilcox investigated the feasibility of several storage concepts for solar thermal application. The most promising alter-native to the plant's oil-and-rock storage system was the moving-bed thermal energy storage system (MBTESS), which included discharging heat exchangers that transferred heat from sand (the storage medium), on the shell side of the exchanger, to tubes containing water or steam (see Figure 5-1). The MBTESS design employed gravity-induced sand flow, at low velocity, over the tube bundles to be heated. The tubes were arranged in a staggered pattern and inclined at an angle between the angle of repose and the vertical. The shell was also inclined, parallel to the tubes. This configuration reduces flow resistance, minimizes stagnant regions at the top of each tube, and reduces the appearance of voids underneath the tubes. A recommended bed velocity of 0.15-0.30 m/s provides good heat transfer without appreciable tube wear or particle attrition. A flow restrictor below the tube bank keeps the heat exchanger shell full of moving-bed material. The Babcock and Wilcox study predicted an overall heat transfer coefficient of 931 to 1162 W/m^2 K from the sand moving bed to steam, based on the work of Denloye and Botterill (1977). Dubberly et al. (1983) also investigated the sand moving-bed heat exchanger and predicted performance comparable to the Babcock and Wilcox results (Wright et al. 1981).

A shell-and-tube design has the disadvantage of being limited in operating temperature by the strength of the tube materials. The temperature limit depends on many factors including operating pressure, tube-wall thickness, and tube material. Because no steam is produced in a solid-particle/air heat exchanger, the operating pressures will be inherently lower than in the MBTESS heat exchanger. In this section, no attempt is made to evaluate candidate tube materials and their associated temperature limits. The analysis of the solid particle/air heat exchanger is limited to aspects of performance such as heat transfer and pressure drop.
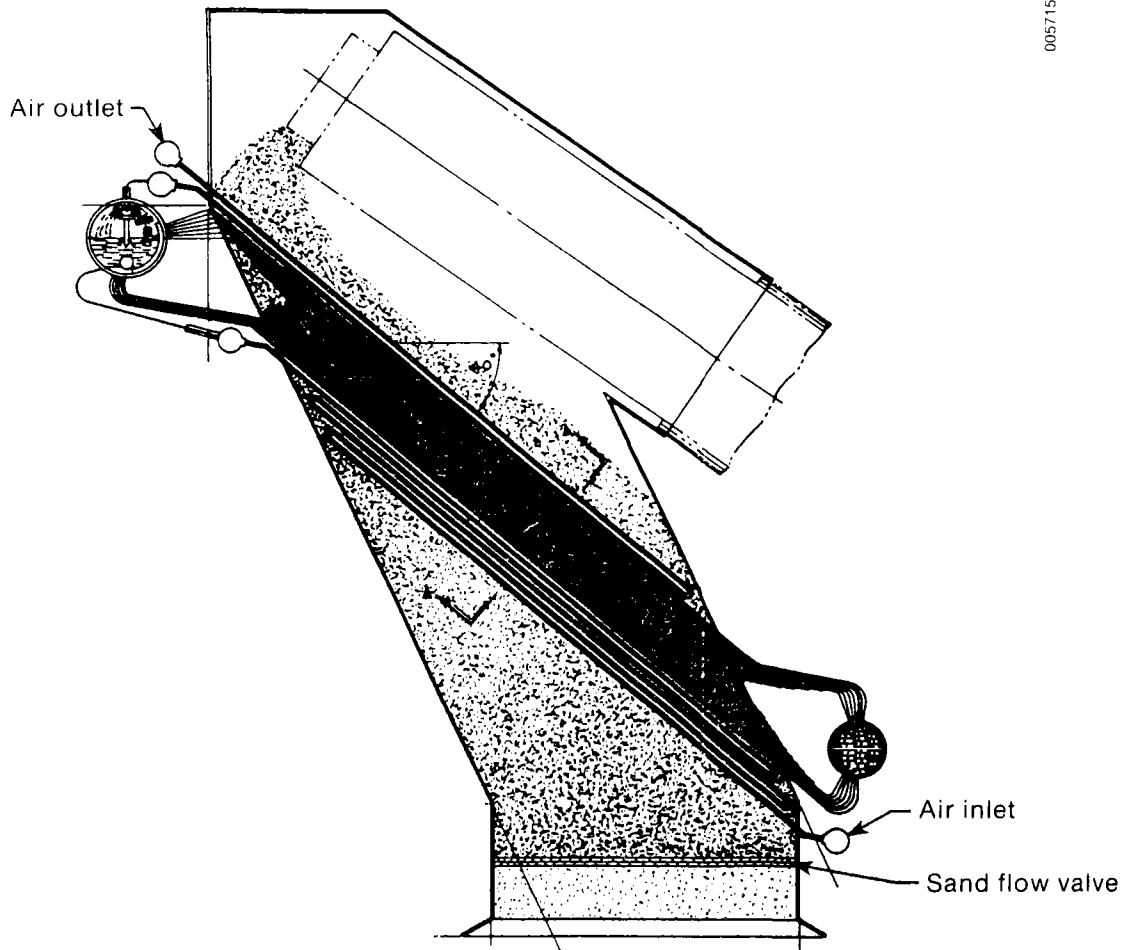
Source: Wright et al. 1981.

Figure 5-1. Configuration of the Moving-Bed Heat Exchanger

5.1 Sizing the Heat Exchanger

To make a fair comparison with the DCHX, the inlet and outlet temperature con-
ditions for the particles and air sides were identical for the shell-and-tube
exchanger, with:

$$T_{ai} = 150^{\circ}C$$

$$T_{ao} = 970^{\circ}C$$

$$T_{si} = 1000^{\circ}C$$

$$T_{so} = 581^{\circ}C \ .$$

The desired rate of heat transfer from the alumina particles to the air in the exchanger Q was 100 MW_t. Characteristics of the alumina particles were given as:

particle diameter d = 0.5 mm

specific gravity = 4.0

specific heat, c_{ps} = 837.2 J/kg K

thermal conductivity = 8 W/m K (on average).

The foregoing analysis is based on the configuration studied by Babcock and Wilcox, which has the alumina particles on the shell side and air on the tube side. Brinn et al. (1948) analyzed heat transfer from granular materials moving downward inside vertical tubes. They observed rodlike flow behavior for Ottawa sand in 0.022-m inside diameter tubes. Extending their correlations to our materials, properties, and conditions, the tube-side heat transfer coefficient for a nominal 0.0254-m diameter tube is only about 8 W/m^2 K. Because the Babcock and Wilcox study predicted much higher overall heat transfer coefficients for particles on the shell side, we chose to follow their work. For purposes of this study, the materials we considered to fabricate the tubes were Incoloy 825 for the first few rows experiencing the highest temperatures, and stainless steel for the remaining tubes. Sensitivities examined in the foregoing analysis include:

o Effect of outlet air temperature requirement on heat exchanger area and pressure drop
o Effect of internally finned tubes on required heat exchanger area and pressure drop
o Effect of particle-side heat transfer coefficient on overall heat transfer coefficient and hence on required heat transfer area
o Effect of air-side Reynolds number on required heat exchanger area and pressure drop.

5.2 Thermal Analysis

Counterflow heat transfer in a shell-and-tube heat exchanger may be expressed by:

$$Q = UA\Delta T_{1m} \ , \tag{5-1}$$

where A is the surface area of the heat exchanger, U is the overall heat transfer coefficient, and ΔT_{1m} is the log-mean temperature difference between the two streams. The log-mean temperature difference is known and may be found from:

$$\Delta T_{lm} = \frac{(T_s - T_a)_B - (T_s - T_a)_A}{\ln\left[\frac{(T_s - T_a)_B}{(T_s - T_a)_A}\right]} \cdot \tag{5-2}$$

In the preceding equation, and henceforth in this section, the subscript s refers to the alumina solid particles, the subscript a refers to air, and A and B refer to opposite ends of a counterflow heat exchanger configured as in Figure 5-2.

To solve for the required heat transfer area, we must compute the overall heat transfer coefficient U from:

$$U = \frac{1}{\frac{1}{H_p} + R_p + \left(\frac{1}{H_a} + R_a\right)\frac{D_o}{D_i} + \frac{Y_w}{K_w}\frac{D_o}{D_w}}, \tag{5-3}$$

where

$$D_w = \frac{D_o - D_i}{\ln(D_o/D_i)} \cdot \tag{5-4}$$

Alumina inlet
(T = 1000°C)

Air outlet
(T_{ao} = 970°C)

A

B

Air inlet
(T = 150°C)

Alumina outlet
(T = 581°C)
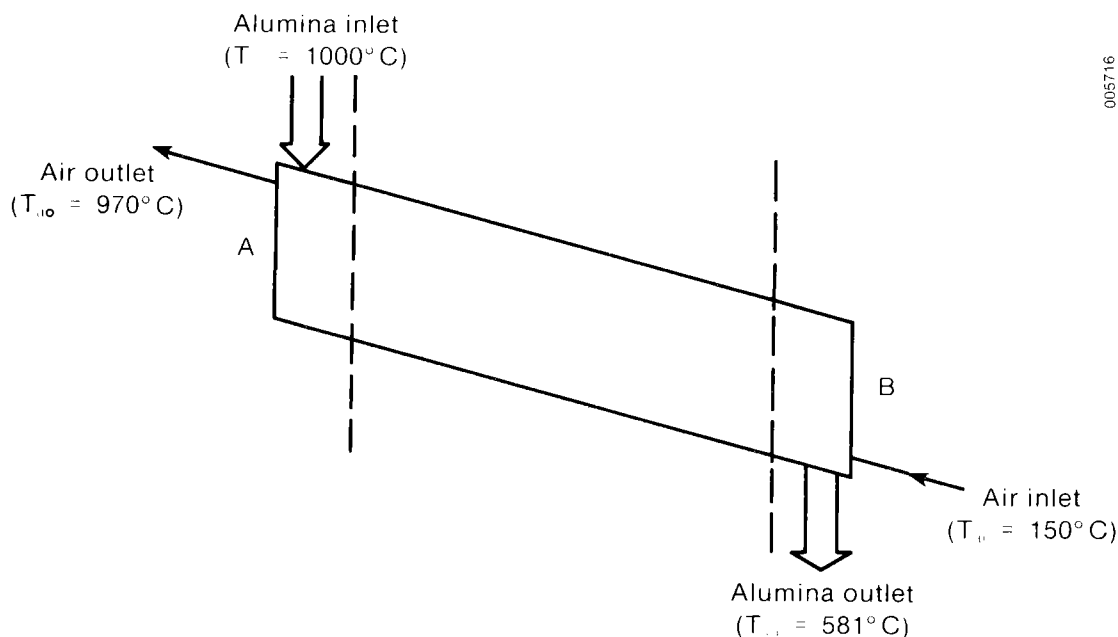
005716

Figure 5-2.   Schematic of Moving-Bed Shell-and-Tube Heat Exchanger

In the previous equations, H_p is the heat transfer coefficient on the particle or shell side, H_a is the air-side (tube-side) heat transfer coefficient, R_p and R_a are fouling resistances, D_o and D_i are the outside and inside diameters of the tubes, Y_w is the wall thickness, and K_w is the wall thermal conductivity.

The expression describing the tube-side heat transfer coefficient H_a is (Carnavos 1979):

$$Nu_a = 0.023 \, Re_a^{0.8} \, Pr_a^{0.4} \, F \, , \qquad (5-5)$$

where F is a heat transfer adjustment factor for fin-tube geometry (F = 1 for smooth tubes), Nu_a is the air-side Nusselt number, Re_a is the air-side Reynolds number, and Pr_a is the air-side Prandtl number. The air heat transfer coefficient H_a is then found from the definition of Nu_a:

$$H_a = \frac{Nu_a K_a}{D_h} \, , \qquad (5-6)$$

where D_h is the hydraulic diameter of the tube and K_a is the thermal conductivity of air. Table 5-1 gives characteristics for a smooth tube and a finned tube used in the following analysis.

The alumina-side (shell-side) heat transfer coefficient is found from (Kurochkin 1966):

$$Nu_s = 0.0214 \, Pe^{0.21} \frac{D_o}{d_s} \, , \qquad (5-7)$$

where

$$Pe = \frac{V_o c_{ps} \, \gamma_b \, D_o}{K_s} \, .$$

In the above equations, d_s is the mean particle diameter, V_o is the bed velocity, c_{ps} is the specific heat of the alumina, γ_b is the bulk density, K_s is the thermal conductivity of the alumina particles, and Pe is the Peclet number. The bed velocity was 0.15 m/s, based on the design developed by Babcock

Table 5-1. Tube Dimensions and
Adjustment Factors

	Smooth Tube	Finned Tube
D_i	22.2 mm	23.7 mm
D_o	27.2 mm	25.4 mm
D_h	22.2 mm	12.2 mm
F	1.0	1.13
F*	1.0	1.07

and Wilcox. Sample calculations for the heat transfer coefficients may be found in Appendix C. For those conditions, the value of H_s is 1468 W/m^2 K, and H_a is 146 W/m^2 K, so that the air side controls the heat transfer. U is 103 W/m^2 K for the case shown in Appendix C.

5.3 Pressure Drop

The pressure drop on the air side (tube side) was a major consideration in the operating cost of the heat exchanger. However, because the air side controls heat transfer (as was seen in our calculations in Appendix C), we wished to have a relatively high velocity in the tubes to enhance heat transfer. In addition to smooth tubes, we investigated internally finned tubes that are designed to improve heat transfer. Carnavos (1979) gives the friction factor for both smooth and finned tubes as:

$$f = \frac{0.046}{Re^{0.2}F^*} , \qquad (5-8)$$

where F^* is a friction factor adjustment for finned-tube geometry. Pressure drop across the tubes in the heat exchanger core may then be found from:

$$\Delta P = \frac{2fV_a^2 L \rho_a}{D_h} , \qquad (5-9)$$

where V_a is the velocity of the air, L is the tube length, and D_h is the hydraulic diameter. This expression does not account for entrance or exit effects, which we assume are negligible compared to the core friction. Sample calculations appear in Appendix D.

5.4 Parametric Analysis

Because the greatest unknown is the thermal performance of the moving bed on the shell side of the heat exchanger, we first examined the influence of H_p, the particle-side heat transfer coefficient, on the required area. The model presented by Kurochkin (1966) results in a value of H_p = 1468 W/m^2 K, which is reasonable compared to values of overall heat transfer coefficient for sand to steam predicted by the Denloye and Botterill model by Wright et al. From Figure 5-3, we see that beyond H_p approximately equal to 800 W/m^2 K, there is little impact on the heat transfer surface required because the air side controls heat transfer. This result indicates that our value for H_p is a reasonable choice for this analysis, as predictions of the area requirement do not significantly change for H_p between 800 and 1700 W/m^2 K.

We next examined the effect of changing the conditions on the air side to improve heat transfer. Figure 5-4 shows the effect of increasing the Reynolds number on the tube side from 10,000 to 50,000. Figure 5-5 illustrates the impact on pressure drop. Another way of improving heat transfer is through the use of finned tubes. Using the characteristics of the internally finned tube described in Table 5-1, we compared the performance of smooth tubes to
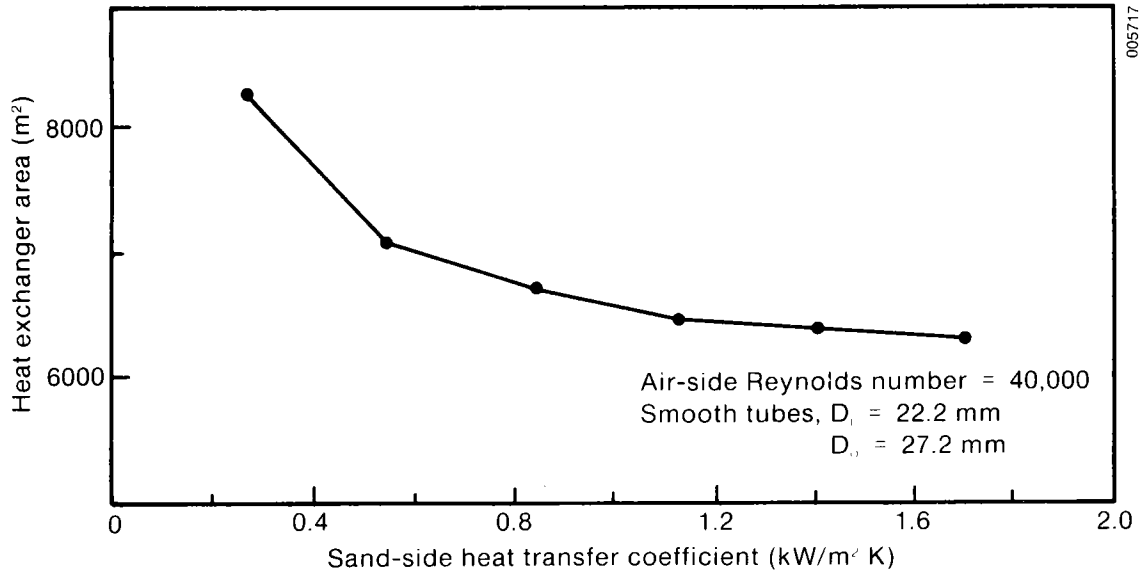
Figure 5-3. Effect of Improving Sand-Side Heat Transfer Coefficient on Total Area Requirement
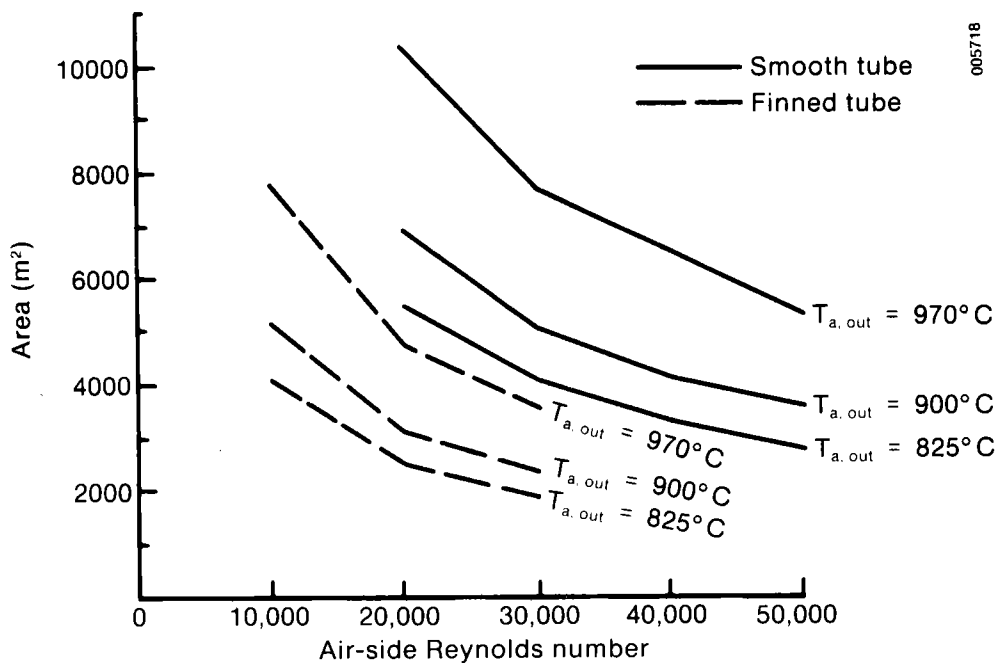
Figure 5-4. Effect of Air-Side Flow Rate on Required Heat Transfer Area
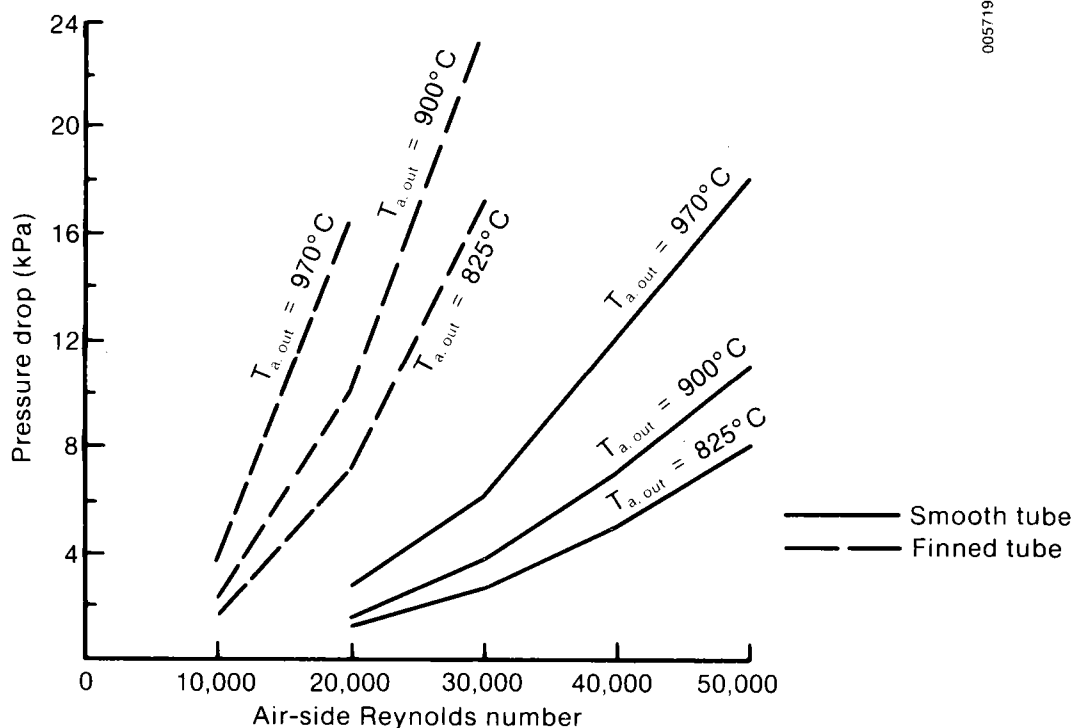
Figure 5-5. Effect of Air-Side Flow Rate on Pressure Drop

finned tubes as a function of Reynolds number (also in Figures 5-4 and 5-5). Finally, we looked at the effect that relaxing the outlet air temperature requirement has on the required heat transfer area. The DCHX easily attained the outlet temperature of 970°C because of the heat transfer characteristics of fluidized beds. With the shell-and-tube configuration, such a high outlet temperature is not as easily attained and affects the required area and the pressure drop. These results appear as well in Figures 5-4 and 5-5.

5.5 Cost Estimates

We estimated capital costs for the heat exchangers discussed in the previous section based on techniques described in Peters and Timmerhaus (1980). The cost of a U-tube heat exchanger with 2.54-cm (1-in.) stainless steel tubes operating at 1034 kPa (150 psi) is given as $280/m^2 ($26/ft^2) in 1981 dollars. This is for a heat exchanger area of 409 m^2 (4400 ft^2), the largest for which data are given (Peters and Timmerhaus 1980, p. 670). The same heat exchanger constructed with Incoloy 825 tubing would cost $463/m^2 ($43/ft^2) (Peters and Timmerhaus 1980, p. 677). For our cost estimate, we assumed a capital cost of $540/m^2 ($50/ft^2) in 1981 dollars. This cost was increased by a Lang factor of 3.5 to account for delivery and installation. We used the methods described in Section 4.0 to determine O&M costs and auxiliary power costs, and to calculate the annual levelized costs.

For comparison to the DCHX, we chose a baseline case for the shell-and-tube heat exchanger that included smooth tubes, T_{ao} at 970°C, Re_a of 50,000, requiring a heat exchanger area of 5300 m^2. Table 5-2 gives the costs for this baseline configuration. This configuration has an energy cost of $2.91/GJ, less than one-half the cost of the original DCHX configuration. Figure 5-6 shows heat exchanger costs for other outlet temperatures, other

values of Re_a, and for both smooth and finned tubes. For both types of tubes, we assumed the same cost of $540/m^2$.

Using the Solar Thermal Technology Program's cost methodology, the shell-and-tube configuration has a cost of $2.03/GJ.

Table 5-2.   Cost Estimate for Baseline Shell-and-Tube Configuration in 1981 Dollars

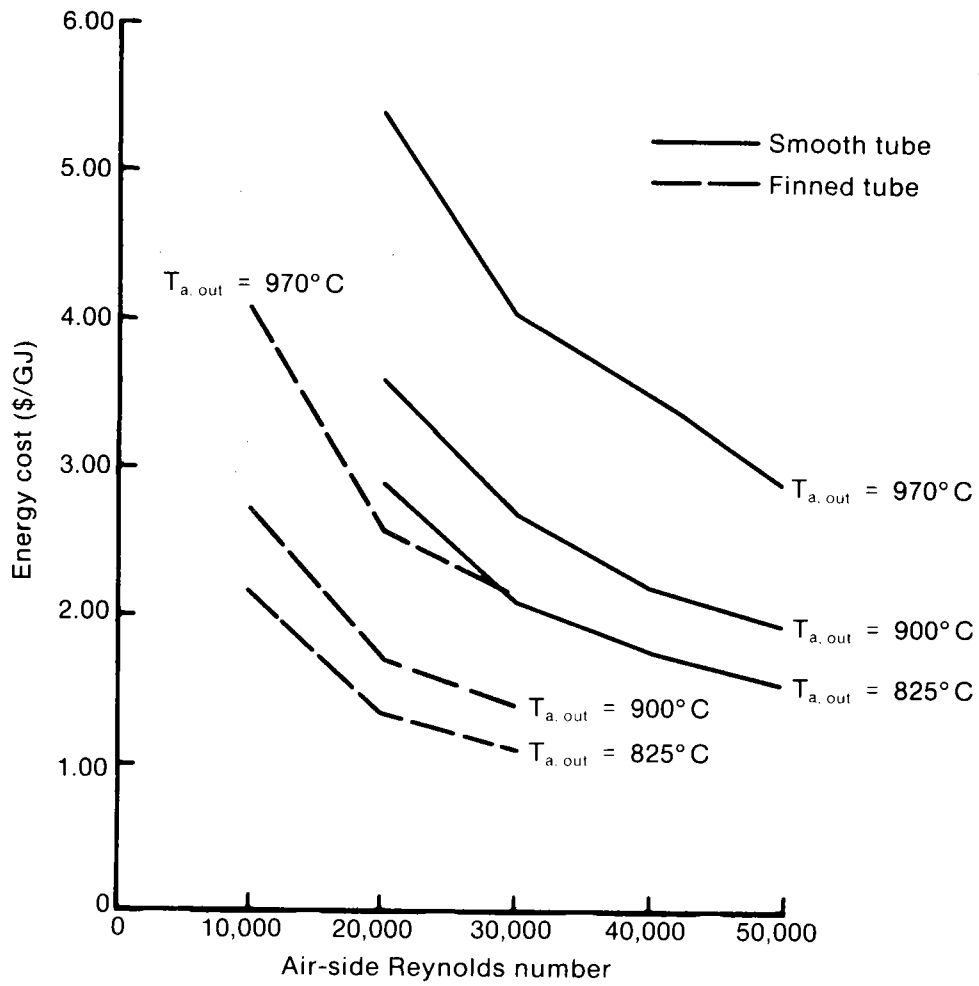|	Total (10^6 $)	Annual Levelized (10^6 $)
Capital investment		
Heat exchanger	10.06	2.24
Piping	0.40	0.09
Total capital investment	10.46	2.33
Annual costs		
Heat exchanger auxiliary power	0.08	0.15
Operation & maintenance	0.63	1.19
Total annual costs	0.71	1.34
Total annual levelized cost		3.67
Total annualized cost per unit of energy transferred		0.0105 $/kWh$_t$ 2.91 $/GJ 3.07 $/$10^6$ Btu

Figure 5-6.   Effect of Air-Side Flow Rate on Heat Exchanger Cost

6.0 CONCLUSIONS AND RECOMMENDATIONS

A direct-contact heat exchanger system was designed to transfer heat at a rate of 100 MW_t from 1000°C solid particles to air at 10 atm pressure. The annual levelized cost of thermal energy delivered from the system was estimated for two direct-contact configurations. The original configuration was based on the best information available on the state of the art of the various technologies involved and has an annual levelized cost per unit of delivered energy of $6.66/GJ. The best case configuration allowed for reasonable progress resulting from future development activities in several technologies and has a cost of $2.30/GJ. Much of the cost of the direct-contact configurations is in the solids-handling equipment--particle feeders and defeeders and the cyclones--and not in the heat exchanger itself. As an alternative to direct contact, a shell-and-tube heat exchanger was designed for the same service. The cost of this heat exchanger per unit of delivered energy is estimated to be $2.91/GJ.

These costs were calculated using a cost methodology developed by the SERI Solar Energy Storage Program. In addition, a cost methodology from the Solar Thermal Technology Program was used to allow comparison to the Solar Thermal cost goals. Using this methodology, the original configuration cost $4.64/GJ, the best case configuration cost $1.56/GJ, and the shell-and-tube configuration cost $2.03/GJ. All these costs are high compared to the Solar Thermal cost goal of $8.52/GJ ($9.00/10^6 Btu) for thermal energy delivered from a solar central receiver.

The direct-contact heat exchanger (DCHX) is a technically feasible option, though development is needed in several areas. Fluidized-bed behavior is well characterized, but data on fluidized-bed behavior with the particles that will actually be used in the system would greatly increase the confidence of design. We must resolve design details such as grid design for good air distribution, minimum stable bed depth, and the number of downcomers needed between stages to maintain uniform temperatures in the beds. Because of the high temperatures in the uppermost beds in the heat exchanger, materials for grid construction need to be examined.

Development of lockhopper valves to handle abrasive solids is needed to extend the temperature range of state-of-the-art valves beyond the current 650°C at 10 atm for 2000 cycles. Valves are needed that will operate at 1000°C at 10 atm pressure for 10,000 cycles. In particular, development of improved valve seat materials is needed. Confirmation of valve reliability is important because providing the capability for on-line valve maintenance significantly increased system cost.

For cyclone design, data are required on the extent of particle attrition in the receiver, in storage, and in transport. These attrition rates will determine the loading of fines into the cyclones, which in turn will dictate the number of cyclone stages needed and perhaps the pressure drop. Another important need is the confirmation of cyclone performance at high temperature and pressure. Advances in turbine technology allowing higher particle loadings would also be a benefit.

The DCHX can be economically competitive with shell-and-tube configurations if the valves noted above become available and if future developments indicate that only one stage, or perhaps no stages, of cyclones are needed. These assumptions were made for the best case configuration for which a DCHX system with one stage of cyclones is estimated to cost $2.30/GJ. This cost will be reduced if O&M costs are found to be less than the 6% of total capital cost assumed in this study. More information is needed on O&M costs for this type of system.

The shell-and-tube heat exchanger, unlike the direct-contact configuration, does not require extensive solids-handling equipment. Therefore the shell-and-tube heat exchanger has a lower cost that could be reduced even further by reducing the outlet air temperature or possibly by using tubes with heat transfer enhancement on the air side. In this study, we have not evaluated tube design or tube materials for the high-temperature regions of the heat exchanger. These issues appear to be the major technical uncertainties of the shell-and-tube configuration and may limit the operating temperature. Also, there seems to be less commercial experience with this type of heat exchanger than there is with equipment such as cyclones and fluidized beds.

This study is an evaluation of a particular subsystem, not a full system study. The specific values of many parameters used in the course of the study will significantly affect the cost and performance of the balance of the central receiver system. These parameters include solids mass flow rate, solids outlet temperature, and air outlet temperature. System studies will be needed to evaluate the impact of these parameters and to determine what portion of system cost should be allocated to the heat exchanger.

7.0 REFERENCES

Battleson, K. W., Apr. 1981, Solar Power Tower Design Guide, SAND81-8005, Livermore, CA: Sandia National Laboratories.

Boericke, R. R., R. Hantman, J. Kuo, and T. Mullen, Aug. 1980, "Assessment of Turbine Erosion by PFB Combustion Products," Proceedings of the 6th International Conference of Fluidized-Bed Combustion, Washington, DC: U.S. Department of Energy, CONF-800428, Vol. 2, pp. 724-728.

Bohn, M. S., Nov. 1983, Air/Molten Salt Direct-Contact Heat-Transfer Experiment and Economic Analysis, SERI/TR-252-2015, Golden, CO: Solar Energy Research Institute.

Brinn, M. S., S. J. Friedman, F. A. Gluckert, and R. L. Pigford, June 1948, "Heat Transfer to Granular Materials--Settled Beds Moving Downward through Vertical Tubes," Industrial and Engineering Chemistry, Vol. 40, No. 6, pp. 1050-1061.

Burolla, V. P., J. M. Hruby, and B. R. Steele, Aug. 1984, "High-Temperature Solar Thermal Energy Absorption with Solid Particles," Livermore, CA: Sandia National Laboratories. Presented at the Intersociety Energy Conversion Engineering Conference, San Francisco, CA, 19-24 Aug.

Carnavos, T. C., 1979, "Heat Transfer Performance of Internally Finned Tubes in Turbulent Flow," New York: ASME. Presented at the National Heat Transfer Conference, San Diego, CA, 6-8 Aug.

Denloye, A. O. O., and J. S. M. Botterill, 1977, "Heat Transfer in Flowing Packed Beds," Chemical Engineering Science, Vol. 32, Great Britain: Pergamon Press, pp. 461-465.

Department of Energy, Jan. 1983, Lockhopper Valve Testing and Development Program, DOE/METC/SP-193, Morgantown, WV: Morgantown Energy Technology Center.

Dubberly, et al., Nov. 1983, Comparative Ranking of Thermal Storage Systems, Volume II: Cost and Performance of Thermal Energy Storage Concepts in Solar Thermal Systems, SERI/TR-631-1283, Golden, CO: Solar Energy Research Institute.

EPRI, June 1978, Technical Assessment Guide, EPRI PS-866-SR, Palo Alto, CA: Electric Power Research Institute.

Falcone, P. K., J. E. Noring, and J. M. Hruby, Feb. 1985, "Assessment of a Solid-Particle Receiver for a High-Temperature Solar Central Receiver System," SAND 85-8208, Livermore, CA: Sandia National Laboratories.

General Electric, June 1978, CFCC Development Program, Commercial Plant Hot Gas Shrouded Ducting Evaluation, FE-2357-33, Schenectady, NY: General Electric Company.

Knowlton, T. M., and D. M. Backhorchin, 1978, "Effect of Two Variables on Cyclone Performance," Coal Processing Technology, Vol. IV, pp. 122-127.

Kunii, D., and O. Levenspiel, 1977, Fluidization Engineering, Huntington, NY: Robert E. Krieger Publishing Co., Inc.

Kurochkin, Y. P., 1966, "Heat Transfer between Tubes of Different Sections and a Stream of Granular Material," Journal of Engineering Physics, Vol. 10, No. 6, pp. 759-763 (USSR).

Leith, D., and Dilip Mehta, 1973, "Cyclone Performance and Design," Atmospheric Environment, Vol. 7, Great Britain: Pergamon Press, pp. 527-549.

Martin, J., and J. Vitko Jr., Jan. 1982, ASCUAS: A Solar Central Receiver Utilizing a Solid Thermal Carrier, SAND 82-8203, Livermore CA: Sandia National Laboratories.

National Coal Board (IEA Grimethorpe) Ltd., Dec. 1983, Experimental Results of Test Series 2 Hot Commissioning Test Program, DOE/ET10393-1530, Morgantown, WV: Morgantown Energy Technology Center.

Parker, R., R. Jain, and S. Calvert, Apr. 1981, "Particle Collection in Cyclones at High Temperature and Pressure," Environmental Science Technology, Vol. 15, No. 4, pp. 451-458.

Peters, M., and K. Timmerhaus, 1980, Plant Design and Economics for Chemical Engineers, 3rd Edition, New York: McGraw Hill.

Whitaker, S., 1972, "Forced Convection Heat Transfer Correlations for Flow in Pipes, Past Flat Plates, Single Cylinders, Single Spheres, and for Flow in Packed Beds and Tube Bundles," AIChE Journal, Vol. 18, pp. 361-371.

Williams, T. A., 1985, "Long-Term Performance and Cost Goals for Solar Thermal Technology," PNL-SA-13036, Richland, WA: Pacific Northwest Laboratory. Presented at the ASME Winter Annual Meeting, Miami Beach, FL, 17-22 Nov.

Wright, et al., Feb. 1981, "Selection and Conceptual Design of an Advanced Thermal Energy Storage Subsystem for Commercial-Scale (100-MWe) Solar Central Receiver Power Plant," SAND80-8190, Livermore, CA: Sandia National Laboratories (prepared by Babcock and Wilcox).

Zenz, F. A., Feb. 1962, "Use Fluid Data for Solids Flow Rates," Hydrocarbon Processing and Petroleum Refiner, Vol. 41, No. 2, pp. 159-168.

Zenz, F. A., Inc., 1982, State-of-the-Art Review and Report on Critical Aspects and Scale-Up Considerations in the Design of Fluidized-Bed Reactors--Final Report on Phase I, DOE/MC/14141-1158, Morgantown, WV: U.S. Department of Energy, Morgantown Energy Technology Center.

Zenz, F. A., Inc., 1983, State-of-the-Art Review and Report on Critical Aspects and Scale-Up Considerations in the Design of Fluidized-Bed Reactors--Final Report on Phase II, DOE/MC/14141-1304, Morgantown, WV: U.S. Department of Energy, Morgantown Energy Technology Center.

APPENDIX A.   COSTING METHODOLOGY FOR SERI'S SOLAR ENERGY STORAGE PROGRAM

To ensure comparable cost projections, a consistent methodology and constant financial and economic parameters should be used both by SERI in-house researchers as well as by subcontractors.

The cost methodology adapted is the one developed by the Jet Propulsion Laboratory [1].

The basic approach of the methodology is to devise an estimate of the costs incurred by the owner/operator of the system as a result of purchasing, installing, and operating the solar energy system under consideration. These costs, aggregated over the system lifetime and converted to an annual basis, are divided by the expected yearly system output. The result is an estimate of the levelized annual cost per unit of output. This levelized cost is the price that must be charged per unit of output so that the resultant revenues would exactly recover the full cost of the system over its expected life. If the levelized annual cost per unit is less than the levelized cost of the same output provided by other means, the system is cost-effective.

The nomenclature and symbols used in this section are explained in Table A-1.

The basic equation for the levelized cost is

$$LOC = AC/O .\tag{A-1}$$

The levelized annual system cost in Y_b dollars is computed from the capital expenditures and their timing, as well as the operating and maintenance cost stream. Note that replacement item capital costs are treated as capital expenditures.

The levelized annual system cost is given by:*

$$AC = (1 + g)^{-d} [FCR \cdot CI_{pv} + CRF_{K,N} (O\&M_{pv} + FL_{pv})] .\tag{A-2}$$

The annualized fixed charge rate (FCR) is the factor by which CI_{pv} must be multiplied to obtain the contribution of capital investment to the levelized annual system cost.

The capital recovery factor (CRF) represents the uniform annual amount (payment) that must be made to fully amortize the capital investment (loan) over N years at the interest rate of K.

$$FCR** = \frac{1}{1 - T} \left(CRF_{K,N} - \frac{T}{N}\right) + b\tag{A-3}$$

---

*Present value refers to the first year of commercial operation, Y_{co}.

**Disregarding investment tax credit. With investment tax credit FCR is given in Eq. A-4.

Table A-1. Nomenclature

Symbol	Description
a	Investment tax credit fraction
AC	Levelized annual system cost in Y_b dollars
ACRS	Accelerated cost recovery system
b	Annual insurance and "other tax" fraction
CI	Capital expenditures
CRF	Capital recovery factor
d	Time difference
DPF	Depreciation factor for sum-of-the-years-digits depreciation
FCR	Annualized fixed charge rate
FL	Fuel cost
g	Annual rate of general inflation
g_c	Annual escalation rate for capital costs
g_f	Annual escalation rate for fuel costs
g_o	Annual escalation rate for operation and maintenance costs
j	Time difference
K	Cost of capital (rate of return on capital, discount rate)
LOC	Levelized annual cost per unit of output
n	Accounting lifetime (depreciation life or tax life)
N	System operating lifetime
O&M	Operating and maintenance costs
p	Time difference
Q	Annual system output as measured in MJ
SDF	Depreciation factor for statutory accelerated depreciation
T	Effective corporate income tax rate
V	Levelized annual value of system output
V_o	Value of system output in year Y_{co} expressed in Y_b dollars
Y_b	Base year for constant dollars
Y_{co}	First year of commercial operation
Y_p	Price year for cost information
Y_t	Year t

Subscript

n	Accounting lifetime
N	System operating lifetime
o	Cost year Y_{co} expressed in Y_b dollars
pv	Present value (year Y_{co} value)
t	Time

$$FCR = \frac{CRF_{K,N}}{1 - T} [1 - (T \cdot DPF_{K,n}) - a] + b \tag{A-4}$$

$$CRF_{K,N} = K/[1 - (1 + K)^{-N}] . \tag{A-5}$$

The present value of the capital expenditures and of the operating and maintenance costs is computed using typical discounting formulas. In calculating the present value of the operating and maintenance costs, we assume that these costs are uniform streams over the system lifetime.

$$CI_{pv} = (1 + g_c)^P \sum_t CI_t \left(\frac{1 + g_c}{1 + K}\right)^j \tag{A-6}$$

$$O\&M_{pv} = (1 + g_o)^P \cdot O\&M_o \left(\frac{1 + g_o}{K - g_o}\right) \left[1 - \left(\frac{1 + g_o}{1 + K}\right)^N\right] \quad \text{if } K \neq g_o \tag{A-7}$$

$$(1 + g_o)^P \cdot O\&M_o \cdot N \qquad\qquad\qquad \text{if } K = g_o$$

$$p = Y_{co} - Y_p \tag{A-8}$$

$$j = Y_t - Y_{co} + 1 \tag{A-9}$$

$$d = Y_{co} - Y_b . \tag{A-10}$$

Note that CI_{pv} and $O\&M_{pv}$ are in year Y_{co} dollars. Adjustment to Y_b dollars is made when calculating AC.

$O\&M_o$ is the cost in year Y_{co} expressed in Y_p dollars. CI_t is the capital investment during year Y_t expressed in Y_p dollars.

For nonuniform operating and maintenance costs, $O\&M_{pv}$ is calculated from:

$$O\&M_{pv} = (1 + g_o)^P \cdot \sum_{j=1}^N O\&M_t \left(\frac{1 + g_o}{1 + k}\right)^j . \tag{A-11}$$

Based on the present value estimates for the capital expenditures, the recurrent costs, and operating and maintenance costs, the annual levelized system cost is calculated. This annualized system cost is equal to a cost stream of equal annual payments that has a present value equal to that of all the system costs (i.e., capital expenditures and operating, maintenance, and fuel costs).

For storage subsystem analysis, where several options for storage are considered, and where no annual system output can be associated with the subsystem (but only a storage capacity), present worth for capital costs, operation and maintenance costs, and fuel costs (gas, oil, or electricity) may be used in the trade-off.

For accounting purposes, the capital investment must be depreciated over a number of years. For the equipment under consideration the accounting life-time is 15 years. According to the tax law of 1981, the accelerated cost recovery system (ACRS) may be used. For investments after 1985, the depreciation factor for statutory accelerated depreciation is:

$$SDF_{K,N} = \frac{1}{n(1 + K)} \left\{ 1 + \frac{2}{CRF_{K,(n-1)}} - \frac{2(1 + K)}{nK^2} \left[1 - \frac{1 + nK}{(1 + K)^n} \right] \right\}. \quad (A-12)$$

The accelerated depreciation schedule for a public utility (15-year accounting life) is shown in Table A-2.

Annual Output Value

The basic equation for the levelized cost requires an estimate of the system output.

The output value should also be expressed as a levelized annual value using the same discount and inflation factors given in Table A-3. To calculate the levelized value of the output the following expression is used.

$$V = V_0 \left(\frac{1 + g}{K - g} \right) \left[1 - \left(\frac{1 + g}{1 + K} \right)^N \right] \cdot CRF_{K,N}. \quad (A-13)$$

Table A-2. **Accelerated Depreciation Schedule for Public Utility Placed into Service after 31 December 1985 (in percent)**

If the year since installation is:	Applicable percentage
0	7
1	12
2	12
3	11
4	10
5	9
6	8
7	7
8	6
9	5
10	4
11	3
12	3
13	2
14	1

Table A-3. Financial Parameters for Preliminary Economic Analyses

Symbol	Description	Value
N	System operating lifetime (years)	30
n	Accounting lifetime (years)	15
K	Cost of capital (rate of return on capital, discount rate)	0.10^a
$CRF_{K,N}$	Capital recovery factor (10%, 30 years)	0.10608
g	Rate of general inflation	0.06
g_c	Escalation rate for capital costs	0.06
g_o	Escalation rate for operating and maintenance costs	0.06
g_f	Escalation rate for fuel costs	0.08
Y_b	Base year for constant dollars	1981
Y_{co}	First year of commercial operation	1990
Y_p	Price year for cost information	1981
	Raw land cost	$1.25/m^2$
	1990 costs in 1981 dollars for:	
	Natural gas	$6.30/GJ
	Residual oil (No. 6)	$7.49/GJ
	Distillate oil	$8.91/GJ
	Liquid gas	$6.83/GJ
	Coal	$2.28/GJ
	Electricity	$12.89/GJ
FCR	Annualized fixed charge rate	0.19216
b	Annual insurance + "other tax" fraction	0.02
a	Investment tax credit fraction	0.10
T	Effective corporate income tax rate	0.50

[a]Typical for utility applications. Cost for industrial applications may be higher.

For the given values of the discount factor and the inflation rate, the above expression for the levelized annual output value reduces to:

$$V = 1.88584 \, V_o \; .$$

The financial parameters to be used are given in Table A-3.

Capital Investment Estimation

Cost estimation for capital equipment shall use the methodology and factors given in Refs. 2 and 3.

Cost Comparisons

For energy storage cost estimates, the capital investment in Eq. A-6 can be approximated by:

$$CI_t = F_1[F_2(A) + F_3(B)] ,\qquad\qquad\text{(A-14)}$$

where

A = energy and power related capital costs of system

B = storage medium cost

F_1 = nondirect costs factors

F_2 = installation cost factor for A

F_3 = installation cost factor for B.

The magnitude of the factors F_1, F_2, and F_3 vary widely for various groups that have made cost estimates. Table A-4 shows the values for these factors.

For SERI work, the factor per Ref. 3 shall be used. Deviations from these factors must be justified.

Table A-4. F-Factors

Source	F_1	F_2[b]	F_3[c]	$(F_1) \times (F_2)$
Ref. 3	1.95	1.80	1.0	3.51
Industry practice[a]				
Maximum	2.5	2.0	2.0	5.0
Minimum	--	--	1.0	3.0
JPL	1.2	1.0	1.0	1.2
SNLL	1.155	--	--	TBD
SNLA	1.25	--	--	TBD
Solar Thermal Cost Goals Committee	1.25	TBD	TBD	TBD
Copeland (6/81-2/82)	1.44	1.8	1.0	2.59

[a]According to Stearns-Roger Services, Inc.

[b]The installation cost factor is based on the primary equipment cost. It gives an estimate for the labor cost to install the equipment.

[c]F_3 is the labor cost factor to install the storage medium.

REFERENCES

1. Doane, J. W., R. P. O'Toole, R. G. Chamberlain, P. B. Bos, and P. D. Maycock, The Cost of Energy from Utility-Owned Solar Electric Systems--A Required Revenue Methodology for ERDA/EPRI Evaluations, ERDA/JPL-1012-76-3, Pasadena, CA: Jet Propulsion Laboratory, June 1976.

2. Peters, M. S., and K. D. Timmerhaus, Plant Design and Economics for Chemical Engineers, 3rd Edition, New York: McGraw-Hill Book Company, 1980.

3. Cost and Performance of Thermal Storage Concepts in Solar Thermal Systems, Final Report Phases 1 and 2, SERI/TR-XP-0-9001-1-A and -B. November and December 1981. Prepared by Stearns-Roger Services Inc., Denver, CO. Available from NTIS.

APPENDIX B

CRITICAL REVIEW

OF THE STATE OF THE ART

OF PARTICLE-GAS HEAT EXCHANGERS

ELIZABETH FISHER

DAVID H. JOHNSON

SOLAR ENERGY RESEARCH INSTITUTE
1617 COLE BLVD.
GOLDEN, CO 80401

OBJECTIVES OF THIS ACTIVITY

COLLECT AND REVIEW EXISTING INFORMATION ON SAND TO AIR
DIRECT CONTACT HEAT EXCHANGERS AND RELATED EQUIPMENT
OPERATING AT HIGH TEMPERATURE AND PRESSURE.

DETERMINE THE OPTIONS FOR EACH COMPONENT OF THE SAND
TO AIR DCHX SUBSYSTEM TO BE INCLUDED IN A CONCEPTUAL
DESIGN AND COST ESTIMATE.

APPROACH

CHOOSE A BASELINE SET OF COMPONENTS WHICH BEST SATISFY
BASIC PERFORMANCE CRITERIA AND FOR WHICH SUFFICIENT
INFORMATION EXISTS TO DEVELOP AN OPTIMIZED DESIGN FROM
WHICH COST MAY BE ESTIMATED.

IF POSSIBLE, IDENTIFY AN OPTION FOR EACH COMPONENT OF
THE BASELINE WHICH HOLDS THE POTENTIAL FOR IMPROVED
PERFORMANCE.

OUTLINE

I.COMPONENTS
    A.HEAT EXCHANGER
        1.OPTIONS
            a.FLUIDIZED BED
                i.SINGLE-STAGE
                ii.MULTI-STAGE
            b.FALLING BED
                i.FREE
                ii.HINDERED
            c.MOVING BED
            d.CASCADING BED
            e.STAGED CYCLONES
        2.HEAT TRANSFER
            a.CONVECTION AND CONDUCTION ONLY
            b.INCLUDING RADIATION
        3.FLUID MECHANICS
    B.FEEDER
        1.LOCK HOPPER
        2.PISTON
        3.POCKET
        4.SCREW
        5.INERTIAL PLUG
        6.RAM
    C.SEPARATOR
        1.AIR QUALITY REQUIREMENTS
        2.OPTIONS
            a.CYCLONE
            b.ELECTROCYCLONE
            c.FILTER
            d.PACKED BED
    D.COMPRESSOR
    E.INSULATION

II.INDUSTRY
    A.INVENTORS AND MANUFACTURERS
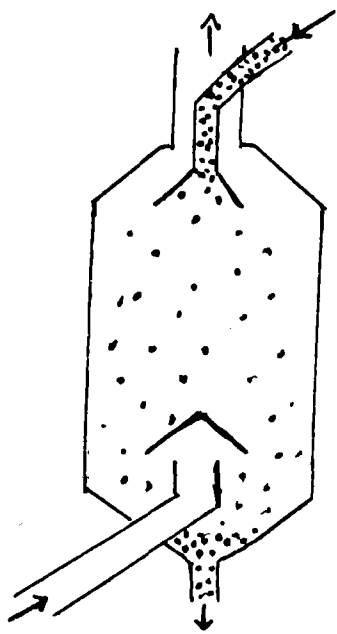   B.APPLICATIONS
        1.WASTE HEAT RECOVERY
        2.CAT CRACKING
        3.MHD
        4.PRESSURIZED FLUIDIZED BED

Baseline DCHX Subsystem
And Options To Be Explored

FEEDER

BASELINE: PISTON
OPTION: INERTIAL PLUG

SAND/AIR
DIRECT
CONTACT
HEAT
EXCHANGER

SEPARATOR

BASELINE: STAGED CYCLONE
OPTION: ELECTROCYCLONE FOR
LAST STAGE(S)

BASELINE: MULTISTAGED
FLUIDIZED BED

OPTION: FALLING BED

COMPRESSOR

FREE FALLING BED

SINGLE-STAGE FLUIDIZED BED
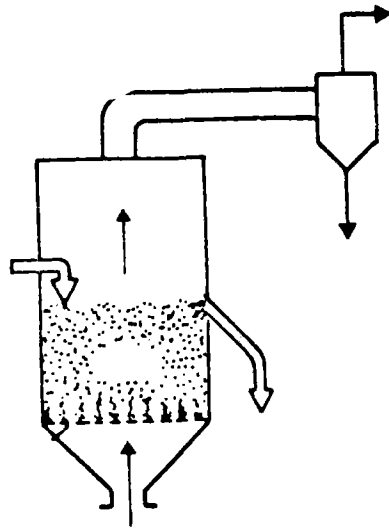
HINDERED FALLING BED

MULTI-STAGE
FLUIDIZED BED

CASCADING BED

STAGED CYCLONES

PRECIPITATOR

KILN EXH FAN

DUST RETURN

RAW MEAL FEED

TO BY-PASS

KILN

MOVING BED

HOT AIR
OUTLET

M

COLD AIR
INLET

H
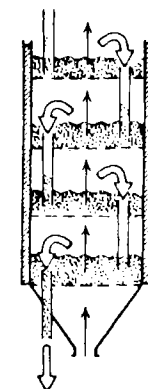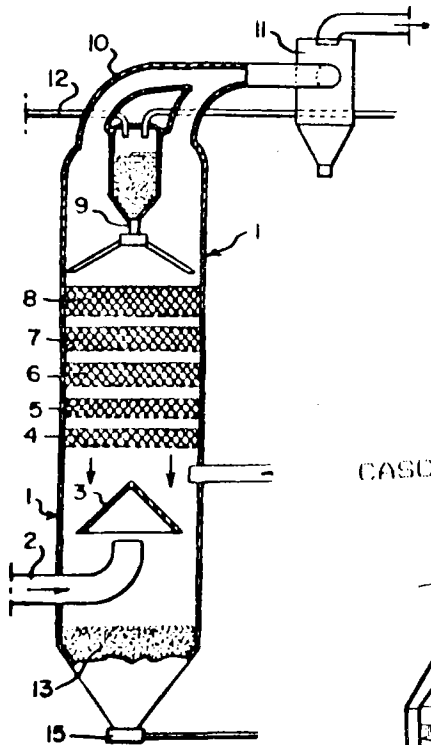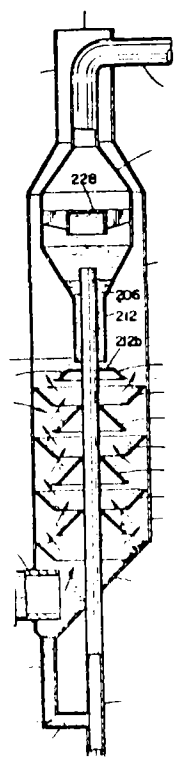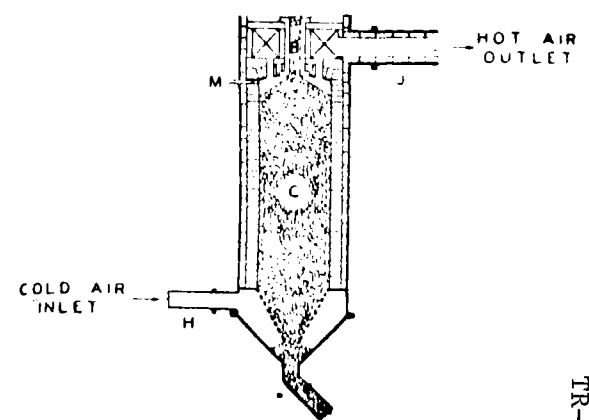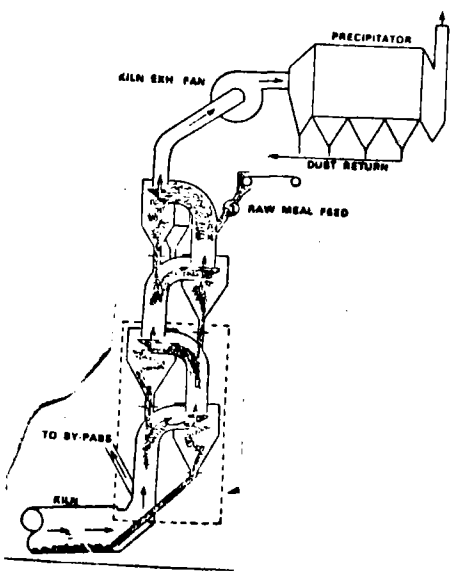
Information on Particle/Gas Heat Exchangers

	Heat Transfer (Ambient)	Heat Transfer (High T)	Heat Transfer (High P)	Fluid Mechanics (Ambient)	Fluid Mechanics (High T)	Fluid Mechanics (High P)
Free Falling Bed	2	1		2		
Hindered Falling Bed	2			2		
Multistage Fluidized Bed	2	2	2	2	2	2
Moving Bed	1	1		2		

2 = DIRECTLY RELATED INFORMATION

1 = INFORMATION FROM ANOTHER SYSTEM THAT CAN BE APPLIED.

FLUIDIZED BED
FLUID MECHANICS
AT AMBIENT TEMPERATURE AND PRESSURE

REFERENCES: ERGUN (1952), ERGUN AND ORNING (1949)

SUMMARY: THE PRESSURE DROP ACROSS A FIXED AND EXPANDED BED IS GIVEN BY

$$\frac{\Delta P}{L} = 150 \frac{(1-\epsilon)^2}{\epsilon^3} \frac{\mu U_M}{D_P^2} + 1.75 \frac{(1-\epsilon)}{\epsilon^3} \frac{\rho U_M}{D_P}$$

WHEN THE PRESSURE DROP EQUALS THE BOUYANT WEIGHT OF THE PACKING PER UNIT VOLUME OF THE BED,

$$\frac{\Delta P}{L} = (1-\epsilon) (\rho_P - \rho_F) g ,$$

THE BED BEGINS TO EXPAND. WHILE THE BED EXPANDS THE PRESSURE DROP REMAINS CONSTANT AND THE VOID FRACTION IS GIVEN BY SUBSTITUTING EQUATION 2 IN EQUATION 1.

THE EXPANSION IS HOMOGENEOUS UNTIL THE BED ATTAINS THE LOOSEST STABLE CONFIGURATION OF THE SOLIDS (FOR SPHERES THIS IS A CUBICAL PACKING WITH   = 0.47). AN ADDITIONALINCREASE IN FLOW RATE CAUSES BUBBLES OF GAS TO PASS THROUGH THE BED. THE BED IS NOW FLUIDIZED.

FLUIDIZED BED
FLUID MECHANICS
EFFECT OF GREATER THAN AMBIENT TEMPERATURE

REFERENCE: BOTTERILL, TEOMAN, AND YUREGIR (1982 A AND B)

EXPERIMENTAL
CONDITIONS:

PRESSURE: AMBIENT
GAS: AIR
GAS INLET
 TEMP.: $20^{\circ}C$ TO $960^{\circ}C$
PARTICLE
 MATERIALS: SAND, COAL ASH, ALUMINA, GLASS BALLOTINE

PARTICLE MEAN DIAMTERS (MM): SAND - 0.38, 0.46, 0.53, 0.66, 0.78, 0.89, 1.28, 2.32; COAL ASH - 0.82 WITH A WIDE DISTRIBUTION; ALUMINA - 0.37, 0.98, 1.12; GLASS BALLOTINE - 1.04

PARTICLE SHAPE FACTORS: SAND - 0.90, 0.80, 0.84, 0.92, 0.97, 0.95, 0.74, 0.64; COAL ASH - UNDETERMINED; ALUMINA - 0.88, 0.56, 0.54; GLASS BALLOTINE - 1.00

MEASUREMENTS: MEASURED THE MINIMUM FLUIDIZING GAS SPEED AND THE VOIDAGE AT MINIMUM FLUIDIZATION

RESULTS: E_{MF} VARIES WITH TEMPERATURE.

VARIATION OF U_{MF} WITH TEMPERATURE AGREES WELL WITH ERGUN EQUATION WHEN VARIATION OF E_{MF} IS TAKEN INTO ACCOUNT.

THERE IS A TRANSITION BETWEEN TYPE B&D BEHAVIOR WHEN $Re_{MF} = 12.5$ AND $Ar = 26000$

COMMENTS: NO EXPLANATION GIVEN FOR WHY E_{MF} VARIES WITH TEMPERATURE.

FLUIDIZED BED
FLUID MECHANICS
EFFECT OF GREATER THAN AMBIENT PRESSURE

REFERENCE: KAWABATA ET.AL. (1981)

EXPERIMENTAL CONDITIONS:

TEMPERATURE: AMBIENT
GAS: AIR
GAS PRESSURE: 0.1 MPA TO 0.8 MPA
PARTICLE
 MATERIALS: SILICA SAND
PARTICLE MEAN
 DIAMETERS (MM): 0.30, 0.43, 0.60
APPARATUS: TWO DIMENSIONAL COLUMN OF 10 x 300 MM
              INSIDE CROSS-SECTION AND 450 MM HEIGHT

MEASUREMENTS:
 MINIMUM FLUIDIZATION VELOCITY, BED EXPANSION, BED HEIGHT
 FLUCTUATIONS, AND BUBBLE SIZE DISTRIBUTION, RISING VELOCITY,
 AND FREQUENCY AS A FUNCTION OF PRESSURE WITH PARTICLE SIZE AS
 A PARAMETER.

RESULTS:
 THE MINIMUM FLUIDIZATION VELOCITY DECREASES WITH PRESSURE AND
 THIS EFFECT IS GREATER FOR LARGER PARTICLES. THIS BEHAVIOR
 IS IN AGREEMENT WITH THE ERGUN EQUATION.

 THE BED EXPANDS FASTER WITH EXCESS GAS SPEED AT HIGH PRESSURE THAN
 AT LOW AND THIS EFFECT IS GREATER FOR LARGER PARTICLES, BUT THE
 BED HEIGHT FLUCTUATIONS ARE UNCHANGED BY PRESSURE. THESE RESULTS
 ARE ATTRIBUTED TO AN INCREASE IN THE WIDTH OF BUBBLES WITH PRESSURE
 RESULTING IN DECREASED BUBBLE VELOCITY AND INCREASED HOLDUP AND
 THUS BED EXPANSION WITHOUT AN INCREASE IN BED HEIGHT FLUCTUATIONS.

COMMENT:
 MEASUREMENT OF BUBBLE CHARACTERISTICS DIFFICULT AND MAY HAVE
 LARGE ERROR. RESULTS IN 3-D MAY BE DIFFERENT THAN IN 2-D.

HEAT TRANSFER: FLUIDIZED BEDS: RADIATION

REFERENCES: Chen and Chen (1981); Botterill et al (1982)

CHEN AND CHEN

Model for bed-to-wall heat transfer including radiation in a bubbling fluidized bed

* A portion of the wall is in contact with either a bubble or a "packet" of the solid-gas "emulsion". The emulsion is at bed temperature when it first comes into contact with the wall ; it loses heat to the wall by conduction and radiation before it is swept away.

* Heat transfer when a bubble is in contact with the wall is treated as radiation between parallel plates. (The wall and the bubble/emulsion interface are the plates.) When the emulsion is in contact with the wall, heat transfer is treated as a combination of conduction and radiative heat exchange between a wall and a scattering, absorbing, and emitting medium.

To apply this model, it is necessary to know:
    * residence time of an emulsion packet at the wall
    * fraction of time the wall is in contact with bubbles
    * absorption and back-scattering coefficients of emulsion packets
    * effective emissivity of the bubble-emulsion interface
   * wall emissivity
    * emulsion packet emissivity.

Many of these quantities are not readily available. Thus, it is difficult to use the model.

Using estimates of these values based in part on the properties of fixed beds, Chen and Chen achieved good agreement with the experimental results of an earlier investigator. It is not clear how sensitive the predictions are to the choice of values for the unknown quantities.

BOTTERILL ET AL.

Experiment of the behavior of fluidized beds at high temperatures.

Experimental Conditions: see FLUID MECHANICS: FLUIDIZED BEDS: HIGH TEMPERATURE
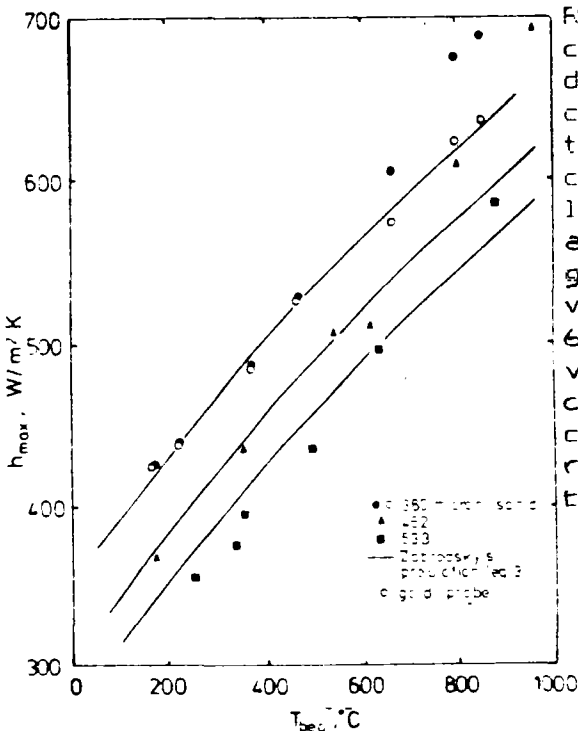
Results: Botterill et al. measured heat transfer coefficients from a fluidized bed to surfaces of different emissivities in order to determine the contribution of radiation. They found (see graph) that the measured maximum heat transfer coefficient was well predicted by the empirical correlation of Zabrodsky at low temperatures and when a cold probe was used. (Radiative transfer to a gold surface is small because of the low emissivity of gold.) However, for temperatures above 600 C and materials with reasonably high emissivities, they measured a larger heat transfer coefficient. In some cases, the heat transfer coefficient was as much as 14% higher. No correlation is provided for the radiative contribution.

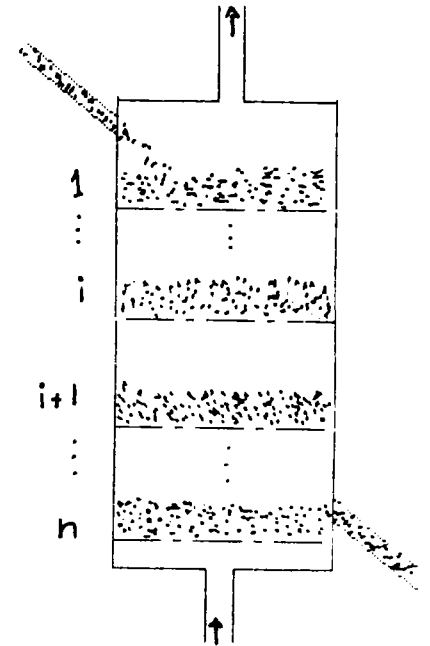# HEAT TRANSFER IN MULTI-STAGE FLUIDIZED BEDS AT HIGH TEMPERATURES

REFERENCES: Feyman and Laguerie (1980); Hood (1981)

IDEAL N-STAGE FLUIDIZED BED

* gas and particles leaving a given stage
  are at the same T

* wall losses and radiation are insignificant

efficiency $\quad \eta \equiv \dfrac{T_{g,out} - T_{p,out}}{T_{p,in} - T_{g,in}} = \dfrac{\gamma(\gamma^{n-1}-1)}{\gamma^{n+1}-1}$

where $\quad \gamma = \dfrac{\dot{m}_g \, c_{p,g}}{\dot{m}_p \, c_{p,p}}$
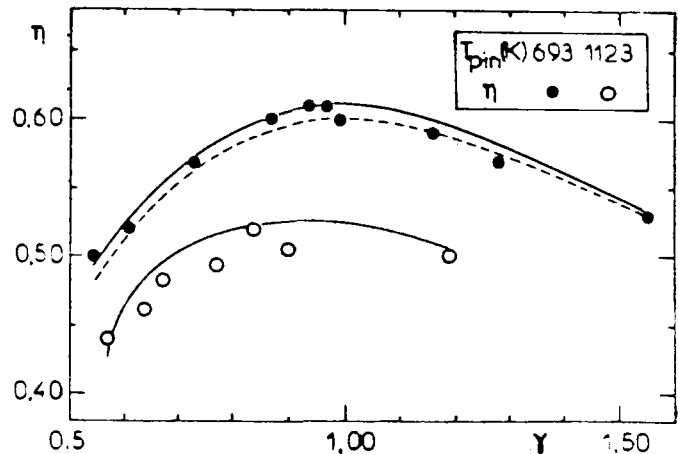
AT HIGH TEMPERATURE:

wall losses and radiative backmixing become important

model of Feyman and Laguerie includes:

* radiation between upper surface of bed and distributor plate above
(black bodies)

* conduction through wall

model of Hood includes:

* wall in radiative balance

* convection between gas and wall

* screens (radiation shields)

HEAT TRANSFER: MULTISTAGE FLUIDIZED BEDS: RADIATIVE HEAT TRANSFER

REFERENCES: Peyman and Laguerie (1980); Hood (1981).

PEYMAN AND LAGUERIE
MODEL
   * Gas and particles in a given stage are is thermal equilibrium with each other and with the distributor plate below them.
   * Radiative heat transfer occurs between the upper face of the fluidized bed and the lower face of the distributor plate above it, which act as black bodies. The wall acts as a refractory.
   * Radiative heat transfer has reduces the efficiency of a multistage fluidized bed because it has a "backmixing" effect.

$$\dot{m}_p\left(c_{p,p,i-1}T_{i-1} - c_{p,p,i}T_i\right) = \dot{m}_g\left(c_{p,g,i}T_i - c_{p,g,i+1}T_{i+1}\right) + L_i\left(T_{wi} - T_s\right)$$
$$+ R_{i,i+1}\left(T_i^4 - T_{i+1}^4\right) - R_{i-1,i}\left(T_{i-1}^4 - T_i^4\right)$$

EXPERIMENT
   * 4-stage heat exchanger
   * sand cooled by air
   * scale: diameters of stages: 145 mm, 185 mm
            height of beds: 75mm
   * particles: sand with mean diameter 0.29mm
   * temperature: inlet solids at 420 and 850 C
   * pressure: ambient

HOOD
MODEL
   * modification and extension of the model of Peyman
   * Convection occurs between the wall and the gas travelling between the fluidized bed and the next distributor plate
   * The wall does not act as a refractory.
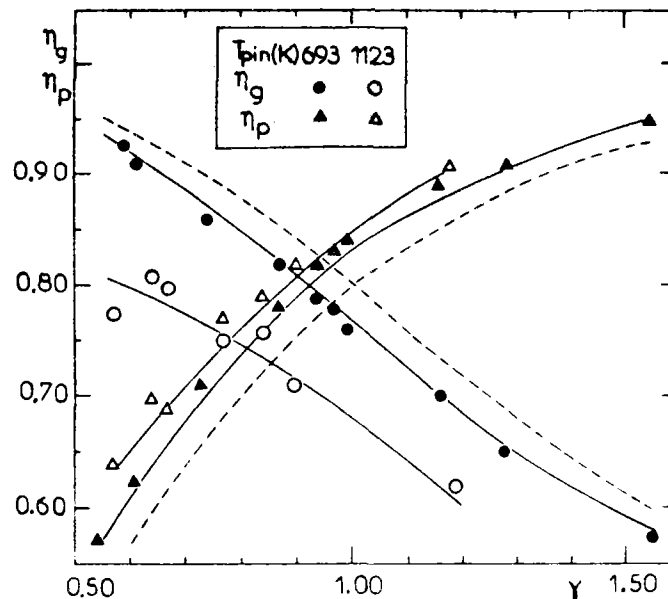   * Model can include screens (i.e. radiation shields) below the distributor plates.
EXPERIMENT
   * apparatus of Peyman
   * Only two stages were used when the screens were inserted.
   * Experiment agrees with the predictions of Hood's model to within 4% for temperature.

Results of Peyman, where

$$\gamma = \dot{m}_g c_{p,g} / \left(\dot{m}_p c_{p,p}\right)$$

$$\eta_g = \left(T_{g,out} - T_{g,in}\right) / \left(T_{p,in} - T_{g,in}\right)$$

$$\eta_p = \left(T_{p,in} - T_{p,out}\right) / \left(T_{p,in} - T_{g,in}\right)$$

SERI

HEAT TRANSFER: FALLING BED

REFERENCES: Kato et al (1983); Sanderson and Howard (1977)

Sanderson and Howard measured the heat transfer coefficient between heated air and particles and compared their results to the predictions of a simple model of heat transfer from a gas to a falling droplet or particle. They used terminal velocity correlations for single rigid spheres falling through a gas.

Experimental Conditions:
   * column dimensions: diameter: 0.15 m; height: 1.5 m.
   * particles: steel shot with mean diameter 364 microns
   * pressure: atmospheric
   * temperature: air inlet temperatures up to 154 C; LMTD up to 53 C
   * Rig and measurements were simple, and thus more representative of industrial than laboratory conditions.

Results:
A typical theoretical prediction for the heat transfer coefficient was 6.3E2 W/m K. Experimental results agreed reasonably well with the predictions except for some tests in which a high air flow rate produced a flow maldistribution at the column inlet. Poor flow conditions reduced the heat transfer coefficient. In some tests, screens were inserted to increase the residence time of particles in the column. This also made the air flow more uniform. No correlation was provided for the effect of screens.

Kato et al. measured heat transfer rates for the drying of alumina particles in a hindered falling bed heat exchanger.

Experimental Conditions:
   * column dimensions: 3 columns used-- d=.105 m, h=.6 m; d=.077 m, h=.4 m; d=.052 m, h=.4 m.
   * particles: alumina with diameter 832, 527, 480, 317 microns
   * pressure: atmospheric
   * temperature: gas inlet: 35 to 95 C; particle inlet: 14 to 35 C.

Results:

A correlation for the Nusselt number was obtained in terms of the void fraction and the particle Reynolds number.

Hindered Falling Bed
Fluid Mechanics
At Ambient Temperature and Pressure

Reference: Large, Guigon, and Bergougnon (1981)

**Experimental
Conditions:**

    Gas: Air

    Packing: 15 x 15 mm metal Pall rings

    Particle
     Material: Sand; particle mean diameter (mm) 0.19

Measurements: Visualization of flow patterns, pressure drop, solids hold-up

Results: The dry pressure drop of the packing is a significant portion of the total pressure drop.

At low superficial gas velocities sand trickled uniformly through the column

At high superficial gas velocities sand migrated vertically and sand and gas segregated radially.

The net solids hold-up increased with gas and solids flow rate up to the unstable regime.

The fraction of solids suspended in the gas was constant at 0.6 when the solid and gas flow rates varied.

Comment: The hydrodynamics of hindered falling beds depends on bed diameter.

The analogy between solid particle/gas flow and liquid/gas flow is very limited because the solid particles lack surface tension.

HEAT TRANSFER: FALLING CLOUD

REFERENCE: Sanderson and Howard (1977)

Sanderson and Howard measured the heat transfer coefficient between heated air and particles and compared their results to the predictions of a simple model of heat transfer from a gas to a falling droplet or particle. They used terminal velocity correlations for single rigid spheres falling through a gas.

Experimental Conditions:
* column dimensions: diameter: 0.15 m; height: 1.5 m.
* particles: steel shot with mean diameter 364 microns
* pressure: atmospheric
* temperature: air inlet temperatures up to 154 C; LMTD up to 53 C
* Rig and measurements were simple, and thus more representative of industrial than laboratory conditions.

Results:
A typical theoretical prediction for the heat transfer coefficient was $6.3E2$ W/m^2 K. Experimental results agreed reasonably well with the predictions except for some tests in which a high air flow rate produced a flow maldistribution at the column inlet. Poor flow conditions reduced the heat transfer coefficient. In some tests, screens were inserted to increase the residence time of particles in the column. This also made the air flow more uniform. No correlation was provided for the effect of screens.

SERI ◉

REFERENCES: GUZDAR AND HARVEY (1982), HAWRYCH (1981)

APPLICATIONS: FEEDING COAL AND BIOMASS TO HIGH PRESSURE
               GASIFIERS

TYPES:

LOCK HOPPERS - LARGE BINS WITH VALVES TO SHUT OFF
               SO THAT THEY CAN BE PRESSURIZED WITH
               A GAS AFTER FILLING.

PISTONS - SMALL LOCK HOPPERS WITH A PISTON REPLACING
          COMPRESSED GAS.

POCKETS (TWO TYPES):

ROTARY - SMALL LOCK HOPPERS ON A SHAFT WITH
         VALVES REPLACED BY SEAL BETWEEN
         BLADES AND HOUSING.

LINEAR - SMALL LOCK HOPPERS WITH HIGH
         PRESSURE AIR DISPLACED BY WATER.

SCREWS (TWO TYPES):

EXTRUDERS - A COMPACTED PLUG OF FEED
            MATERIAL IS FORMED AT LOW SPEED.

COMPRESSORS - A LOOSE PLUG OF FEED MATERIAL IS
              FORMED AT HIGH SPEED.

INERTIAL PLUGS (TWO TYPES):

GRAVITATIONAL - A MOVING BED OF FEED MATERIAL
                HIGH ENOUGH TO WITHSTAND ΔP

CENTRIFUGAL - A LOOSE PLUG OF FEED MATERIAL
              IS FORMED BY CENTRIFUGAL FORCE.

RAM - A COMPACTED PLUG OF FEED MATERIAL IS FORMED AND
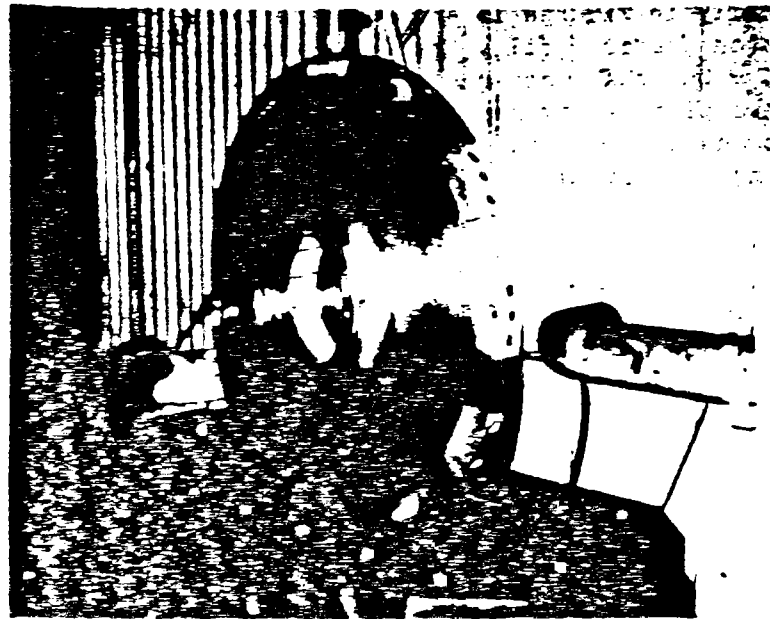   PUSHED INTO THE HIGH PRESSURE REGION.
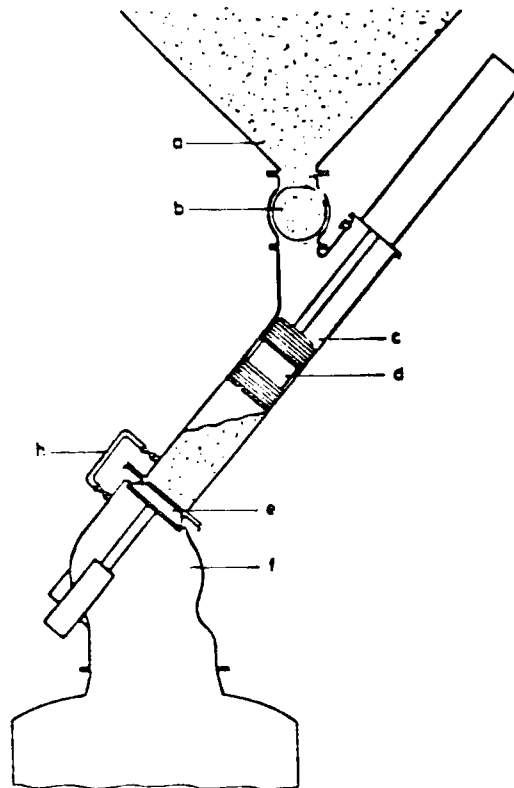
FIGURE 13. ROTOR
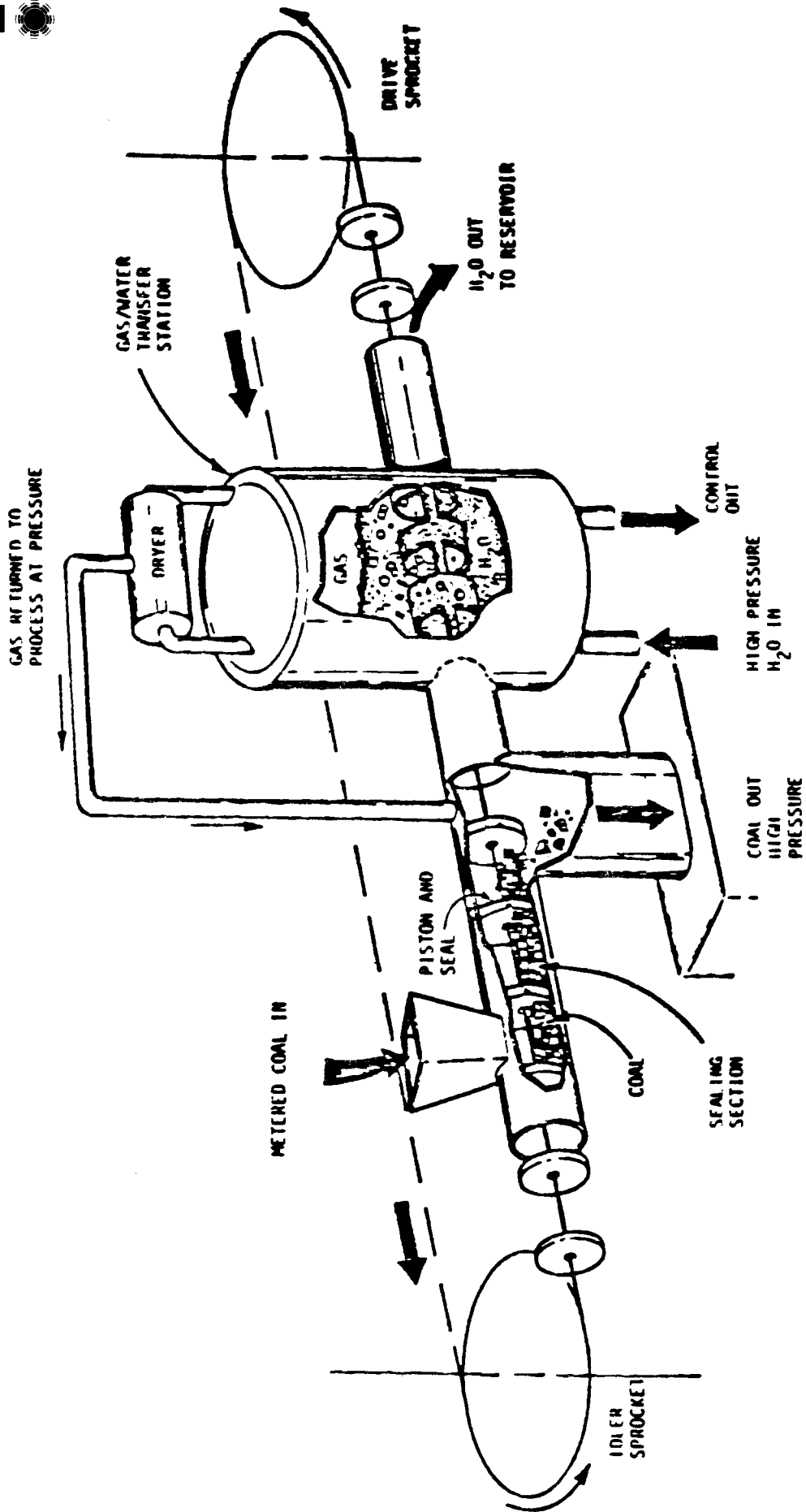

FIGURE 14. SCHLEFFER PISTON FEEDER
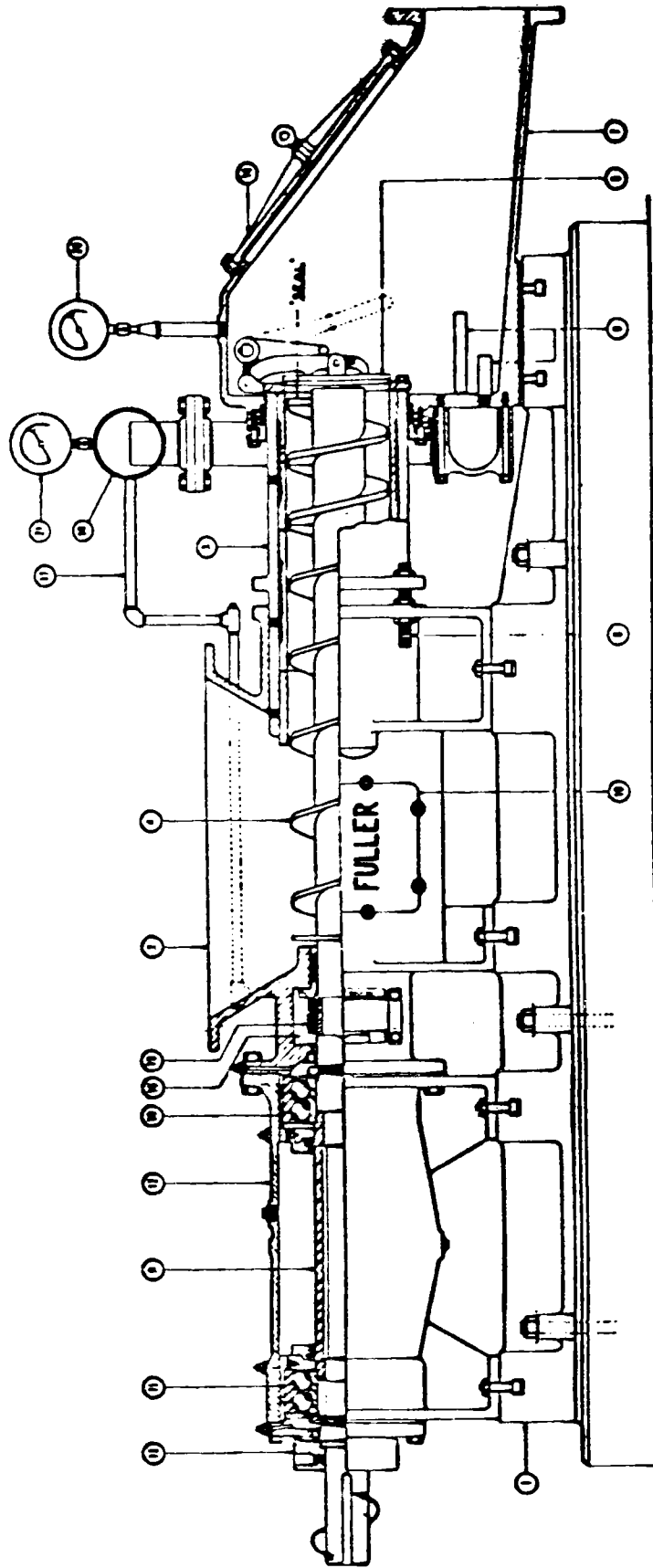
FIGURE 20. CUTAWAY VIEW

Figure 6. Fuller-Kinyon Pump

with hydrogen (not shown) the low end of the specific power range is reached by about 10 tons/hr. For high mass flow or light gas, performance for biomass should approach that for coal. Figure 12 shows a sketch of the Lockheed Kinetic Extruder and Figure 13, a photograph of the rotor.

Piston Feeder

A piston feeder is conceptually the same as a mini-lock hopper with a displacer piston to conserve the high pressure gas. Many types of piston feeders have been developed only three of which are described here briefly.

A Schlepper type piston feeder (14) is being developed by Lurgi to provide semicontinuous feed to its gasifier and to minimize gas compression costs. Figure 14 shows a schematic of this feeder. The cylinder is filled with coal from a bunker with the piston on its upper end position and the bottom outlet closed. It appears that a limited charge must be metered in order to provide smooth piston passage past the fill port. The piston then moves down to seal the cylinder compartment and hold the coal drops into the reactor. The piston is forced down to the lower cylinder end displacing almost all coal and gas from the cylinder. Bottom valve closure and piston retraction complete the feed cycle. A demonstration feeder is currently being built by Lurgi and is expected to be tested shortly (14).
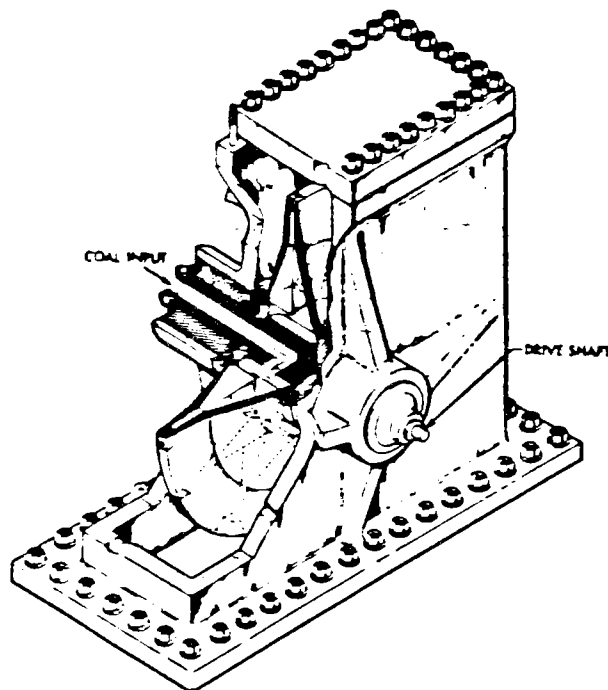

FIGURE 12. LOCKHEED KINETIC EXTRUDER

Sand/Air Heat Exchanger Feeder Ratings

E= Excellant G= Good F = Fair P= Poor U= Unacceptable

Requirement / Type	Controlled And Metered Feed Rate	Pressure Seal To 20 Atmospheres	Handle Particles of 1.0 to 0.1 m.m. Diameter	Economic Operation	Low Capital Cost	Reliable And Safe Operation	Potential To Operate At 1000°C
Lock Hopper (11)	Intermittent, Requires Pressurized Storage Hopper — P	Lurgi Pilot Plant Unit Operated To 1200 psi — E	Can Handle Any Size Up To 4", small particles wear valves — F	Pressurized Air Requirement Leads To High Operational Cost — U	Factor of 2 Greater than other Types — U	Years of Operational Experience, Problems with Valves and Holdup — F	Hopper Adaptable To High Temperature, Valves may not be — F
Piston (22)	Multiple Pistons Smooth Feed Rate Compared To Hopper — F	Ingersoll-Rand Unit Operated To 500 psi — E	Any size up to 4" but small particles may cause wear — G	Mechanical Action Leads To Low Power — E	A few percent less than Specific screw at 300 psi — G	Under Development. Can be Designed To Be Fail Safe — G	Piston Heads and Cylinder adaptable to High Temp. — G
Pocket Rotary	Quasicontinuous Controllable — G	Limited To 120 psi by Blade Leakage — U	Small particles will wear blades — F	requires pressurized air — P	Fairly simple Construction — F	Years of operating experience, blade wear a problem — F	Rotor can be adapted — G
Linear	Quasicontinuous controllable over wide range — G	Foster-Miller unit operated To 1000 psi — E	Small particles will wear plug — F	pressurized air replaced by water — E	15% more than screw or piston — F	500 hours of Testing. Fail Safe — G	Use of water unsuitable at high temp. — U
Screw	Continuous, Controllable over wide range — E	Fuller-Kinyon Pump Operated to 75psi — U	Can be designed to handle small particles — G	High speed rotation leads to medium operating expense — F	30% more than Centrifugal Inertial Plug — G	Internal "Flapper" Valve Can Provide Fail Safe Design — F	screw expensive to adapt, Flapper valve may give trouble — F
Inertial Gravitational	Continuous Controllable — E	Limited By Height of Column — G	very small particles without wear — E	mechanical lifting is Efficient — E	Simplicity Leads To Low Cost — E	Years of Low ΔP experience Not Fail Safe — F	Cylinder easily adaptable — G
Centrifugal	Continuous, Controllable over a range — E	Lockheed unit Tested To 400 psi — E	very small particles with little wear — E	Low specific power below 500 psi — G	Simplicity Leads To Low Cost — E	100 Hours of Testing. Not Fail Safe — P	Rotor and Feed pipe adaptable — G

AIR-SOLIDS SEPARATORS: AIR QUALITY REQUIREMENTS FOR THE TURBINE

REFERENCE: Boericke et al. 1977

Evaluation of the problem of turbine blade erosion by particles, directed
towards power generation from pressurized fluidized bed combustion.
Gases from presurized fluidized bed combustors (PFBC) have similar temperature
(790 to 950 C) and pressure (approx. 16 atm.) to the air leaving the heat
exchanger in our application. PFBC turbine blade environment is somewhat
harsher because the combustor gases are corrosive.
Boericke at al. based their recommendations for allowable particulate
concentration on several tests, the conditions of which are summarized below:

| TEST	PRESSURE	TEMPERATURE	LENGTH OF TEST
coal-fired locomotive	4.8 atm.	?	2000 hrs
GE erosion rig	1 atm.	480-870 C	600 hrs
PFB cascade	5.6 atm.	840 C	2x1000 hrs
Cat-cracker	3 atm.	650 C	used in industry

RESULTS
    * Erosion increases rapidly with particle size. Particles smaller than 8
microns do not cause measureable erosion.
    * Cat-cracker experience, which involves erosion by a highly abrasive
catalyst similar to the particulate matter of our heat exchanger, indicates
ssomewhat higher allowable particle concentrations than the combustion tests.
However, materials available for turbine blades at those temperatures are more
erosion-resistant than high-temperature materials.

In applying the results of these tests to the particular turbine of interest,
Boericke noted that:
    * Increasing the pressure increases the particle flowrate for a given
concentration.
    * Erosion rate is proportional to V^n , where V is the relative velocity of
the particles and the blade, and n is aconstant between 2 and 5. $n \simeq 2.3$ for
some materials of interest.
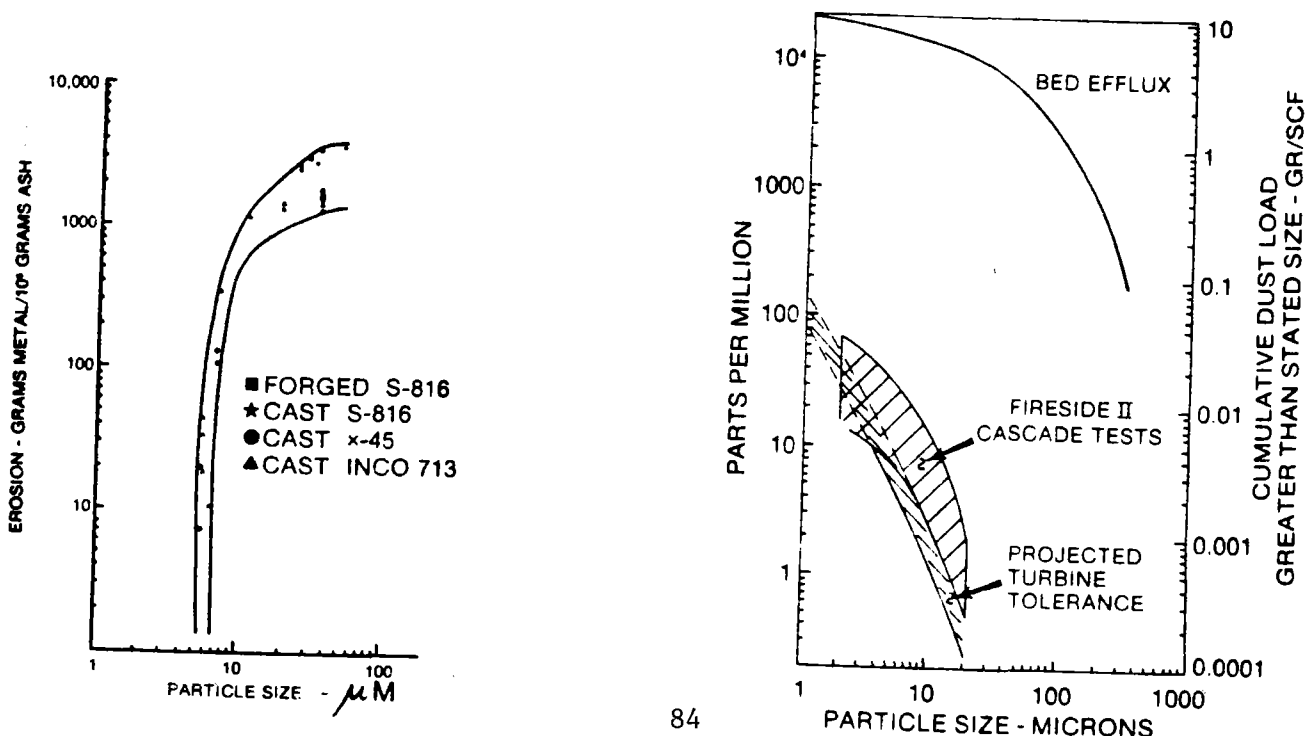
SEPARATORS

REFERENCES: Boericke et al.(1981); Brooks et al.(1981); Casal and Martinez-Benet (1983); Fraas et al.(1979); Keairns et al.(1980); Mathers et al. (1980); Parker et al.(1981); Rennhack (1982); Strauss (1975); Westinghouse

CYCLONES:
* have been used in series to clean gases from pressurized fluidized bed combustors.
* last cyclone must be high-efficiency (i.e.small).
* most data on collection efficiency must be extrapolated to high temperature and high pressure.

ELECTROCYCLONES:
* not yet tested at full scale.
* dust is charged, then separation in cyclone is improved by applying electric field.
* high-efficiency electrocyclones can be larger than equivalent conventional cyclone.

FILTERS:
* at present not available for our temperatures.
* mineral-fiber filters are being developed.

PACKED BEDS:
* dirty gases pass through packed or moving bed of granular material.
* have been used at 500 C.·
* temperature range can probably be extended.
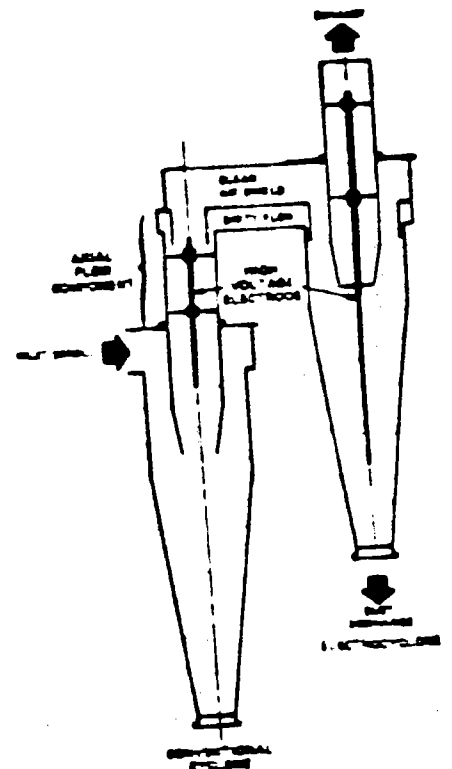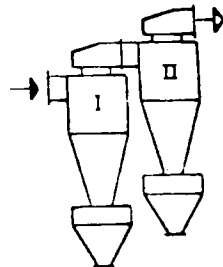
AIR-SOLIDS SEPARATORS: CYCLONES: EFFECT OF TEMPERATURE AND PRESSURE

REFERENCES: Parker et al. (1981); Rennhack (1982)

Information on cyclone efficiency must be extrapolated to our extreme temperature and pressure conditions. There is contradictory evidence on the effect of increasing temperature and pressure.

Rennhack predicts that cyclone collection efficiency will decrease with an increase in temperature or pressure. His prediction is based on the effect of temperature and pressure on gas properties and thus on the drag force acting on particles. Collection efficiency in cyclones decreases when the drag force increases, because drag acts against the centrifugal force that drives the particles outward and separates them from the air. The graph below shows how the minimum separable particle diameter varies with temperature and pressure.
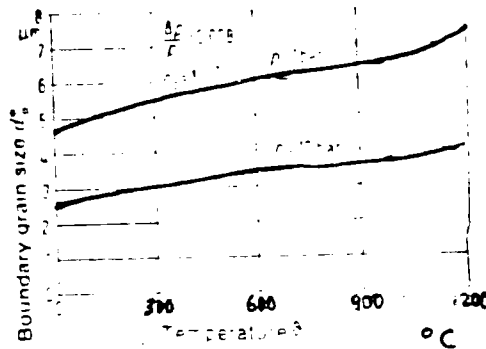

Parker et al. performed experiments and compared their results to the theoretical predictions of Leith and Licht.
Experimental conditions:
* 2-in cyclone
* inlet temperatures from ambient to 693 C
* pressures from atmospheric to 2530 kPa (25 atm)
Results: Collection efficiency decreased with increasing temperature and increased with increasing pressure. (See graph below.) The pressure dependence was contrary to theory, which predicted that pressure would have little effect. Parker et al. present an empirical correlation but no theoretical explanation for their results.

particle aerodynamic diameter, μm
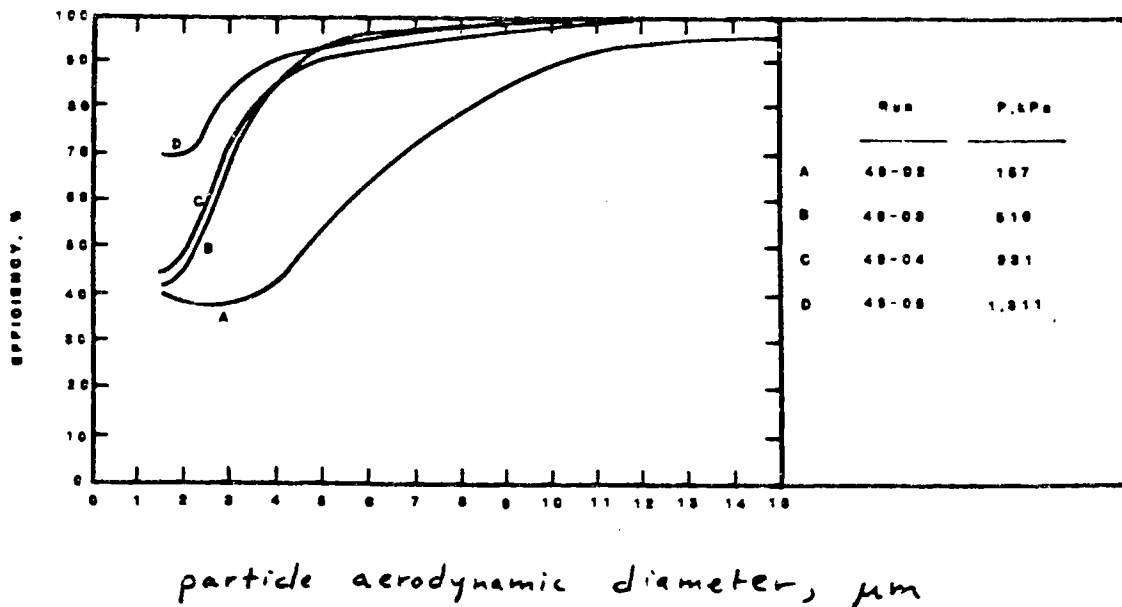
AIR-SOLIDS SEPARATORS: ELECTROCYCLONES

REFERENCE: Boericke et al. (1981)

Collection efficiency of conventional cyclones decreases as size increases. Thus, high-efficiency cyclones required for the final stage of clean-up for pressurized fluidized bed combustor gases are small (approx. 10 in. diameter). High-efficiency electrocyclones can be much larger, since their efficiency depends on voltage rather than size. Boericke et al. describe how the electrocyclone works and report on the results of an analytical model and experiments on an 18-inch electrocyclone. GE is now involved in the design and testing of larger models.

In the drawing, an electrocyclone is shown following a conventional cyclone. Dust particles are charged as they leave the first cyclone. Inside the electrocyclone, they are pushed to the wall by an applied electrical force as well as by the centrifugal force acting in all cyclones.

Force balance:

$$3\pi\mu d_p U_w = \frac{1}{3}\pi d_p^3 \rho_p \frac{V_t^2}{D} + q E_a$$

drag   centrifugal   electrostatic

Analytical model:
Electrocyclone is represented by a simplified two-dimensional model divided into five zones. Particle migration from zone to zone is expressed in a set of coupled differential equations. An analytical solution has been found, and is presented in another paper.

Experiment:
   * 18-in. electrocyclone operating at ambient temperature and pressure
   * Results agreed very well with the predictions of the model for low flowrates, where the electrostatic force is dominant. For higher flowrates, the measured efficiency was lower than predicted.
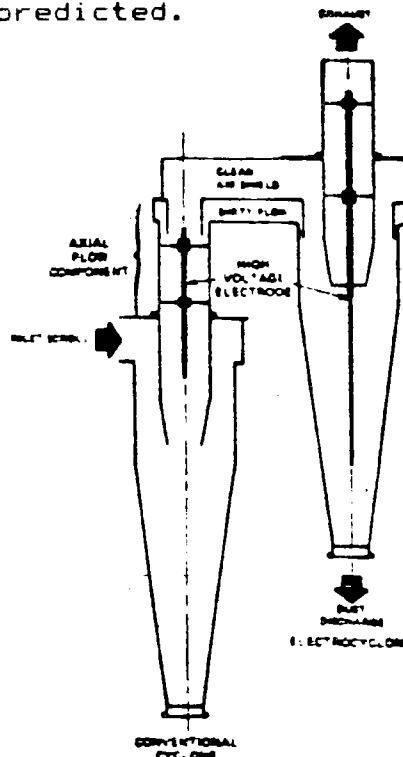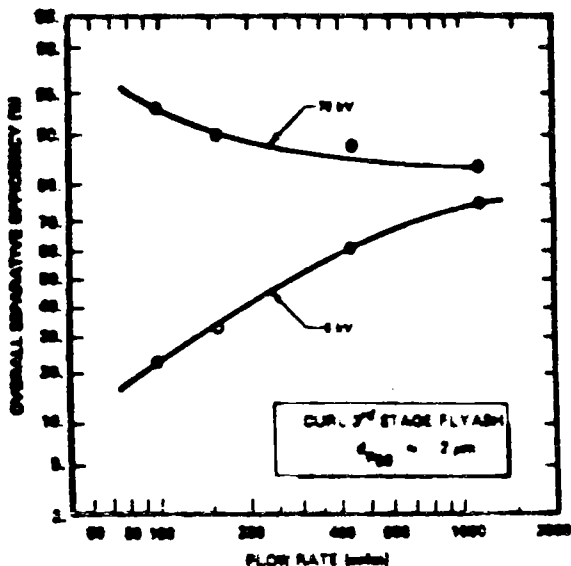
INSULATION

REQUIREMENTS:

* withstand 1000 C
* abrasion resistant

DESIGN:

* internal insulation, probably with an innermost abrasion-resistant layer.
* pressure vessel shell
* external insluation.

MANUFACTURERS:

* Babcock and Wilcox
* Carborundum
* Johns-Manville

COMMENTS:

* Our temperature requirements are not unusual.

* Since abrasion depends on particle velocity, size, and impact rate, as well as on particle and insulation hardness, manufacturers were reluctant to predict erosion rate. However, they did not think that our application would involve exceptional erosion problems.

* High-density insulation is more appropriate for abrasion resistance, but is a poorer insulator and more subject to thermal shock than low-density insulation. It may be necessary to control warm-up to guard against thermal shock.

* High-density insulation is available for our temperatures with a hardness rating of 9 (where diamond =10).

SERI

THERMOELECTRON CORP.
Waltham, MA 02254.   617-890-8700
Dr. Bill Cole

ThermoElectron is working on a particle-air heat exchanger for recovering
waste heat from flue gases and preheating clean air for combustion. This
work is sponsored by DOE Idaho Operations Office. The results will be in
the public domain once reports have been approved by DOE. Until then, there
is little performace information available.

Experimental Conditions:
    * scale: apparatus has cross-sectional area 0.46 m.
    * particles: alumina
    * temperature: hot gases enter at 1090 C; air is preheated to 540 C.
(The preheat temperature is the highest desired for industrial combustors.
The heat exchanger can be modified to produce hotter air.)
    * pressure: atmospheric

Design:
    * Exhaust gases enter the upper chamber and fluidize a bed of alumina
particles, transferring heat to them.
    * The particles travel to the lower chamber, where they are fluidized by
cold combustion air. The air is heated and leaves the chamber.
    * The particles are carried pneumatically back to the upper chamber.
This leg acts as a heat exchanger too, since heat is transferred to the air
that carries them upward.
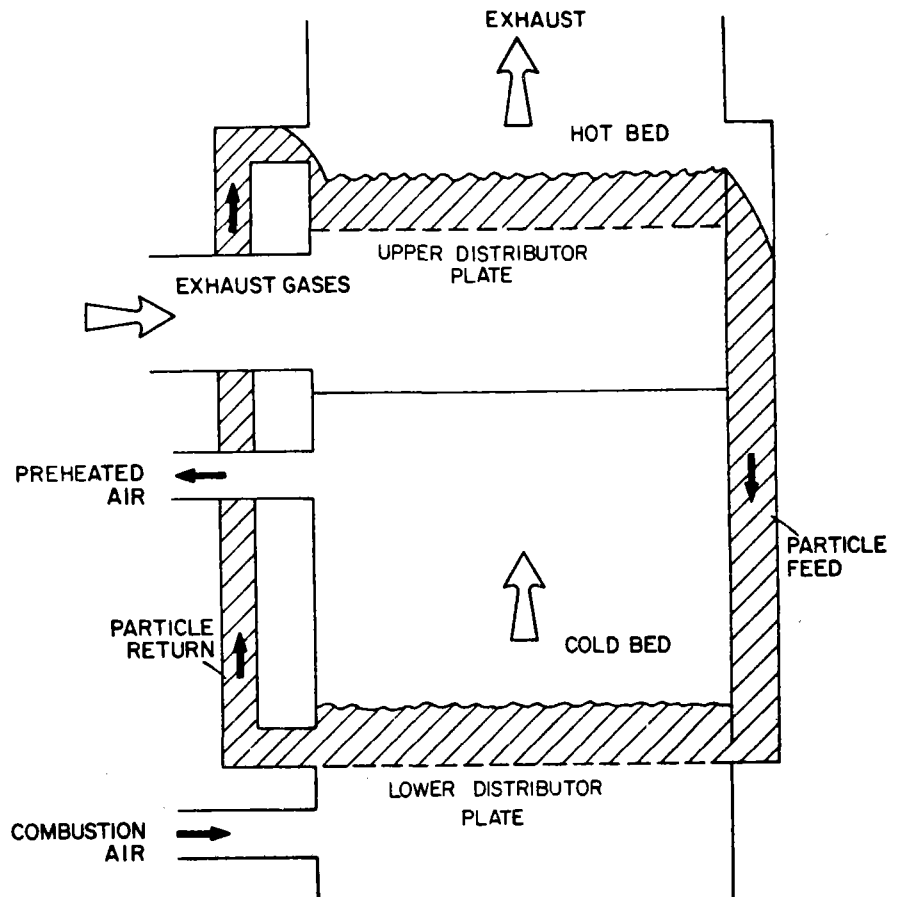
ECONOTHERM
15 Cedar Lane (P.O. Box 309)
Englewood, NJ 07631. 201-567-9767
Mr. J. Paul Vandenhoeck

REFERENCE: Vandenhoeck

Econotherm has designed gas-particle-air heat exchangers that are in use for waste heat recovery in the aluminum and foundry industries.

Operating conditions:
    * scale: full-scale
    * particles: sand or ceramic pellets
    * temperature: inlet gas temperatures up to 1100 C
    * pressure: atmospheric

Design:
    * two chambers
    * Particles are heated by hot flue gases in the upper chamber.
    * Particles heat clean air in the lower chamber.
    * Particles form a seal between the two chambers. From the bottom of the second chamber, they are carried pneumatically back to the top of the heat exchanger.
    * Heat transfer occurs in shallow fluidized beds and, apparently, in a free-falling section.

Comments:
    * The heat exchanger is refractory-lined. Vandenhoeck reports that abrasion was not noticeable in a foundry waste-heat heat exchanger of this type even after two years' operation.
    * Sand is satisfactory for relatively low-temperature applications, but it sinters at high temperatures.

90
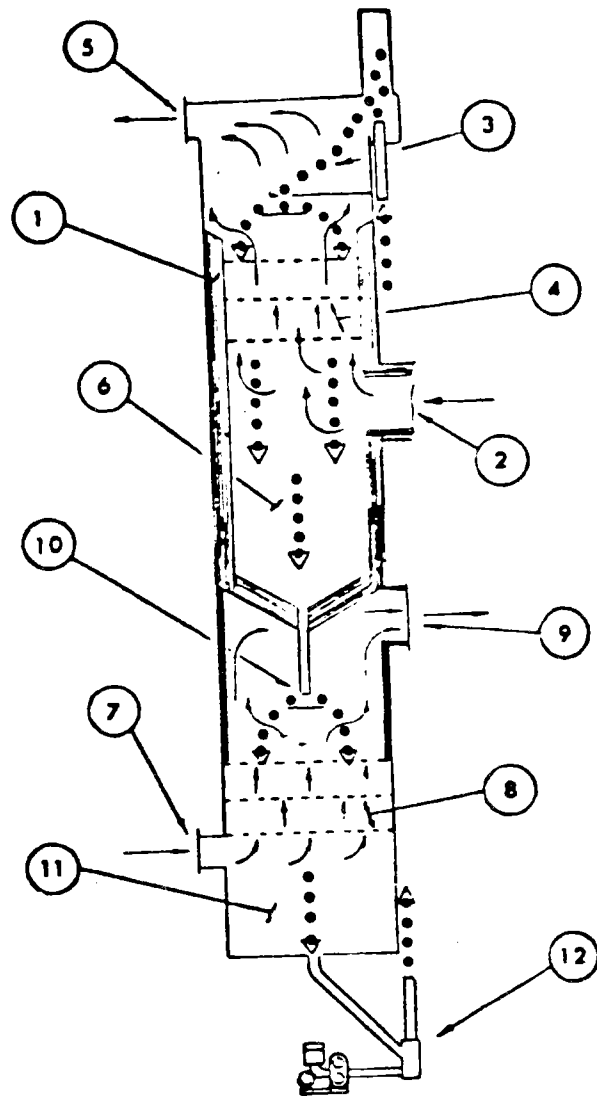
THERMAL SYSTEMS
Woburn, MA.   617-933-7880
Dr. Andy Syska

REFERENCE: Massey et al.(1979)

At Thermal Systems, Dr. Syska has done extensive experimental work on particle-air heat exchangers for waste heat recovery. To date, this work was done under contract to other companies and is proprietary. However, sometime in 1984, some of Thermal Systems' concepts will be developed by ThermoElectron with funding from DOE. The results of those investigations will be in the public domain.

Tests performed at Thermal Systems:
    * scale: working prototypes on industrial scale
    * particles: from 200 to 1200 microns
    * temperature: air preheated up to 1090 C.
    * pressure: atmospheric.

The reference to Massey et al. (a patent) gives information about a heat exchanger invented at Thermal Systems a few years ago. According to Dr. Syska, this design would no longer be recommended.
    * Hot dirty gas enters the device at A and pneumatically conveys the particles upward as it transfers heat to them.
    * The gas and particles enter a larger chamber, in which the particles settle. The gas moves upward and out of the system at B.
    * The particles form a seal between the chamber and a larger chamber that surrounds it. They fall into the larger chamber and then fall through a system of baffles, exchanging heat with a stream of clean air.
    * The clean air enters the heat exchanger at D and leaves, preheated, at C. The particles travel in a closed loop.
    * Note that the particles are heated in cocurrent heat exchange; they are cooled in countercurrent heat exchange.
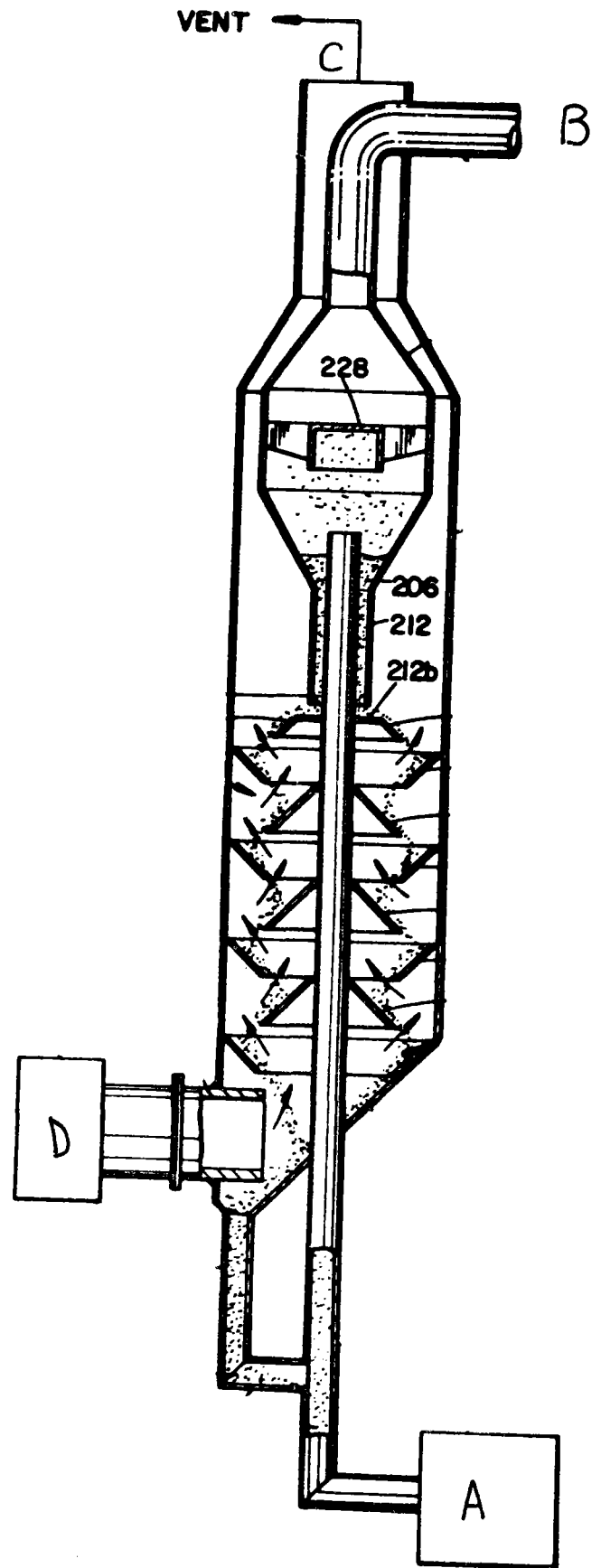
TUNZINI-NESSI ENTERPRISES
1 Place Honore de Balzac
95108   Argenteuil-Cedex,   France
3-411-5454

REFERENCES: Meunier (1978 a and b);
Meunier et al. (1983)

Tunzini-Nessi   is   working   with
researchers   at   the   Universite   de
Technologie   de   Compiegne   on   the
development of the packed bed heat
exchanger. Applications include flue gas
waste   heat   recovery,   regenerating
foundry sand, and obtaining useful heat
by burning mine tailings.

Experimental conditions:
    * scale: 0.3-m-diameter column at the
university;   demonstration   plant   in
progress.
    *   temperature: 500   C   at   the
university; 1200 C in the demonstration
plant
    * pressure: ambient

Design:
    * countercurrent heat exchanger
    * layers of packing increase particle
residence   time   and   improve   the
uniformity of both particle and gas
flow.
   * fluidized bed is used for the
hottest contacting at the bottom, since
the packing and packing supports can not
resist very high temperatures (1500 C).

Note:
The   device   shown   is   for   heating
particles with hot flue gases. A device
for heating gases with hot particles
would have a slightly different design:
    * The fluidized bed would be omitted
or placed at the top of the column.
    * The diameter of the column would be
larger   at   the   top   than   the   bottom
beacuse of the change in density of the
gas.
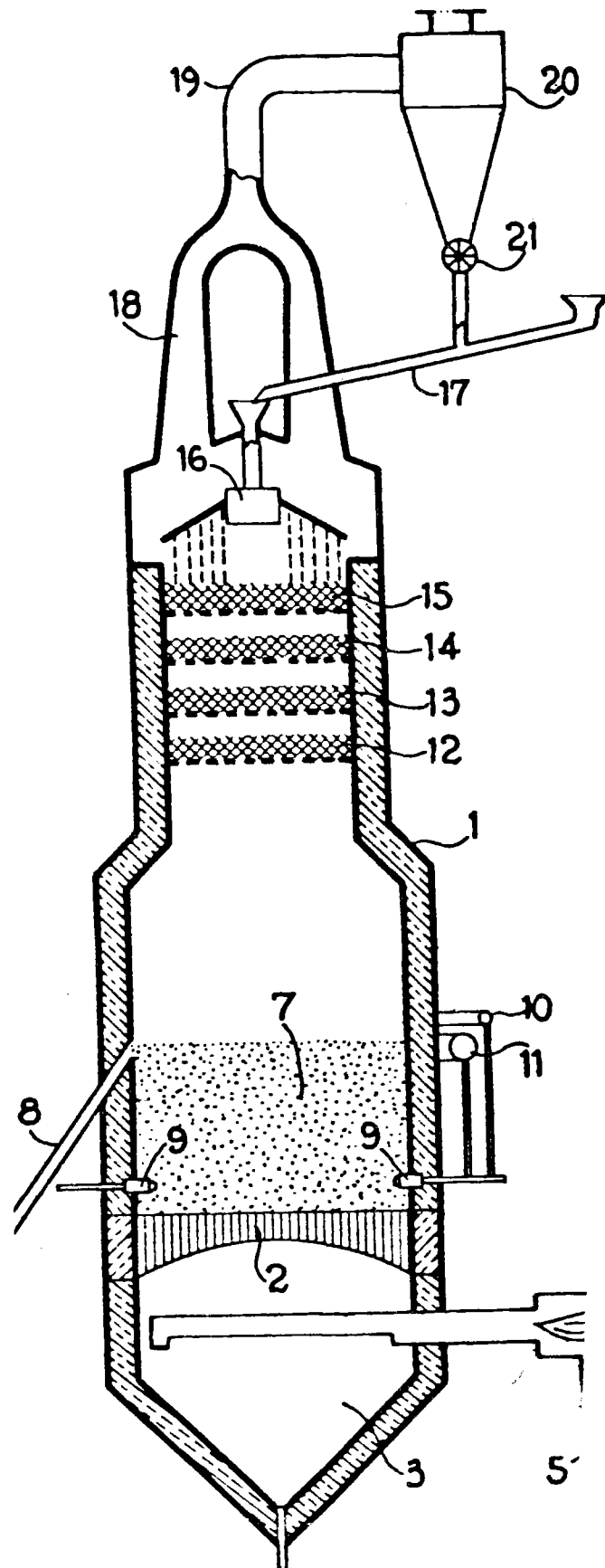
THE FALLING CLOUD HEAT EXCHANGER
(STONE PLATT FLUIDFIRE LTD.)

REFERENCES: SAGOO 1981 A AND B, SAGOO 1979, EAVES 1978

APPLICATION: HEAT RECOVERY FROM HOT CONTAMINATED GASES
FLOWING UP A CHIMNEY

OPERATING
  CONDITIONS:

GAS: AIR

GAS INLET TEMPERATURE: (U. OF ASTON) 100, 160
215°C (PILOT PLANT) 200, 300°C

GAS PRESSURE: AMBIENT

PARTICLE MATERIAL: ALUMINA, STEEL

PARTICLE DIAMETER: 0.40 MM, 0.38 MM

TERMINAL VELOCITY: 2.62 M/S, 5.27 M/S

COLUMN DIMENSIONS: (U. OF ASTON) 0.3 M
DIAMETER X 1.9 M HIGH (PILOT PLANT) 1.1 M
DIAMETER X 4.3 M HIGH

TEST RESULTS: MEASURED HEAT RECOVERY RATE, HEAT TRANSFER
COEFFICIENT, AND THERMAL EFFICIENCY FOR BENCH
SCALE MODEL (U. OF ASTON) AND PILOT PLANT.
PUBLISHED RESULTS FROM THE BENCH SCALE MODEL
ARE ONLY QUALITATIVE. RESULTS FROM THE PILOT
PLANT WERE LIMITED BY THE PLANT CAPACITY.

COMMENTS: REFERENCED REPORTS ARE OF VERY POOR TECHNICAL
QUALITY, BUT SOME PRACTICAL LESSONS CAN BE
LEARNED FROM THE RECORDED EXPERIENCE OF BUILDING
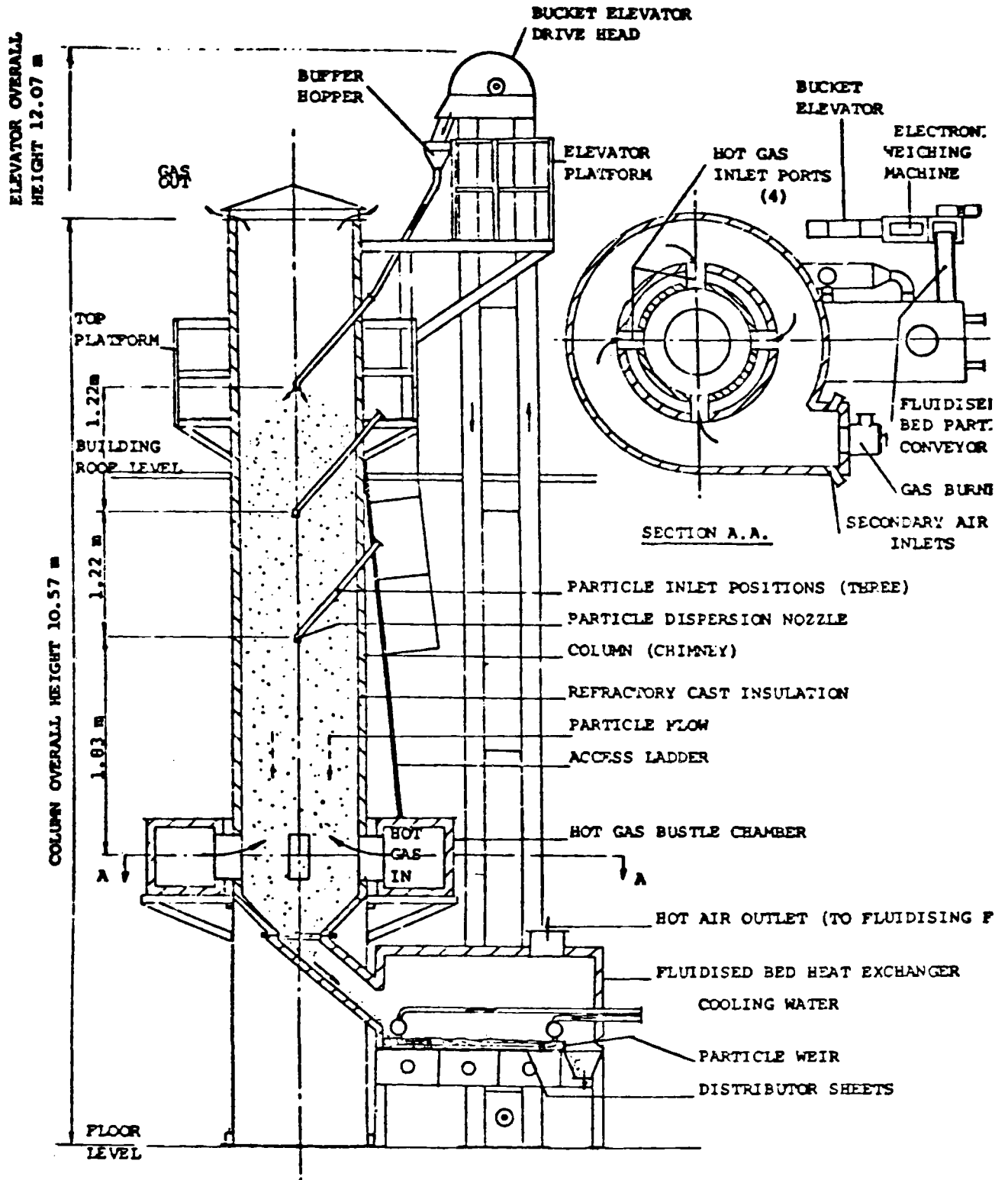AND OPERATING A PILOT PLANT.

FIG 1: THE FALLING CLOUD HEAT EXCHANGER - COMMERCIAL PILOT PLANT

SERI ⊛

SOURCES IN LITERATURE SEARCH

ENGINEERING INDEX-- 1982-- topics such as:
    heat recovery
    heat exchangers
    heat transfer
    fluid mechanics

CURRENT CONTENTS, Engineering Series, VOL.14 (1983)

JOURNALS NOT COVERED BY CURRENT CONTENTS, such as:
    German Chemical Engineering
    International Chemical Engineering
    Applied Energy

SURVEYS, such as
    Sandia Particle Library Listing (updated 4/19/83)
    Geldart's Survey of Gas Fluidization Research

CONVERSATIONS with:
    Dr. M. Bergougnou (University of Western Ontario)
    Dr. T. Reed (SERI)
    Dr. J. Taborek (Science Applications, Inc.)
    Dr. W. Thielbahr (DOE Idaho Operations Office)

COMPUTER SEARCHES IN COMPENDEX (equivalent to Engineering Index 1973-83) -- topics such as:
    moving bed/ heat transfer
    falling/ heat exchanger
    direct contact/ heat exchange/ particle/ gas

CURRENT ENERGY PATENTS 1982 and 1983.

APPENDIX C. SAMPLE CALCULATIONS FOR THERMAL ANALYSIS OF SHELL-AND-TUBE HEAT EXCHANGER

Shell-Side Heat Transfer Coefficient

Given:

ρ_s = particle density = 4000 kg/m^3

V_o = bed velocity = 0.15 m/s

ρ_b = bulk density = 2400 kg/m^3

D_o = tube outside diameter = 0.0272 m

K_s = thermal conductivity of alumina $\cong$ 8 W/m K

c_{ps} = specific heat of alumina = 837.2 J/kg K

d_m = mean size of particles = 0.5 × 10^{-3} m.

From Eq. 5-7 (Kurochkin 1966),

$$Nu_p = 0.0214 \, Pe^{0.21} \left(\frac{D_o}{d_m}\right)$$

with:

$$Pe = \frac{V_o \, c_{ps} \, \rho_b \, D_o}{K_p}$$

$$Pe = \frac{(0.15)(837.2)(2400)(0.0272 \text{ m})}{8} = 1025$$

$$Nu_p = 0.0214 \, (1025)^{0.21} \left(\frac{0.0272}{0.5 \times 10^{-3}}\right) = 5.0$$

$$H_p = \frac{Nu_p \, K_p}{D_o} = \frac{(5.0)(8)}{0.0272} = 1468 \text{ W/m}^2 \text{ K} \approx 250 \text{ Btu/h ft}^2 .$$

Tube-Side Heat Transfer Coefficient (Smooth Tubes)

Given:

Re_a = air Reynolds number = 40,000 (varied)

Pr_a = air Prandtl number = 0.72

F = heat transfer adjustment factor = 1 (smooth tubes)

D_H = hydraulic diameter = 0.0222 m = D_i

K_a = air thermal conductivity = 0.0334 W/m K.

From Eq. 5-5,

$$Nu_a = 0.023 \, Re_a^{0.8} Pr_a^{0.4} F$$

$$Nu_a = (0.023)(40,000)^{0.8} (0.72)^{0.4} \approx 97$$

$$H_a = \frac{Nu_a \, K_a}{D_H}$$

$$H_a = \frac{(97)(0.0334)}{0.0222} = 146 \, W/m^2 \, K \; .$$

Overall Heat Transfer Coefficient

Given:

$T_{in,p}$ = particle inlet temperature = 1000°C

$T_{out,p}$ = particle outlet temperature = 581°C

$T_{in,a}$ = air inlet temperature = 150°C

$T_{out,a}$ = air outlet temperature = 970°C

H_a = tube-side heat transfer coefficient = 146 W/m^2 K

H_p = shell-side heat transfer coefficient = 1413 W/m^2 K

R_p = shell-side fouling resistance = 0.0001 m^2 K/W

R_a = air-side fouling resistance = 0.0003 m^2 K/W

Y_w = wall thickness = 2.5×10^{-3} m

K_w = wall thermal conductivity = 11 W/m K.

Compute ΔT_{LM}:

$$\Delta T_{LM} = \frac{(T_p - T_a)_B - (T_p - T_a)_A}{\ln\left[\dfrac{(T_p - T_a)_B}{(T_p - T_a)_A}\right]} = \frac{(581 - 150) - (1000 - 970)}{\ln\left[\dfrac{(581 - 150)}{(1000 - 970)}\right]}$$

$$\Delta T_{LM} = 150.5^\circ C \; .$$

Calculate the average tube diameter:

$$D_w = \frac{D_o - D_i}{\ln\left(\dfrac{D_o}{D_i}\right)} = \frac{0.0272 - 0.0222}{\ln\left(\dfrac{0.0272}{0.0222}\right)} = 0.0246 \; .$$

Calculate U, the overall heat transfer coefficient:

$$U = \left[1/ \frac{1}{H_p} + R_p + \left(\frac{1}{H_a} + R_a \right) \frac{D_o}{D_i} + \frac{Y_w}{K_w} \frac{D_o}{D_w} \right]$$

$$U = 1/ \frac{1}{1413} + 0.0001 + \left(\frac{1}{146} + 0.0003 \right) \frac{0.0272}{0.0222} + \frac{0.0025}{11} = \frac{0.0272}{0.0246} = 103 \ W/m^2 \ K \ .$$

Required Heat Transfer Area

Given:

$$U = 103 \ W/m^2 \ K$$
$$\Delta T_{LM} = 150^o C$$
$$Q = 100 \times 10^6 \ W.$$
$$Q = UA\Delta T_{LM}.$$

Solving for the area,

$$A = \frac{Q}{U\Delta T_{LM}}$$

$$A = \frac{100 \times 10^6}{(103)(150.5)} = 6450 \ m^2 \ .$$

APPENDIX D. SAMPLE CALCULATIONS FOR PRESSURE DROP IN SHELL–AND–TUBE HEAT EXCHANGER

Pressure Drop in Tubes

Given:

$$Re = 40,000$$

$$D_H = 0.0222 \text{ m}$$

$$\rho_a = 0.833 \text{ kg/m}^3$$

$$\mu = 0.000024 \; \rho_a \cdot s$$

$$C_{pa} = 1018 \text{ J/kg K .}$$

Compute air velocity:

$$Re = \frac{\rho_a V_a \; D_H}{\mu} \rightarrow V_a = \frac{Re\mu}{\rho_a D_H}$$

$$V_a = \frac{(40,000)(0.000024)}{(0.833)(0.0222)} = 51.9 \text{ m/s .}$$

Compute friction factor:

$$f = \frac{0.046}{Re^{0.2}} = \frac{0.046}{(40,000)^{0.2}} = 5.53 \times 10^{-3} \; .$$

Compute mass flow rate per tube of air:

$$\dot{m}_t = \rho_a A_t V_a = \frac{(0.833) \; \pi(0.0222^2)(51.9)}{4} = 0.0167 \text{ kg/s .}$$

Compute total mass flow rate of air:

$$Q = \dot{m} \; C_{pa} \Delta T_a \rightarrow \dot{m} = \frac{Q}{C_{pa}\Delta T_a}$$

$$\dot{m} = \frac{100 \times 10^6}{(1018)(970 - 150)} = 119.8 \text{ kg/s .}$$

Compute number of tubes required:

$$NT = \frac{\dot{m}}{\dot{m}_t} = \frac{119.8}{0.0167} = 7173 \text{ tubes .}$$

Compute tube length:

$$A = NT \times A_t = NT \times \pi \, D_o \, L$$

$$L = \frac{A}{NT \; \pi \; D_o} = \frac{6450}{(7173)(\pi)(0.0272)}$$

$$L = 10.5 \text{ m} .$$

Compute pressure drop:

$$\Delta P = \frac{2f \; V_a^2 \; L \; \rho_a}{D_H}$$

$$\Delta P = \frac{2(5.53 \times 10^{-3})(51.9)^2(10.5)(0.833)}{0.0222}$$

$$\Delta P = 11,737 \text{ Pa} .$$

DISTRIBUTION LIST

Howard S. Coleman, Director
Division of Solar Thermal Technology
Department of Energy
Forrestal Building
1000 Independence Ave., S.W.
Washington, DC 20585

Sigmund Gronich
Division of Solar Thermal Technology
Department of Energy
Forrestal Building
1000 Independence Ave., S.W.
Washington, DC 20585

Michael Gurevich
Division of Energy Storage
  Technology
Department of Energy
Forrestal Building (5E-052)
1000 Independence Ave., S.W.
Washington, DC 20585

Jill Hruby
Sandia National Laboratories
Livermore, CA 94550

R. Jain
Air Pollution Technology
5191 Santa Fe St.
San Diego, CA 92126

L. D. Kannberg
Battelle Pacific Northwest
  Laboratory
P.O. Box 999
Richland, WA 99352

Kenneth W. Klein, Director
Office of Energy Storage and
  Distribution
Department of Energy
Forrestal Building (5E-036)
1000 Independence Ave., S.W.
Washington, DC 20585

Charles Mangold
Division of Solar Thermal Technology
Department of Energy
Forrestal Building
1000 Independence Ave., S.W.
Washington, DC 20585

James Martin
Oak Ridge National Laboratory
P.O. Box Y
Building 9204-1
Oak Ridge, TN 37830

Al Mezzina
Brookhaven National Laboratory
Upton, NY 11973

A. I. Michaels
Argonne National Laboratory
Building 362
9700 S. Cass Avenue
Argonne, IL 60439

Frederick H. Morse, Director
Office of Solar Heat Technologies
Department of Energy
Forrestal Building (CE-33)
1000 Independence Ave., S.W.
Washington, DC 20585

Lee G. Radosevich
Solar Programs Division 8431
Sandia National Laboratories
Livermore, CA 94550

Steve Sargent
DOE SERI Area Office
Golden, CO 80401

Craig E. Tyner
Central Receiver Technology
Division 6226
Sandia National Laboratory
Albuquerque, NM 87186

Ron West
4774 McKinley
Boulder, CO   80303

Tex Wilkins
Division of Solar Thermal Technology
Department of Energy
Forrestal Building
1000 Independence Ave., S.W.
Washington, DC   20585

SERI Staff:

Mark S. Bohn	15/3	252
Stanley Bull	15/2	231
Meir Carasso	15/3	252
Robert Copeland	15/3	252
Don Feucht	17/3	100
Barbara Goodman	15/2	231
Herbert J. Green	15/3	252
Bim Gupta	15/3	251
David Johnson	15/3	252
Cecile LeBoeuf	16/1	211
Gerry Nix	15/3	251
Kenneth Olsen	15/3	251
Paul Schissel	16/3	255
Larry Shannon	15/3	250

Document Control Page	1. SERI Report No. SERI/TR-252-2663	2. NTIS Accession No.	3. Recipient's Accession No.

4. Title and Subtitle
Technical and Economic Evaluation of a Solid Particle/Air Direct-Contact Heat Exchanger

5. Publication Date
October 1986

6.

7. Author(s)
J. Green, C. Leboeuf, M. Bohn

8. Performing Organization Rept. No.

9. Performing Organization Name and Address
Solar Energy Research Institute
1617 Cole Boulevard
Golden, Colorado 80401

10. Project/Task/Work Unit No.
4254.10

11. Contract (C) or Grant (G) No.
(C)
(G)

12. Sponsoring Organization Name and Address

13. Type of Report & Period Covered
Technical Report

14.

15. Supplementary Notes

16. Abstract (Limit: 200 words)

A conceptual design of a solid-particle/air heat exchanger system is presented including a multistage fluidized-bed heat exchanger, solid-particle feeders and defeeders, and cyclones. The system is designed for 100°C solid particles that heat air at 10 atm at a 100-MW$_t$ heat rate. This type of heat exchanger could be part of a solar thermal central receiver system that uses solid particles as the heat transfer media. The technical and economic feasibilities of this system are evaluated. As an alternative to direct contact, a shell-and-tube heat exchanger is evaluated as well.

The direct-contact system is technically feasible though additional development is needed in some areas. The annual levelized cost per unit of delivered thermal energy for a direct-contact system based on state-of-the-art technology is estimated to be \$6.66/GJ. If reasonable assumptions are made as to technical progress resulting from future development activities, the cost drops to \$2.30/GJ. The cost of a shell-and-tube heat exchanger for the same service is estimated to be \$2.91/GJ.

17. Document Analysis

a. Descriptors Central Receivers ; Direct Contact Heat Exchangers ; Economic Analysis ; Fluidized Bed Heat Exchangers

b. Identifiers/Open-Ended Terms

c. UC Categories
62, 62a, c

18. Availability Statement
National Technical Information Service
U.S. Department of Commerce
5285 Port Royal Road
Springfield, Virginia 22161

19. No. of Pages
116

20. Price
A06

Form No. 0069 (3-25-82)